AD-A282 166

94-21430

REPORT DOCUMENTATION PAGE

1. AGENCY USE ONLY (Leave blank)	2. REPORT DATE 1/10/94	3. REPORT TYPE AND DATES COVERED Final - 9/1/89 thru 8/31/94

4. TITLE AND SUBTITLE
Soot and NOx Emissions and Combustion Characteristics of Low Heat Rejection Direct Injection Diesel Engines

5. FUNDING NUMBERS
DAAL03-89-G-0103

6. AUTHOR(S)
D.E. Klett, E.M. Afify, M.T. Sadd

7. PERFORMING ORGANIZATION NAME(S) AND ADDRESS(ES)
Mech. Engr. Dept, North Carolina A&T State Univ.
Greensboro, NC 27411

8. PERFORMING ORGANIZATION REPORT NUMBER

DTIC ELECTE JUL 13 1994

9. SPONSORING/MONITORING AGENCY NAME(S) AND ADDRESS(ES)
U. S. Army Research Office
P. O. Box 12211
Research Triangle Park, NC 27709-2211

10. SPONSORING/MONITORING AGENCY REPORT NUMBER
ARO 26765.2-EG-SAH

11. SUPPLEMENTARY NOTES
The view, opinions and/or findings contained in this report are those of the author(s) and should not be construed as an official Department of the Army position, policy, or decision, unless so designated by other documentation.

12a. DISTRIBUTION/AVAILABILITY STATEMENT
Approved for public release; distribution unlimited.

12b. DISTRIBUTION CODE

13. ABSTRACT (Maximum 200 words)

Performance and emissions data were gathered on a normally aspirated single cylinder DI engine with various combinations of ceramic coatings installed. Thin ceramic thermal barrier coatings were applied to the piston crown and bowl, the head and valves, and the cylinder liner. The coated piston and head were run singly and in combination with the cylinder liner to investigate the effects of these different coated surfaces on emissions and performance. Coating the piston crown alone results in generally lower cylinder pressure, lower brake specific fuel consumption and lower NOx emission compared to the baseline engine. Soot emission is typically increased below 2000 RPM and decreased above 2000 RPM. Coating the head alone reduces cylinder pressure, but generally increases specific fuel consumption and NOx and soot emission. The KIVA-II code was used to model the Hydra engine with the thermal coatings. The computer modeling has led to an understanding of the effect of coating the piston on NO production. The hotter piston crown warms the intake air, shortening ignition delay and decreasing the ratio of premixed to diffusion combustion, ultimately resulting in lower peak cylinder temperature and reduced NO. The KIVA-II results agree reasonably well with the experimental data for cylinder pressure and NO and soot emission.

14. SUBJECT TERMS
Diesel Combustion, Low Heat Rejection Engines, NOx Emission
Soot Emission, Thermal Barrier Coatings

15. NUMBER OF PAGES
115

16. PRICE CODE

17. SECURITY CLASSIFICATION OF REPORT	18. SECURITY CLASSIFICATION OF THIS PAGE	19. SECURITY CLASSIFICATION OF ABSTRACT	20. LIMITATION OF ABSTRACT
UNCLASSIFIED	UNCLASSIFIED	UNCLASSIFIED	UL

NSN 7540-01-280-5500

Standard Form 298 (Rev. 2-89)
Prescribed by ANSI Std. Z39-18
298-102

DTIC QUALITY INSPECTED 1

FINAL REPORT

SOOT AND NO$_x$ EMISSIONS AND COMBUSTION CHARACTERISTICS OF LOW HEAT REJECTION DIRECT INJECTION DIESEL ENGINES

By

D. E. Klett
Mechanical Engineering Department
North Carolina A&T State University

E. M. Afify and M. T. Saad
Mechanical Engineering Department
North Carolina State University

January 10, 1994

TABLE OF CONTENTS

CONTENTS CONTINUED

SUMMARY

An experimental and analytical study on the effect of thin ceramic coatings on soot and NOx emissions and performance of a direct injection diesel engine was conducted jointly between North Carolina A&T State University and North Carolina State University.

Performance and emissions data were gathered on a normally aspirated Ricardo Hydra single cylinder DI engine with various combinations of ceramic coatings installed. Thin ceramic thermal barrier coatings were applied to the piston crown and bowl, the head and valves, and the cylinder liner. The coated piston and head were run singly and in combination with the cylinder liner to investigate the effects of these different coated surfaces on emissions and performance for two different pure hydrocarbon fuels, hexadecane and dodecane. Coating the piston crown alone results in generally lower cylinder pressure, lower brake specific fuel consumption and lower NOx emission compared to the baseline engine. Soot emission is typically increased below 2000 RPM and decreased above 2000 RPM. Coating the head alone reduces cylinder pressure, but generally increases specific fuel consumption and NOx and soot emission.

The analytical portion of the study involved modifications to the KIVA-II code and its use to model the Hydra engine with the thermal coatings. Modifications to the code include incorporation of an eddy-break-up combustion model, to replace the standard Arrhenius single reaction model. A time dependent combustion surface temperature was also incorporated to simulate the effects of thermal barrier coatings on cylinder temperature, pressure and NOx production. A soot model was added to the code, following the work of Magnussen and Hjertager. The EBU model gives better results for the diffusional portion of the combustion process, but fails to adequately model the premixed combustion, typically resulting in a lower predicted peak cylinder pressure (and temperature) than predicted by the single reaction model and shown by experiments. Consequently, the EBU model also under-predicts NO emission to a greater degree than the SR model. The KIVA-II modeling has led to an understanding of the effect of coating the piston on NO production. The hotter piston crown warms the intake air, shortening ignition delay and decreasing the ratio of premixed to diffusion combustion, ultimately resulting in lower peak cylinder temperature and reduced NO. The KIVA-II results agree reasonably well with the experimental data for cylinder pressure and NO and soot emission.

LIST OF PUBLICATIONS

Technical Papers Published

Afify, E.M., Klett D.E., Singh, H. and Wei, X., "The Effect of Insulating the Piston Crown on the Performance and NO Emissions of a DI Diesel Engine", Proceedings of the Eighth International Conference for Mechanical Power Engineering, Alexandria, Egypt, April, 1993.

Saad, M., Afify, E.M., Klett D.E. and Singh, H., "Modeling of Combustion and NO Emission in a Direct Injection Diesel Engine", Proceedings of the Eighth International Conference for Mechanical Power Engineering, Alexandria, Egypt, April, 1993.

Saad, M., Afify, E.M. and Klett, D.E., "Multidimensional Modeling of Combustion and NO Emission of the Ricardo Hydra Direct Injection Diesel Engine: KIVA-II Versus Experiment", Proceedings of the ASME IC Engine Division Fall Technical Conference, Morgantown, WV, September, 1993.

Papers in Preparation

"Effect of Selective Insulation on the Combustion, Performance and NO Emission of DI Diesel Engines"

"Modeling of Soot and NO Emissions in a DI Diesel Engine: KIVA-II Versus Experiments"

Theses

Saad, M.T., "Soot and NOx Emissions and Combustion Characteristics of Direct Injection Diesel Engine", PhD Thesis, Mechanical Engineering Department, North Carolina State University, December, 1993.

Vakil, M., "Experimental Investigation of Effect of Ceramic Coatings on Performance and Emissions of a DI Diesel Engine", MS Thesis, Mechanical Engineering Department, North Carolina A&T State University, (In Progress)

LIST OF PERSONNEL AND DEGREES EARNED

David E. Klett, Project Dirctor, Professor of Mechanical Engineering, North Carolina A&T State University

E. M. Afify, Co-Investigator, Professor of Mechanical Engineering, North Carolina State University

Messiha T. Saad, Graduate Research Assistant, PhD, North Carolina State University, 12/93

Xu Wei, Graduate Research Assistant, PhD, North Carolina State University, Expected 5/95

M. Vakil, Graduate Research Assistant, MS, North Carolina A&T State University, Expected 5/94

Nigel Brooks, Undergraduate Research Assistant, BS, North Carolina A&T State University, Expected 12/94

Martin Ashley, Undergraduate Research Assistant, BS, North Carolina A&T State University, 5/92

Raphael Jones, Undergraduate Research Assistant, North Carolina A&T State University, 5/93

Postoria, Aguirre, Undergraduate Research Assistant, North Carolina A&T State University, 5/92

ACKNOWLEDGMENT

1. INTRODUCTION

1.1 PROBLEM STATEMENT

The objective of this work was to study the effects of thin ceramic coatings applied to various internal engine surfaces on the performance and emissions of a direct injection (DI) diesel engine. The study included an experimental investigation coupled with computer modeling using the KIVA II code to gain insight into the combustion effects caused by higher surface temperatures resulting from the use of ceramic coatings. The project was a joint effort between North Carolina A&T State University, where the experiments were carried out, and North Carolina State University, where the bulk of the computer modeling was performed.

The Army, among a number of other agencies and corporations, has maintained an interest in the use of ceramics in diesel engines for a number of years, and many studies have been conducted on various aspects of this topic [1-8]. This study focused on the use of KIVA II to model the combustion process in a particular DI diesel engine with thin ceramic coatings applied to the piston crown, the cylinder head inner surface and the cylinder liner. Experiments were performed on a single-cylinder Ricardo Hydra DI diesel research engine to provide a data base for comparison with the modeled results. Of particular interest were the effects of the coatings on brake specific fuel consumption, NOx emission and soot emission. Two pure hydrocarbon fuels, Dodecane ($C_{12}H_{26}$) and Hexadecane ($C_{16}H_{34}$), were used for the experiments and in the combustion modeling. These fuels were chosen for purposes of reproducibility of experimental results and because the properties are available to facilitate the modeling.

1.2 BACKGROUND

The use of ceramic coatings on combustion chamber surfaces influences the performance and exhaust emissions of DI diesel engines [1-4]. This can be attributed to changes in the combustion process brought about by the modification of the thermal boundary conditions due to the lower thermal conductivity of ceramics relative to metals. The added thermal resistance of thin low conductivity coatings increases the surface temperature, and higher surface temperatures affect the cowustion process in a variety of ways, depending on which combustion chamber surfaces are coated.

1

To better understand the effect of insulating the combustion chamber walls on the performance and exhaust emissions of the engine, a brief review of the combustion process in DI diesel engines is first presented.

The combustion process in DI diesel engines involves two modes of combustion, usually referred as the premixed and the diffusion combustion modes [9]. Premixed combustion occurs early in the process when fuel which has evaporated and mixed with air during the ignition delay period auto ignites. This mode is accompanied by a high rate of heat release which produces a rapid rate of pressure rise. When the premixed fuel/air mixture is depleted, diffusion combustion, characterized by a lower rate of heat release, takes over and controls the remainder of the combustion process.

Modification of the engine design, or variation of its operating conditions, will affect the combustion process in such a way as to vary the ratio of the time duration of the two modes, t_p/t_d, where t_p represents the duration of the premixed mode and t_d represents the duration of the diffusion mode. This ratio plays an important role in determining the effect of engine parameters and other factors on the performance and emissions of the engine. Factors which increase the ignition delay period will increase the premixed combustion duration while decreasing the diffusion combustion duration, causing an increase in the ratio t_p/t_d. This may lead to higher peak cylinder pressure and temperature which may improve thermal efficiency and reduce CO and unburned hydrocarbon (UHC) emissions at the expense of increasing NOx emissions of the engine. Large increases in t_p/t_d will cause a high rate of pressure rise and lead to objectionable diesel knock. Factors such as engine speed, advanced injection timing and the use of low cetane fuels contribute to longer ignition delay and the increase in t_p/t_d. Reducing the ignition delay period causes the premixed combustion duration to decrease while increasing the diffusion combustion duration, i.e. reduces t_p/t_d, prolonging the combustion process. Large decreases in t_p/t_d may cause the diffusion combustion mode to dominate which may lead to loss of power, decrease in thermal efficiency and possible deterioration of engine exhaust emissions. Preheating the intake air and insulating combustion chamber surfaces are among the factors which can decrease ignition delay and t_p/t_d.

Several experimental studies on low heat rejection (LHR) DI naturally aspirated diesel engines [1,3,4,5,6] showed that engine performance and exhaust emissions suffered from lengthening of the combustion process which is indicative of an extreme reduction in the ratio t_p/t_d.

1.3 PERTINENT LITERATURE REVIEW

Few investigators have studied the effect of insulating various combustion chamber surfaces in DI diesel engines and the results have been contradictory in some cases. Miyairi, et. al [3] studied the effect of selective insulation of the cylinder head, piston crown, and cylinder liner, using thick monolithic ceramic inserts, on the performance and emission characteristics of a single-cylinder, normally-aspirated DI diesel engine. They showed that fuel economy and NO emissions of the engine were improved by insulating the cylinder head and liner, but were made worse by insulating the piston crown. Part of the degradation in BSFC with the insulated piston was attributed to the increased reciprocating mass due to the heavy monolithic ceramic piston crown.

Assanis, et. al [2] conducted a series of tests on a supercharged DI diesel engine with and without piston surface insulation to determine the effect of ceramic coating the piston crown on engine performance and emissions. In their study, they emphasized the significance of the heat release profile, and indicated that insulating the piston with a thin coating of PSZ resulted in better engine efficiency and reduced emissions over the baseline engine.

Dickey [1] studied the effect of applying thin ceramic coatings to all combustion chamber surfaces in a supercharged single-cylinder Caterpillar 1Y-540 DI diesel engine. The results showed decreased thermal efficiency, but also decreased specific NOx and UHC for the ceramic coated engine relative to the baseline engine, especially at higher loads.

Daby, et. al [10] conducted tests on a single-cylinder, uncooled, pressurized-intake, DI diesel engine equipped with thick monolithic ceramic inserts on the head and cylinder liner (above top ring travel). The piston was a low-heat-pass articulated design with a ferrous metal top and an aluminum skirt. These tests were conducted to investigate the behaviour of alternative fuels (low cetane, higher density) in conjunction with an uncooled engine. Basline tests were conducted with Phillips diesel control fuel D-2 in the uncooled engine and in a baseline cooled metal engine. The baseline engine, however, had a different stroke and compression ratio than the ceramic engine, and direct comparisons of performance and emissions for the two engines would not be meaningful.

3

2. DESCRIPTION OF EXPERIMENTS

2.1 EXPERIMENTAL APARATUS

The experimental data used for comparison with the KIVA results were obtained from a Ricardo Hydra single-cylinder DI diesel research engine. Table 1 provides the basic specifications of the engine and Figure 2.1 provides a cross-sectional view of the combustion chamber showing the toroidal bowl piston. Measured data included load, speed, crank angle, needle lift, cylinder and fuel line pressure, fuel mass flow rate, air volume flow rate, intake and exhaust gas temperatures, coolant and lube oil temperatures, exhaust smoke opacity and NO and NOx emissions.

Engine loading was via a digitally-controlled DC motoring dynamometer interconnected to the utility grid through a KTK power control and signal conditioning system. Speed, load and injection timing could be remotely controlled from an instrumentation panel which provides readouts of these parameters plus coolant, lubricant, intake and exhaust manifold temperatures. Additional digital thermocouples were used to monitor room air temperature, NOx sampling line temperature and air filter intake temperture. A sling psychrometer was used to determine combustion air humidity. The engine coolant temperature and oil temperature could be individually controlled with a pair of thermostats that regulate the flow of laboratory water through heat exchangers that provide cooling for the engine fluids.

Exhaust smoke opacity was measured with a USPHS Diesel Smokemeter permanently mounted in the exhaust pipe 75 mm downstream from the exhaust port. The smoke meter was calibrated against a set of neutral density gelatin filters. Oxides of nitrogen were measured with a Thermo Environmental Instruments Model 10AR chemiluminescent NO-NOx analyzer in conjunction with a Model 800 heated sample conditioning unit and a heated sampling line. The NOx system was calibrated periodically against 2000 ppm NO in nitrogen calibration gas.

Intake air flow was measured with a Meriam Model 50MC2-2F Laminar Flow Element equipped with a digital manometer to read the pressure differential, and an inclined water manometer for calibration purposes. Fuel mass flow rate was monitored with an AVL Model 730 gravimetric fuel balance.

4

The cylinder pressure, fuel pressure, needle lift and crank angle were recorded with a Data Precision DATA 6000 digital wave form analyzer at a data rate of 25 KHz. The data was stored on diskettes for subsequent computer analysis. Table 2 gives the test matrix of load, speed and injection timings used for the experiments.

Ignition delay and injection duration were determined from the digital wave form data. The 25 KHz data rate translates to 40 microseconds per data point, which then represents the uncertainty for both the ignition delay and the injection duration.
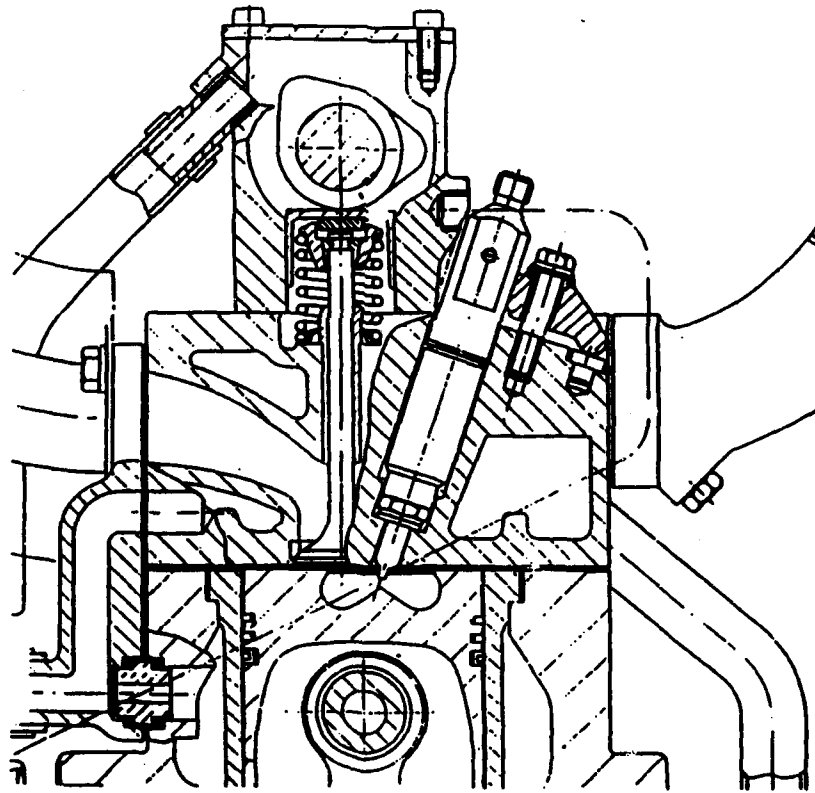
Figure 2.1

Cross Section of Ricardo Hydra DI Diesel Combustion Chamber

TABLE 1 - SPECIFICATIONS OF RICARDO HYDRA DI DIESEL ENGINE

Engine

Number of Cylinder	1
Bore	80.26 mm
Stroke	88.90 mm
Swept Volume	450 ml
Maximum Speed	75 rev/s
Maximum Power	8 KW
Maximum Cylinder Pressure	120 bar
Compression Ratio	20 : 1
Connecting Rod Length	15.80
Squish Height	0.82542 mm
Swirl	3.57
Valve Timing:	Intake Opens	10 BTDC
	Intake Closes	42 ATDC
	Exhaust Opens	58 BBDC
	Exhaust Closes	10 ATDC

Injection System

Injector Pump	Micro Bosch size A type EA 4000 L900
Nozzle	4 holes * 0.21 mm dia. * 155
Nozzle Opening Pressure	250 bar = 25 Mpa
Injector	KBEL 88 PV 1187
Lift Pump	Micro Bosch 9440 030 003

Dynamometer

Manufacturer	McClure
Type	Shunt wound dc with separate excitation
Rating	30 KW continuous
Max. Speed	100 rps
Control	KTK type 6P4Q3D converter for motoring and regenerative loading

6

2.2 CERAMIC COATINGS

The piston, cylinder head, valves and cylinder liner were sent to Adiabatics, Inc. in Columbus, IN for coating. The piston crown and bowl received a 0.25 mm slurry-sprayed coating of partially stabilized zirconia (PSZ) consisting of 85 percent partially calcium stabilized cubic zirconia, 10 percent tungsten cobalt chrome powder, and 5 percent chrome oxide. The head and valves were coated with a 0.5 mm thermal barrier coating incorporating 5 percent hollow alumina spheres in a slurry of 65 percent silica, 15 percent PSZ, 7 percent tungsten chrome powder, and 8 percent chrome oxide.

The cylinder liner was bored 0.2 mm over the entire length plus an additional 0.75 mm in the region above the top ring reversal (TRR). The region above the TRR was plazma sprayed with ytria stabilized zirconia, and then the entire length of the liner was given a 0.2 mm wear coat of slurry sprayed PSZ. The coatings were sealed and densified with a chrome oxide based drain cast slurry.

2.3 TEST MATRIX

A full set of data runs were conducted with each of the two fuels, hexadecane and dodecane, and for each of four different engine builds utilizing different combinations of coated components including: (1) baseline (no coatings), (2) coated piston alone, (3) coated head alone, and (4) coated piston, head and liner together. A full set of runs consisted of the test matrix shown in Table 2 involving four engine speeds, four loads and four injection timings, for a total of 64 runs per engine build, per fuel (512 total runs). After initially investigating the effect of engine coolant temperature on NOx production and observing the expected increase in NOx with increasing temperature, as shown in Figure 2, it was decided to use a constant coolant temperature of 353 K and constant oil temperature of 323 K. A sample data set for hexadecane for one engine speed is shown in Table 3.

TABLE 2 - TEST MATRIX				
INJECTION TIMING (DEG BTDC)	16	18	20	22
BMEP (BAR)	2.24	3.35	3.91	4.47
Speed (RPM)	1000	1500	2000	2500

TABLE 3 EXPERIMENTAL DATA

FUEL: HEXADECANE **FUEL DENSITY: 0.773 gm/cm³** **1500 RPM**

TEST DATA	RUN NUMBER							
	1	2	3	4	5	6	7	8
LOAD N-m	8	8	8	8	12	12	12	12
INJ. TIMING DEG-BTDC	16	18	20	22	16	18	20	22
INTAKE AIR TEMP. K	310	311	312	312	312	312	312	312
WATER TEMP. K	353	353	353	353	353	353	353	353
EXHAUST TEMP K	499	505	515	519	545	551	560	565
SMOKE LEVEL (Amp.)	48	47	47	46	45	45	43	42
SOOT AT STP (g/m³)	.234	.234	.300	.335	.367	.499	.565	.635
SOOT AT EXHAUST (g/m³)	.141	.138	.176	.372	.202	.270	.304	.372
NO$_x$ (PPM)	1300	1550	1750	1900	1900	2150	2300	25.
NO (PPM)	1125	1250	1450	1600	1650	1850	2000	2150
FUEL INJ. g/min	8.2	8	8.3	8.6	10	10.2	10.5	10.9
IGNIT. DELAY (msec)	0.68	0.72	0.8	0.84	0.56	0.64	0.72	0.76
INJ. DURATION (msec)	0.96	1.0	1.04	1.08	1.08	1.12	1.2	1.2
INJ. DURATION (DEG)	8.64	9.0	9.36	9.72	9.72	10.1	10.8	10.8
FUELLING RATE *10⁻⁵ (g/inj)	1092	1066	1106	1146	1332	1359	1399	1452
IGN. DELAY DEG	6.12	6.48	7.2	7.56	5.04	5.76	6.48	6.84
BMEP (bar)	2.24	2.24	2.24	2.24	3.35	3.35	3.35	3.35
POWER OUTPUT W	1257	1257	1257	1257	1885	1885	1885	1885
BSFC g/kwh	391.5	382.0	396.3	410.6	318.3	324.7	334.2	347.0
AIR FLOW RATE (kg/h)	21.25	21.25	21.25	21.25	21.25	21.25	21.25	21.25
AIR FUEL RATIO	42.65	44.28	42.68	41.19	35.42	34.73	33.73	32.50
VOL. EFFICIENCY %	91.38	91.38	91.38	91.38	91.38	91.38	91.38	91.38
ROOM TEMP, F	72	72	72	72	72	72	72	72

TABLE 3 CONTINUED							
FUEL: HEXADECANE		**FUEL DENSITY: 0.773 gm/cm³**					**1500 RPM**

TEST DATA	RUN NUMBER							
	9	10	11	12	13	14	15	16
LOAD N-m	14	14	14	14	16	16	16	16
INJ. TIMING DEG-BTDC	16	18	20	22	16	18	20	22
INTAKE AIR TEMP. K	312	312	312	312	312	312	312	312
WATER TEMP. K	353	353	353	353	353	353	353	353
EXHAUST TEMP K	570	573	583	589	597	602	612	620
SMOKE LEVEL (Amp.)	40	40	39	38	39	37	36	34
SOOT AT STP (g/m³)	.698	.764	.831	.935	.897	.963	1.10	1.35
SOOT AT EXHAUST (g/m³)	.370	.398	.428	.496	.452	.478	.536	.716
NO$_x$ (PPM)	2050	2300	2600	2700	2000	2150	2400	2500
NO (PPM)	1800	2000	2250	2400	1750	2000	2150	2300
FUEL INJ. g/min	10.8	11.0	11.4	11.8	12.0	12.0	12.4	12.9
IGNIT. DELAY (msec)	0.64	0.68	0.76	0.80	0.60	0.68	0.72	0.76
INJ. DURATION (msec)	1.24	1.28	1.32	1.36	1.36	1.40	1.48	1.52
INJ. DURATION (DEG)	11.2	11.5	11.9	12.2	12.3	12.6	13.3	13.7
FUELLING RATE *10⁻⁵ (g/inj)	1439	1465	1519	1572	1598	1598	1652	1718
IGN. DELAY DEG	5.76	6.12	6.84	7.20	5.40	6.12	6.48	6.84
BMEP (bar)	3.91	3.91	3.91	3.91	4.47	4.47	4.47	4.47
POWER OUTPUT (W)	2199	2199	2199	2199	2513	2513	2513	2513
BSFC g/kwh	294.7	300.1	311.0	321.9	286.5	286.5	296.0	308.0
AIR FLOW RATE (kg/h)	21.25	21.25	21.25	21.25	21.25	21.25	21.25	21.25
AIR FUEL RATIO	32.80	32.20	31.07	30.02	29.52	29.52	28.56	27.46
VOL. EFFICIENCY %	91.38	91.38	91.38	91.38	91.38	91.38	91.38	91.38
ROOM TEMP, F	72	72	72	72	72	72	72	72

3. EXPERIMENTAL RESULTS

3.1 PRESENTATION OF DATA

Plots of data for all cases investigated are provided in the appendices. This includes data for fuel consumption (Appendix A), NOx (Appendix B), soot (Appendix C), ignition delay (Appendix D) and exhaust gas temperature (Appendix E). All of the data was included in the appendices in order to have it organized and available for scrutiny by interested parties. A page typically contains four plots, representing four different engine speeds, of the above variables versus load or timing for a common value of the remaining independent variable. Figures for hexadecane fuel precede those for dodecane fuel in each appendix. The following provides a discussion of general trends observed. For convenience, certain example data plots from the appendices are reproduced in the following sections to illustrate these trends. Thus one can rely simply on the examples used here for illustration, or refer to the appendices for additional in-depth evaluation of all cases.

3.2 EFFECT OF COATINGS ON CYLINDER PRESSURE

The effect of coating various combustion chamber surfaces on the cylinder pressure is illustrated in Figure 3.1. The four plots in this figure are for different injection timings. All of the data is for hexadecane fuel, with an engine speed of 1500 RPM and a load of 447 KPa BMEP (the maximum load used for these tests). In all cases, the baseline engine produces the highest cylinder pressure followed in descending order by the coated head, all surfaces coated, and coated piston cases. Some decrease in maximum cylinder pressure can be attributed to decreased volumetric efficiency that occurs with the coated surfaces (all tests were performed under normally aspirated conditions), but changes in the combustion process caused by the surface coatings accounts for most of the decrease as discussed in detail in Chapter 4. This is evident since operating the engine with all of the surfaces coated results in the lowest volumetric efficiency, while coating only the piston crown consistently produces the lowest pressure. Coating only the piston effects the combustion process to the greatest degree of all the insulation schemes and produces the lowest fuel consumption and NOx emission as described in the following sections.

10
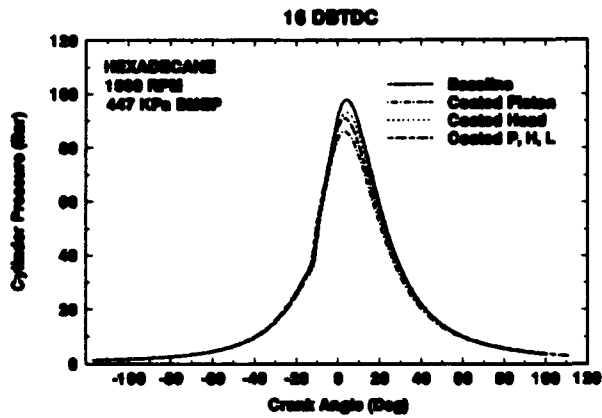
Fig 3.12(a)
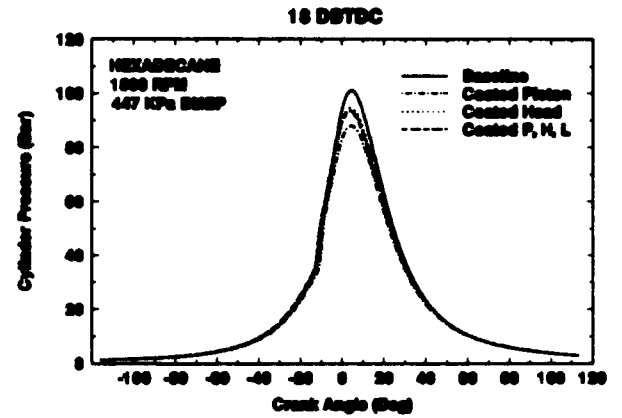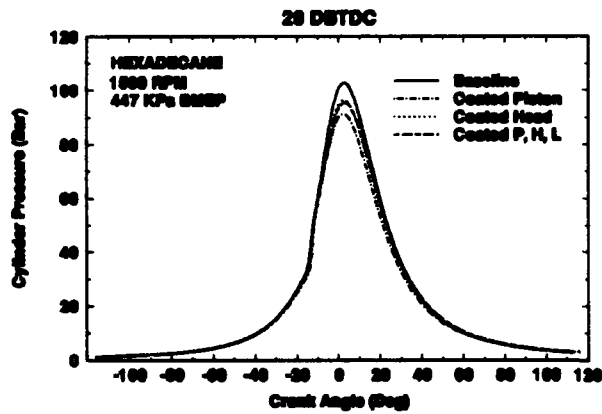
Fig 3.1(b)

. Fig 3.1(c)
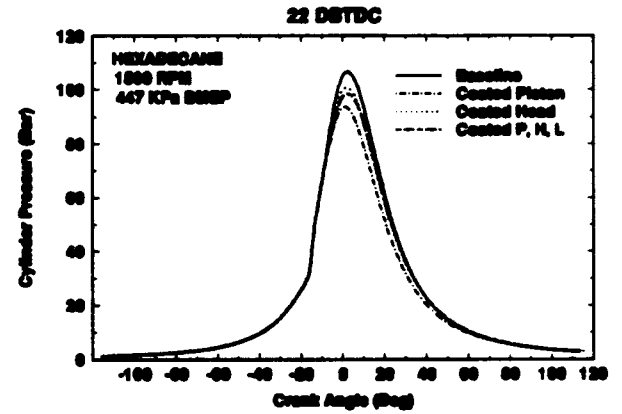
Fig 3.1(d)

Figure 3.1

Cylinder Pressure With Hexadecane Fuel at 1500 RPM and High Load

3.3 EFFECT OF COATINGS ON BSFC

Figure 3.2 compares the brake specific fuel consumption (BSFC) for the four different engine builds as a function of load (BMEP) for an injection timing of 20 DBTDC for hexadecane fuel. Figure 3.3 makes the same comparison for dodecane fuel. Each graph in these figures represents a different engine speed. The injection timing value of 20 DBTDC was chosen arbitrarily for purposes of these comparisons. The same trends are present for the other injection timings tested. The full set of BSFC data is included in Appendix A. The effect of varying the injection timing is to increase BSFC with advancing timing as indicated in Figure 3.4. The general trend exhibited in Figures 3.2 and 3.3 is that specific fuel consumption for the coated-piston case is better than baseline for a number of operating conditions, particularly under low load and at high rpm. The coated-head case produces lower fuel consumption for a few combinations of operating conditions and higher than baseline for others. When all of the surfaces are coated (piston, head and liner), fuel consumption is always worse than baseline, probably due to the reduced volumetric efficiency.

What appear to be anomalous readings in several instances, e.g. the low fuel consumption for the coated piston case at 1000 RPM and a load of 335 KPa and the high consumption for the coated head case at 1000 RPM and 391 KPa, one might at first glance attribute to experimental scatter. However, a review of the entire set of BSFC data in Appendix A show these apparent anomalies to be remarkably consistent at the same engine speed throughout the injection timing range and for both fuels. The strong consistency of trends in the fuel consumption data adds confidence to the validity of the measurements. Uncertainty in the fuel consumption data is estimated to be ±10 gr/kwh indicated by the uncertainty bracket shown in Figure 3.2(a). Apparently, certain combinations of operating conditions (speed, timing and load) can work together to produce either unusually low or unusually high fuel consumption. The lowest overall fuel consumption for hexadecane (270 gr/kwh) and dodecane (260 gr/kwh) is produced by the baseline engine at 2000 rpm, 16 DBTDC and a load of 391 KPa.
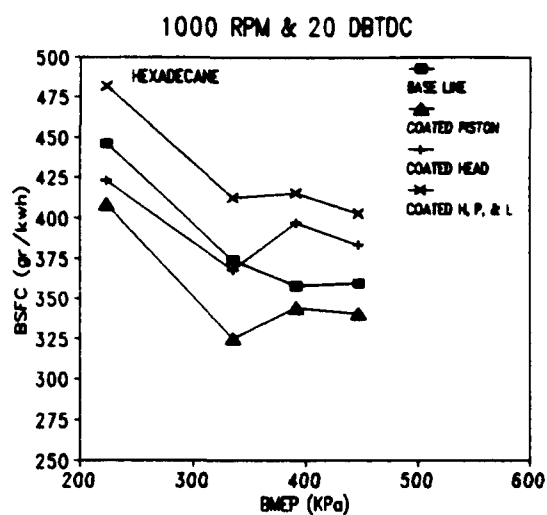
Fig 3.2(a)
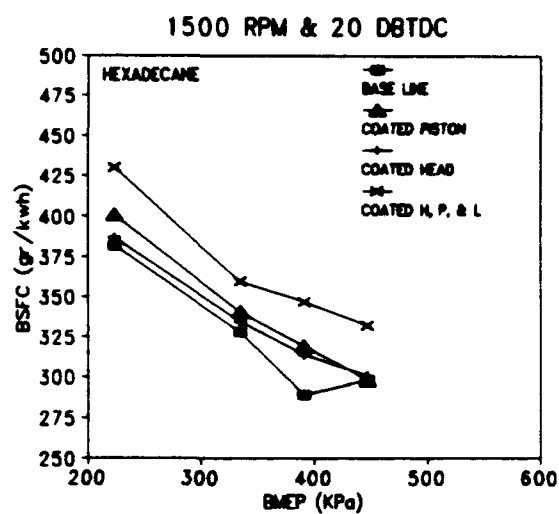
Fig 3.2(b)
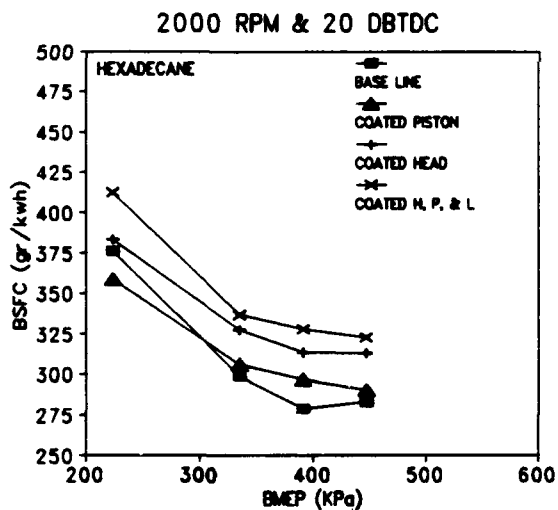
Fig 3.2(c)
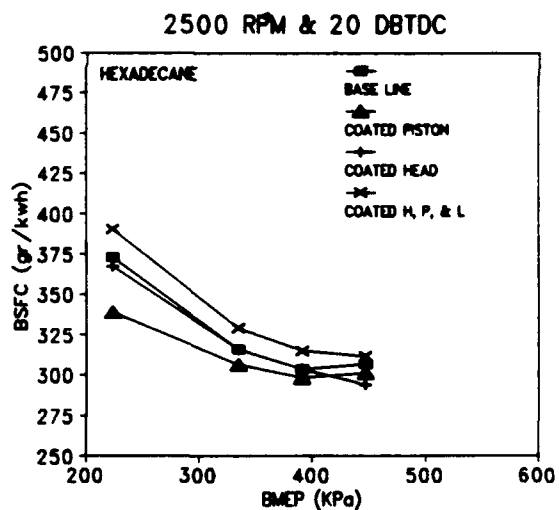
Fig 3.2(d)

Figure 3.2

BSFC Versus Load for Hexadecane Fuel at 20 Degrees BTDC

13

1000 RPM & 20 DBTDC

Fig 3.3(a)

1500 RPM & 20 DBTDC

Fig 3.3(b)

2000 RPM & 20 DBTDC
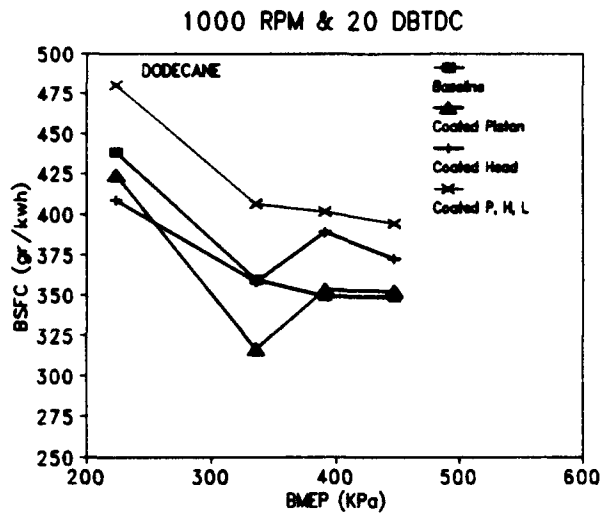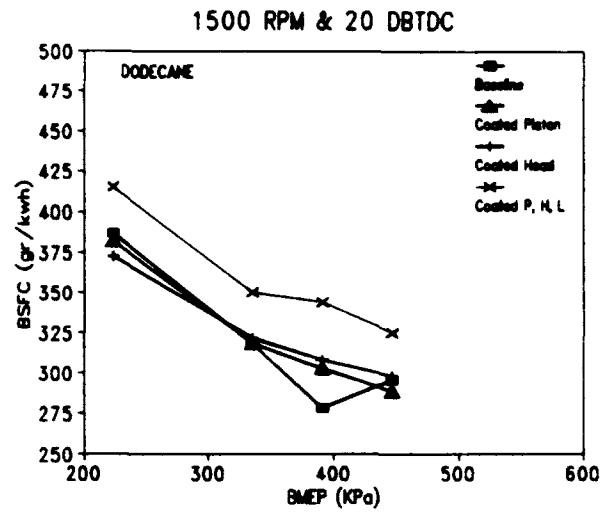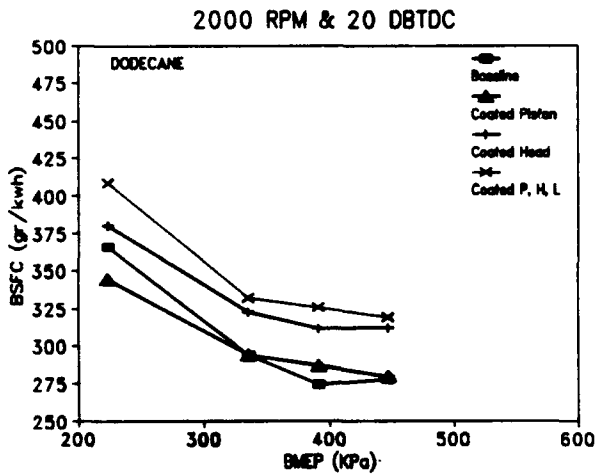
Fig 3.3(c)

2500 RPM & 20 DBTDC
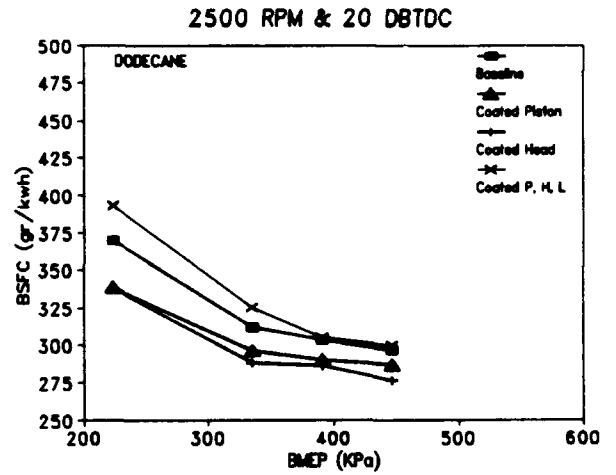
Fig 3.3(d)

Figure 3.3

BSFC Versus Load for Dodecane Fuel at 20 Degrees BTDC
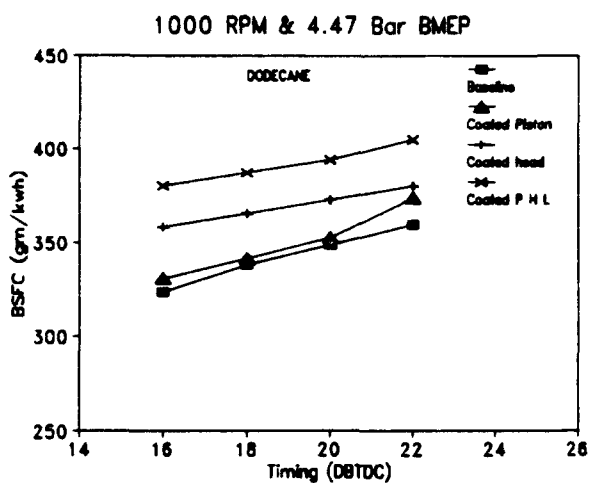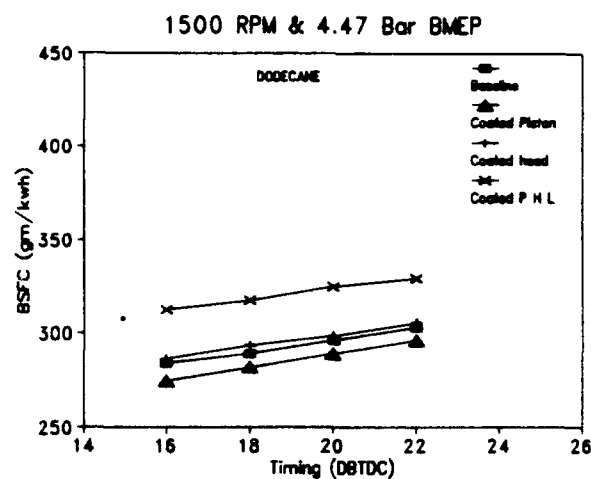
Fig 3.4(a)   Fig 3.4(b)
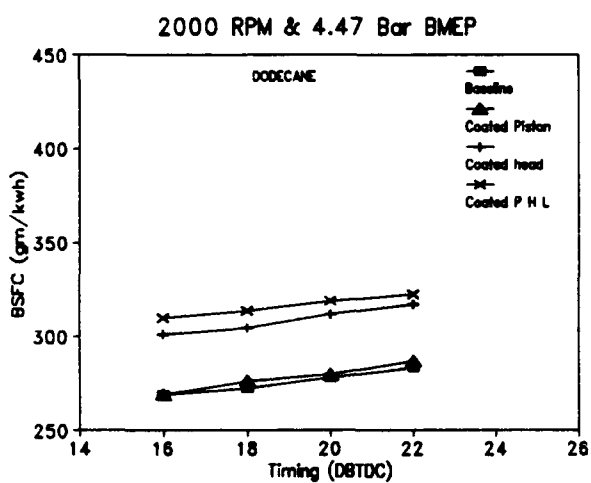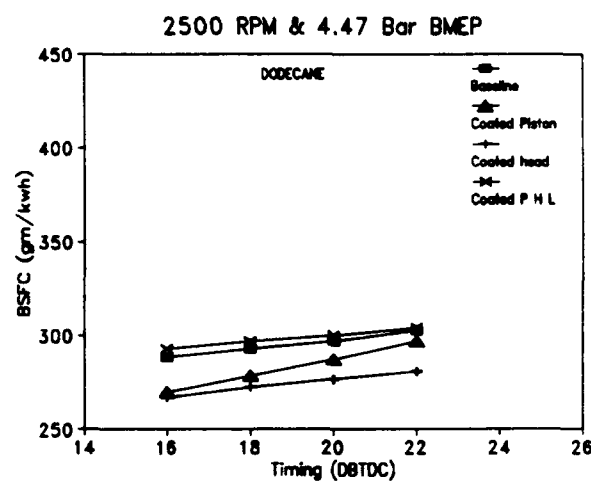
Fig 3.4(c)   Fig 3.4(d)

Figure 3.4

BSFC Versus Timing for Dodecane Fuel at High Load

3.4 EFFECT OF COATINGS ON NOx

Figures 3.5 and 3.6 compare the NOx emission in PPM for each of the four engine builds as a function of load for hexadecane and dodecane, respectively. Again, there are separate plots for each engine speed, and the example data shown is for a timing of 20 DBTDC. Complete data plots for all runs are provided in Appendix B. Uncertainty in the NOx data is estimated at ±50 PPM, approximately represented by the size of the data symbols in the figures.

Ceramic coating the piston crown has a very favorable effect on the NOx emission of this engine. The decrease in NOx for hexadecane at 20 DBTDC timing ranges from zero percent at high speed and low load to 25 percent at low speed and high load. The decrease under high load conditions ranges from 20 to 34 percent depending on injection timing, regardless of engine speed. Possible reasons for the decreased NOx production are related to the effect that the hotter piston surface has on the combustion process as discussed in the next chapter in conjunction with the KIVA modeling results. Lowered NOx emission coupled with improved fuel economy would appear to make coating of the piston crown a desirable engine modification.

Coating of the cylinder head by itself, on the other hand, does not significantly reduce NOx emission and under some operating conditions causes an increase. This is especially true with dodecane fuel, where coating the head causes increased NOx under most conditions. The unimproved or degraded NOx emission, coupled with similarly unimproved or degraded fuel consumption, provide little incentive to ceramic coat the cylinder head.

Operating the engine with coatings on all combustion chamber surfaces, i.e. piston, head and cylinder liner, produces NOx emission values that fall between those for the piston alone and for the head alon^Xx One might expect this result based on the reasoning that the beneficial effects of coating the piston are offset somewhat by the often adverse effects of coating the head. In addition, the insulating effect of coating all three surfaces results in slightly higher cylinder gas temperatures throughout the combustion cycle which will tend to increase NOx as shown by the KIVA modeling results discussed in Chapter 4. Figure 3.7 shows the effect of varying injection timing on NOx emission at high load and four engine speeds for dodecane fuel. The trend is for increasing NOx with advancing injection timing as would be expected due to the increased ignition delay and premixed combustion fraction resulting in higher peak cylinder pressure and temperature.
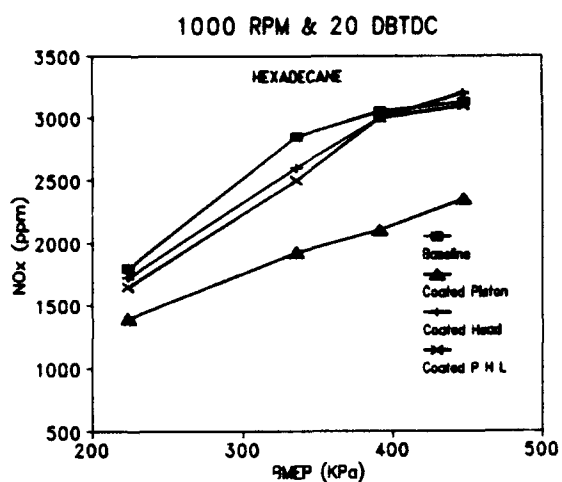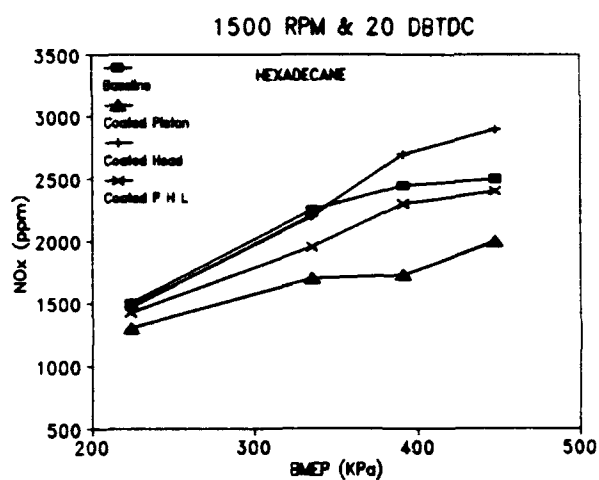
Fig 3.5(a)   Fig 3.5(b)
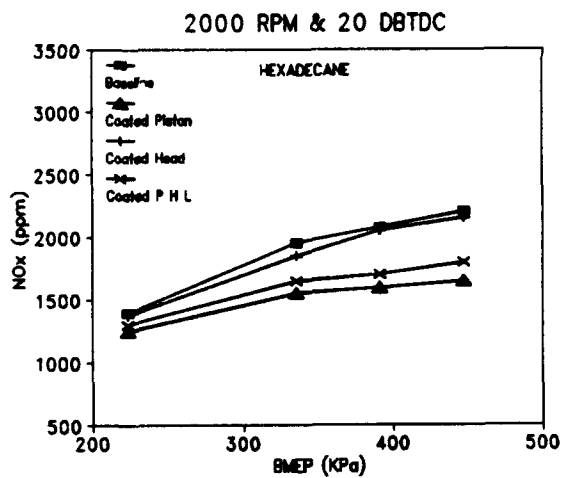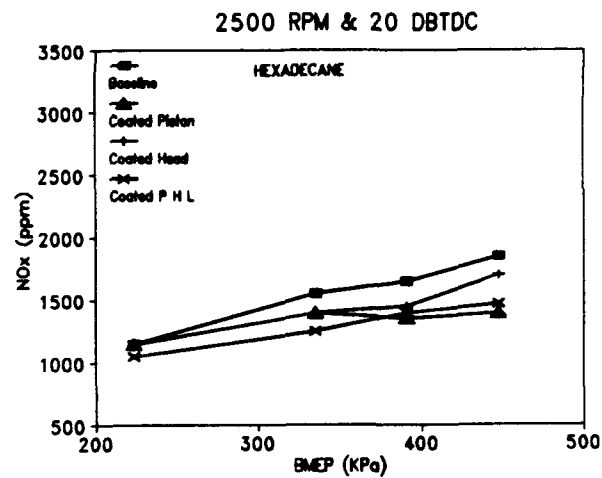
Fig 3.5(c)   Fig 3.5(d)

Figure 3.5

NOx Versus Load for Hexadecane Fuel at 20 Degrees BTDC
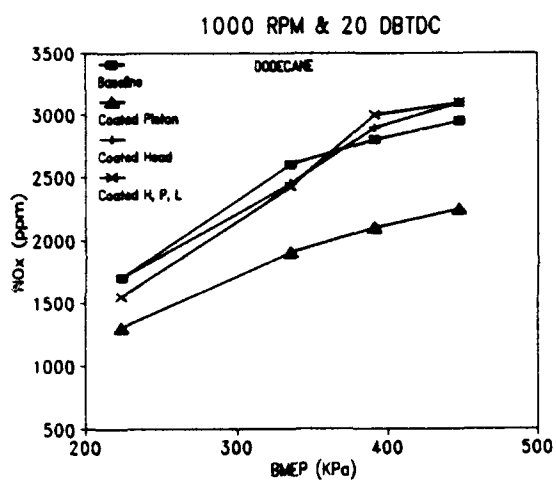
Fig 3.6(a)
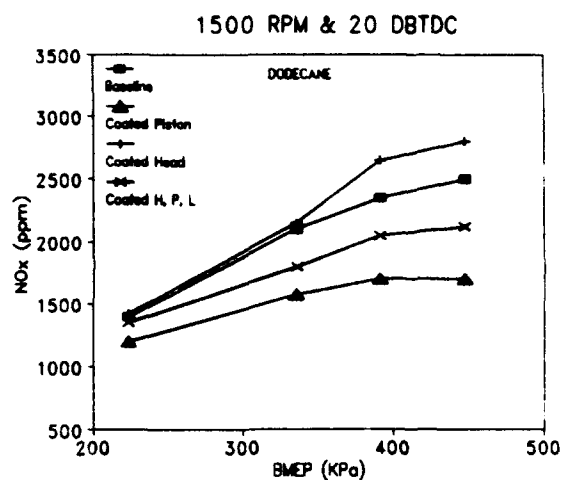
Fig 3.6(b)
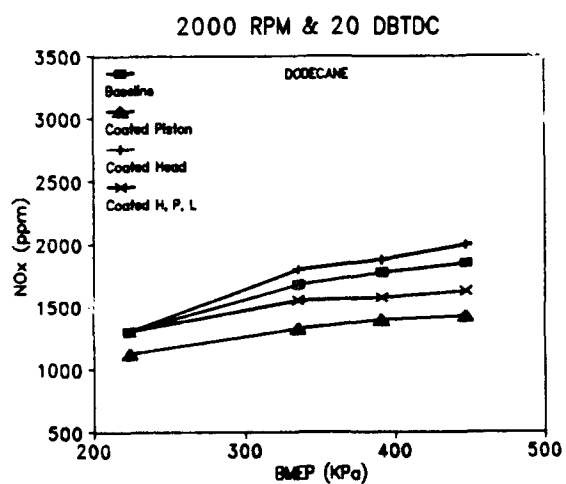
Fig 3.6(c)
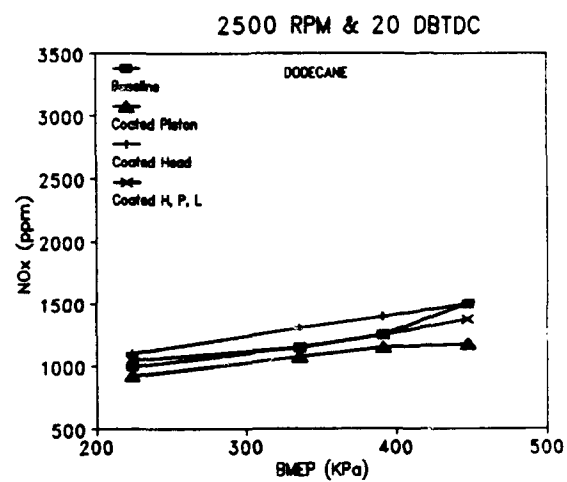
Fig 3.6(d)

Figure 3.6

NOx Versus Load for Dodecane Fuel at 20 Degrees BTDC

18
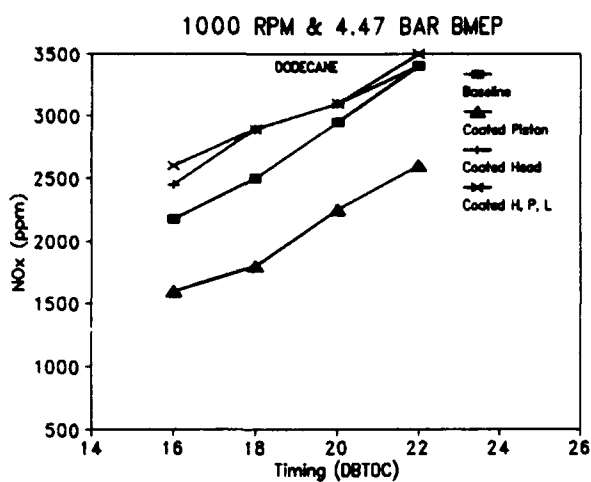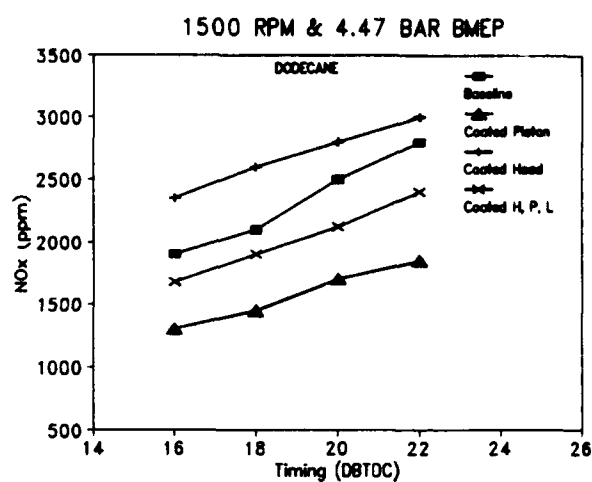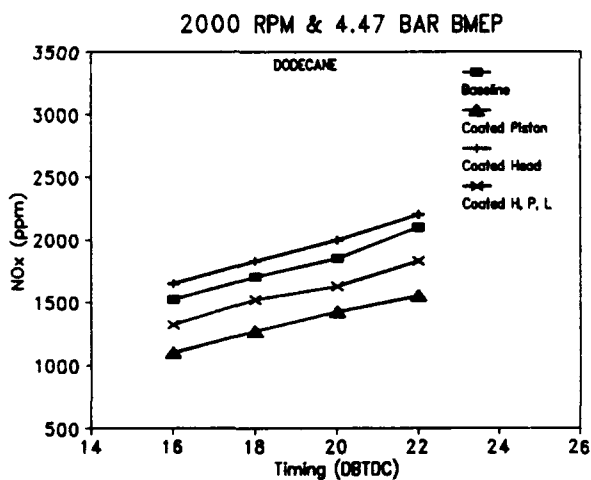
Fig 3.7(a)

Fig 3.7(b)

Fig 3.7(c)
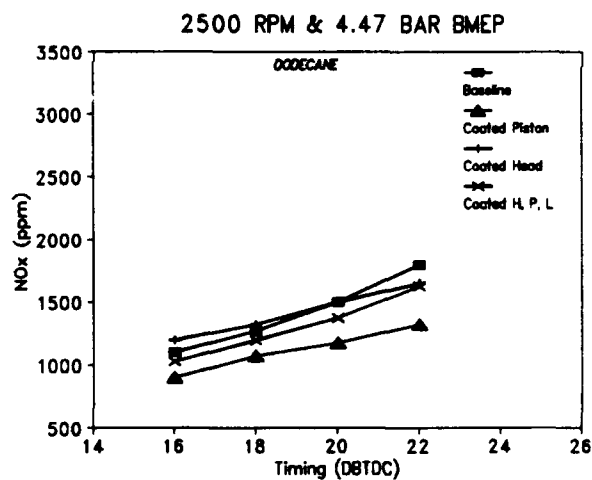
Fig 3.7(d)

Figure 3.7

NOx Versus Injection Timing for Dodecane Fuel at High Load

19

3.5 EFFECT OF COATINGS ON IGNITION DELAY PERIOD

Figures 3.8 and 3.9 show examples of ignition delay versus injection timing at light load for hexadecane and dodecane fuel respectively. Data for all cases is provided in Appendix C. Ignition delay was measured with the digital waveform analyzer used to collect the data by placing the cursor at the point on the needle lift trace where the needle opens and then advancing to the point on the pressure trace where rapid pressure rise begins. At the maximum 25 KHz data rate of the instrument, the time between data points is 0.04 ms, and this is assumed to represent the uncertainty in the ignition delay measurements. The uncertainty of ±0.04 ms is indicated by the brackets in the figures.

The ignition delay values for both fuels lie between 0.4 and 1.1 ms depending mainly on speed and injection timing, and to a lesser extent on load. These values are typical for high cetane fuels.

At low speeds the coated piston appears to decrease the ignition delay relative to the baseline engine as predicted by the KIVA results discussed in the next chapter. The shortened ignition delay is the reason proposed in Chapter 4, based on computer modeling, for reduced cylinder gas temperature and pressure and, consequently, reduced NOx relative to the baseline. In many cases the values of ignition delay for the coated-piston case and the baseline case are within the limits of uncertainty and are therefore inconclusive. In a few cases, the measured ignition delay for the coated-piston case is clearly longer than that for the baseline case, e.g. for hexadecane at 2500 RPM and 335 KPa BMEP (Figure C2(d), Appendix C). For this same case, the NOx emission of the coated-piston engine is slightly less than the baseline engine, in contradiction to our theory for decreased NOx. The conclusion that can be drawn from this is that ignition delay is not the only controlling parameter in the NOx reaction and additional combustion phenomena, of which we do not have a complete understanding at this time, are affected by the ceramic coatings. The lack of in-cylinder gas temperature measurements hinders our ability to completely understand the effect of coatings on the total combustion process.

For the cases of coated head alone and all surfaces coated, no unequivocal statements can be made concerning the effect on ignition delay. For hexadecane fuel, coating the head produces the longest ignition delay values under low load conditions, while coating all the surfaces produces the longest values under high load conditions. For dodecane fuel, coating all surfaces generally produces the longest ignition delays regardless of load.
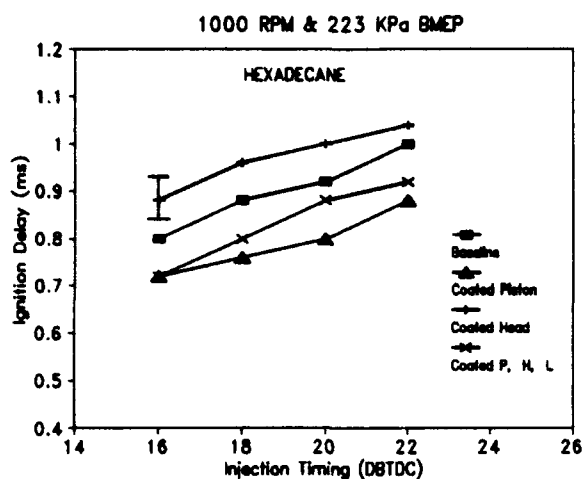
Fig 3.8(a)
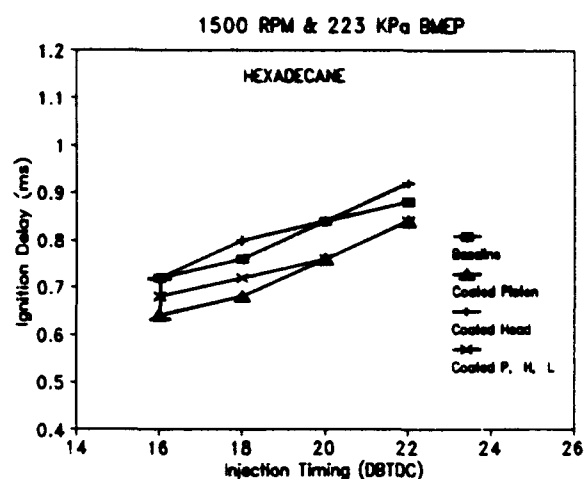
Fig 3.8(b)
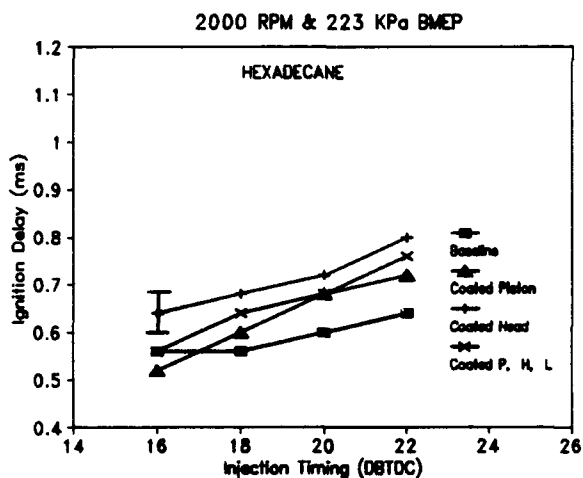
Fig 3.8(c)
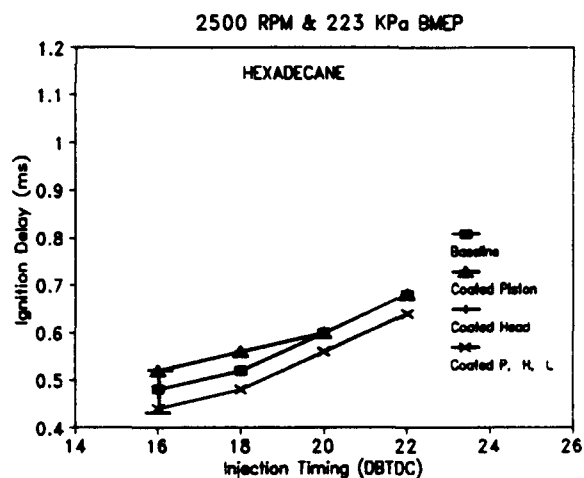
Fig 3.8(d)

Figure 3.8

Ignition Delay Versus Timing for Hexadecane Fuel at 223 KPa BMEP
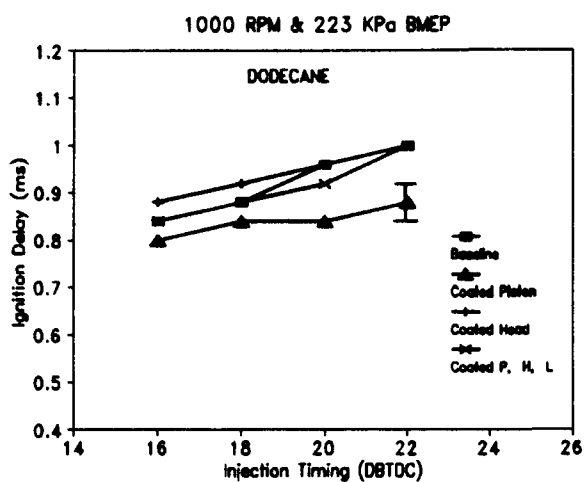
Fig 3.9(a)
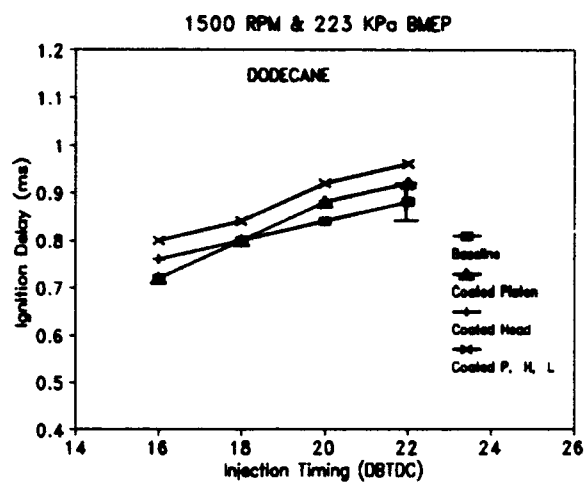
Fig 3.9(b)
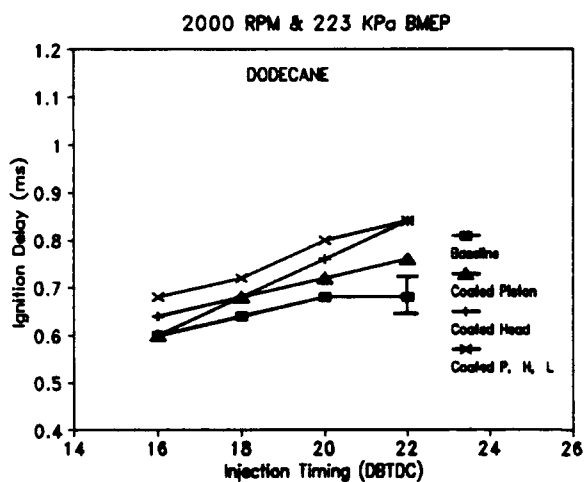
Fig 3.9(c)
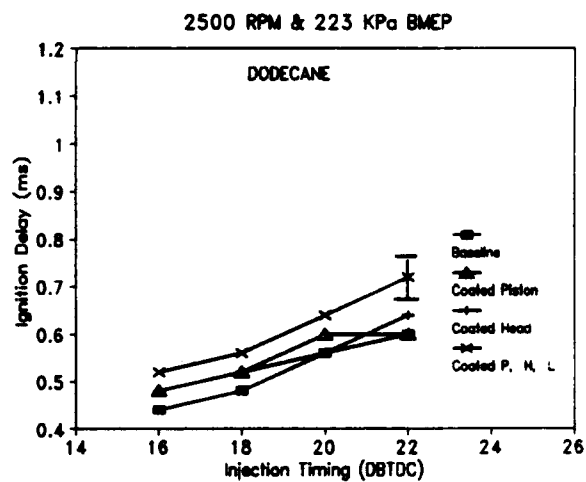
Fig 3.9(d)

Figure 3.9

Ignition Delay Versus Timing for Dodecane Fuel at 223 KPa BMEP

3.6 EFFECT OF COATINGS ON SOOT EMISSION

Soot concentration values in gr/m^3 were calculated from the photocell output of the USPHS smoke opacity meter by calibrating the meter output with a set of neutral density filters and using the concentration versus opacity data from Reference 11. The measurement uncertainty for the soot concentration values is unknown, but the data is useful for observing relative effects of the different coating schemes on soot production.

Figure 3.10 is representative of most of the soot data. It provides soot concentration versus load for hexadecane fuel at 22 DBTDC injection timing for four engine speeds. Most of the trends displayed in this figure hold true for the rest of the soot data which are presented in Appendix D. Coating all of the combustion chamber surfaces has a deleterious effect on soot emission, particularly at lower speeds and higher loads. The effect on soot emission of coating the piston alone depends on engine speed. Coating the piston results in higher soot production than baseline for some engine speeds and lower at others. Likewise, the effect of coating the head alone depends on engine speed. At 1500 RPM the coated head produces relatively low soot emissions, while at 2500 RPM it produces relatively high amounts of soot.

Possible explanations of these results based on computer simulations are not available at this time. The soot modeling described in the following chapter has so far been applied only to the baseline engine. While the results for the baseline case are encouraging, the soot model has not yet been implemented in conjunction with the coated surface temperature model in order to predict the effects of various surface coatings on soot emission. This work is continuing and will be published in technical paper form when completed.
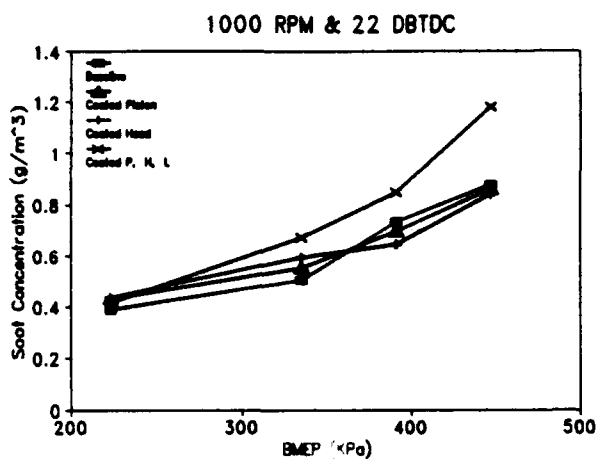
Fig 3.10(a)
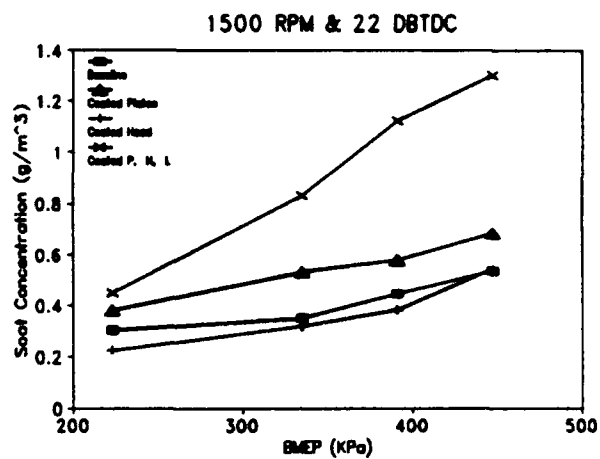
Fig 3.10(b)
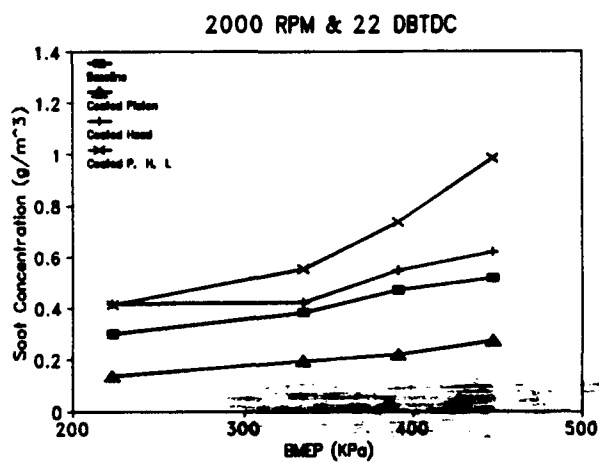
Fig 3.10(c)
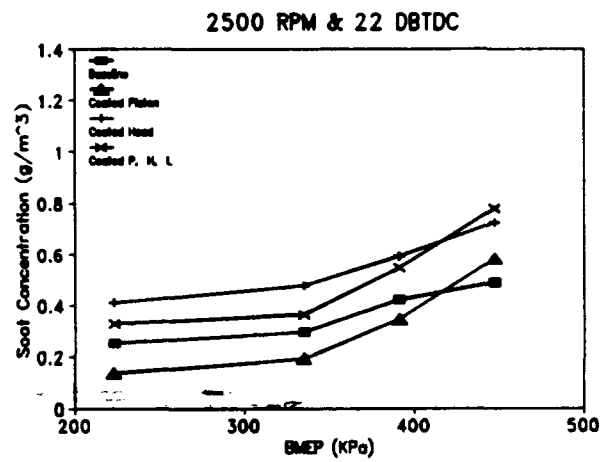
Fig 3.10(d)

Figure 3.10

Soot Concentration Versus Load for Hexadecane at 22 DBTDC

3.7 EFFECT OF COATINGS ON EXHAUST GAS TEMPERATURE

Typical exhaust gas temperature data are shown in Figure 3.11 which shows exhaust temperature versus load for hexadecane at 20 DBTDC injection timing. The same trends are exhibited by the rest of the exhaust temperature data provided in Appendix E. From these figures several interesting phenomena can be noted. Coating the head by itself has little effect on the exhaust temperature relative to baseline except at low speed where it actually reduces exhaust temperature. This trend is predicted by the KIVA results (e.g. see Figure 4.27). A study by Morel, et al. [12] indicated that for a non-insulated diesel engine, 49 percent of the heat loss from the hot cylinder gas occurs through the piston, 32 percent occurs through the head and the remaining 19 percent occurs through the liner. Thus, insulating the head should have less impact on the total heat transfer and the exhaust gas temperature. Peak cylinder gas temperatures are less than baseline due to the effect of the higher surface temperature on the combustion process, as discussed in Chapter 4.

The exhaust temperature for the coated-piston case is typically higher than baseline due to the reduced heat transfer through the piston to the oil. Since approximately half of the heat transfer takes place through the piston, adding a low conductivity coating to the piston crown should significantly reduce heat transfer and increase exhaust temperature.

Coating all of the surfaces produces the highest exhaust temperatures as would be expected due to the larger reduction in heat loss during the expansion stroke when all surfaces are insulated.
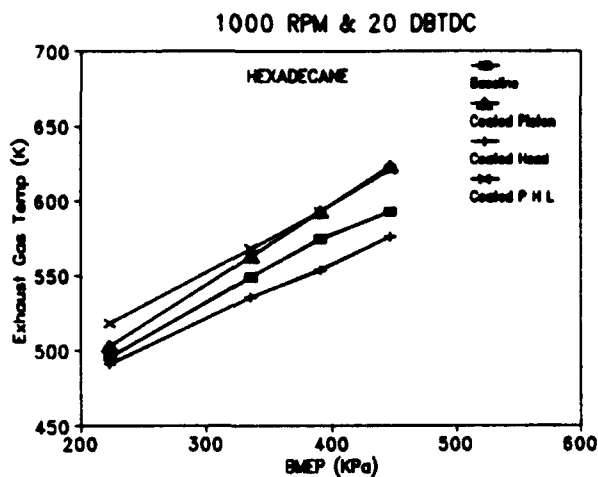
Fig 3.11(a)
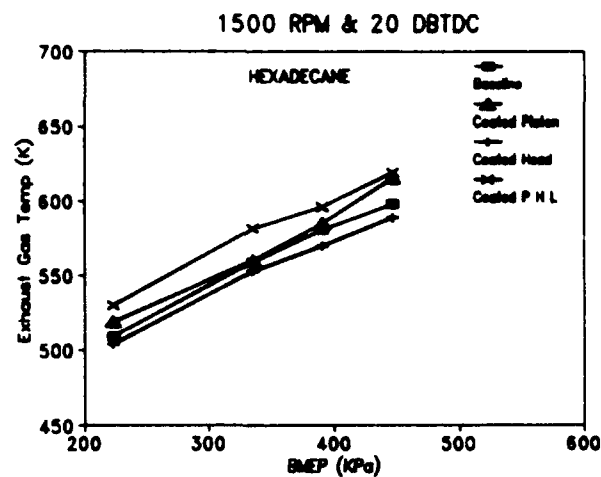
Fig 3.11(b)
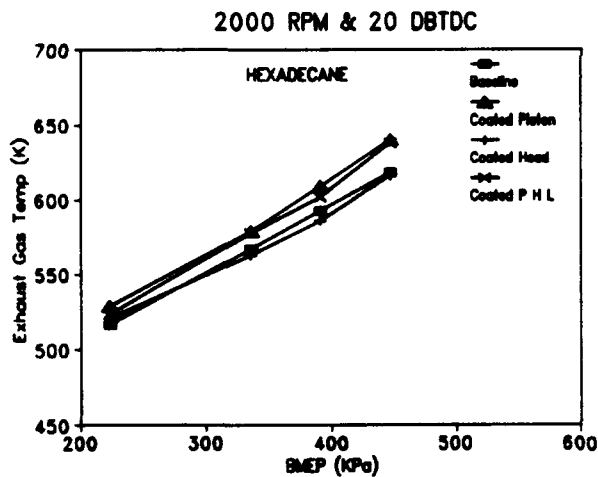
Fig 3.11(c)
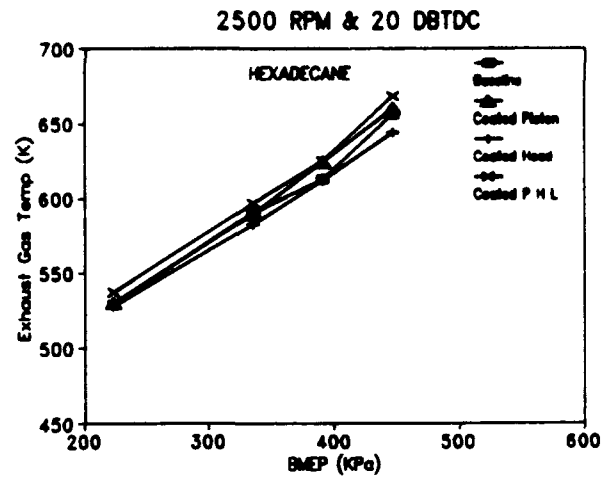
Fig 3.11(d)

Figure 3.11

Exhaust Gas Temperature Versus Load for Hexadecane at 20 DBTDC

4. COMPUTER MODELING

4.1 BACKGROUND

The KIVA-II code, developed at Los Alamos National Laboratory [13], solves either the 2-D or the 3-D unsteady equations of motion of a chemically reactive mixture of ideal gases including the dynamics of a liquid fuel spray and the coupling between the spray and the gas. The code was developed with application to internal combustion engines specifically in mind, and contains a number of features to facilitate this application, such as gas flow, liquid fuel injection, spray dynamics, evaporation, heat transfer, combustion, species transport, and mixing.

KIVA-II was chosen for this work because of the documentation that is available [13,14,15] and the fact that it is being widely used by other researchers in industry, academia and national laboratories to model combustion and emissions in both spark ignition and diesel engines, e.g. Amsden et al.[16], O'Rourk and Amsden [17], Gentry et al. [18], Naber and Reitz [19], Kuo and Reitz [20], Reitz and Diwaker [21], Pinchon [22], Zellat [23], Gibson et al. [24], Varnavas and Assanis [25]. In addition, Ramos [26], and Markatos [27] documented KIVA in their recent books.

The original KIVA-II code employs the Arrhenius single reaction combustion model (SR model). This model is suitable for premixed combustion systems such as spark ignition engines. However, in diesel engines the combustion process is mainly diffusional after a short premixed period. The mixing-controlled eddy-break-up model (EBU model) developed by Magnussen et al. [28-31] provides a better physical representation of the diffusional combustion process.

In this study, KIVA-II was modified to include the EBU combustion model, and results from both models are compared with experiments. New model constants were introduced for the original Arrhenius combustion model. These constants were used for different combinations of load, injection timing and speed and were found to give good agreement between the predicted combustion and experiments for both hexadecane and dodecane fuel.

As part of this work, a soot model was also added to KIVA-II. The model for the rate of soot formation developed by Tesner et al. [32,33] was implemented to calculate the amount of soot formation, and the model of soot combustion developed by Magnussen

27

and Hjertager [28] concerning the behavior of soot in turbulent flames, was implemented to compute the oxidation rate of soot.

4.2 GENERAL STRUCTURE OF KIVA-II CODE

The gas-phase solution procedure in KIVA-II is based on a finite volume method called the ALE (Arbitrary Lagrangian-Eulerian) method which facilitates calculations with curved and changing boundaries. Spatial differences are formed on a finite-difference mesh that subdivides the computational region into a number of small cells that are hexahedrons. The code features a Stochastic Particle Technique, an efficient and accurate method for solving the spray dynamics, based on the Monte Carlo and discrete particle methods. The transient solution is marched out in a sequence of finite time increments called cycles or timesteps. On each cycle the values of the dependent variables are calculated.

The KIVA-II computer program consists of a set of subroutines controlled by a short main program. It was written specifically for use on the CRI Cray family of computers, operating under the Cray Time Sharing System (CTSS) and using the Cray FORTRAN (CFT and CFT77) compilers.

All computational runs were made on the CRAY Y-MP at the North Carolina Supercomputing Center (NCSC). KIVA-II contains statements peculiar to the CFT and CFT77 compilers that permit vectorization of many of the loops in the subroutines. The vectorization of the code improved the run time by a factor of five. A typical run for the Ricardo Hydra engine simulation, including the soot model, begining at 138 degrees BTDC and ending at 90 degrees ATDC, required about 1200 CPU seconds on the Cray Y-MP.

4.3 COMPUTATIONAL PARAMETERS

For simplicity, a 2-D axisymmetric simulation of the combustion in the Ricardo Hydra direct injection diesel engine was used. Figure 4.1 shows the KIVA-II computational mesh of the Ricardo Hydra combustion chamber at 138° BTDC (point of intake valve closure), and again at TDC. The mesh has 23 cells in the radial direction, 1 cell in the azimuthal direction and 24 cells in the axial direction (nx=23, ny=1, nz=24).
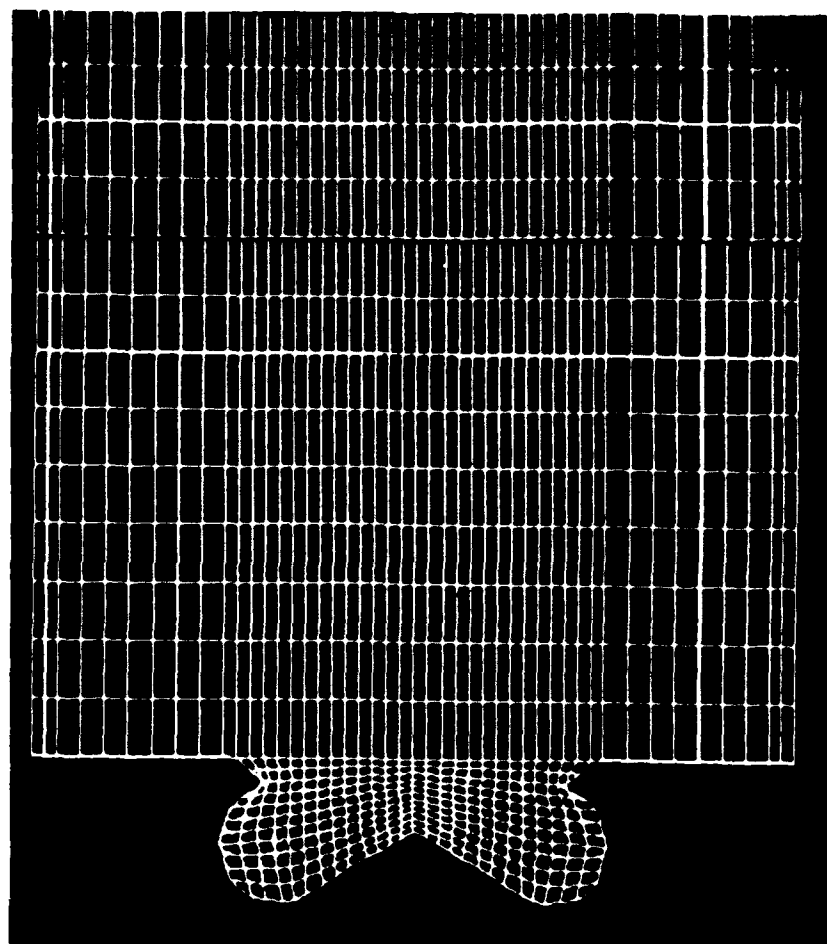
At 138 DBTDC
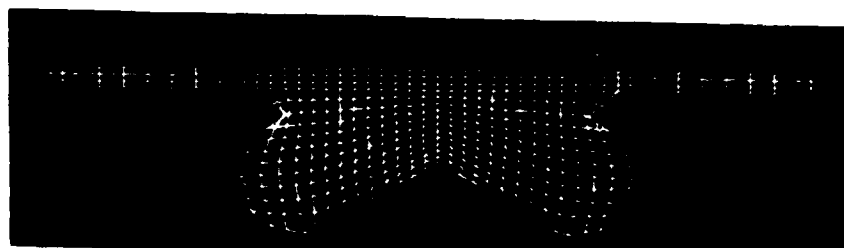
At TDC

Figure 4.1
Computational Mesh Used to Model Ricardo Hydra DI Engine

The calculations were started when the intake valve closed and ended at 90 degrees crank angle ATDC. The initial species was air which was assumed to be 21 percent oxygen and 79 percent nitrogen. The initial densities of the oxygen and nitrogen were assigned so that the initial pressure in the combustion chamber as the intake valve closed was 96 Kpa. The initial air temperature was assumed to be 310 K.

To calculate the dynamics of the spray, the model requires the radii and velocities of the droplets at the injector [15]. The magnitude of the injection velocity, V_{inj}, is determined from

$$V_{inj} = \frac{m_{inj}}{\rho_f \pi r_{inj}^2 t_{inj}}$$ (4.1)

where:

m_{inj} is the injected fuel mass, g/cycle.

ρ_f is the fuel density, g/cm^3

r_{inj} is the injector nozzle radius, cm

t_{inj} is the injection duration, s.

The sauter mean radius was assumed to be 9.5 micron. The model requires the injection angle, injected fuel mass, fuel density, and injection duration. These values were taken from the experimental data.

4.4 COMBUSTION MODELS

4.4.1 Single Reaction Model

The single reaction Arrhenius model is the standard combustion model built into the KIVA-II code. Oxidation of the fuel is assumed to be modeled by a one-step global kinetics scheme. The complete set of chemical reactions is given below.

Two different fuels were used in both the experiments and the modeling, viz hexadecane $(C_{16}H_{34})$ and dodecane $(C_{12}H_{26})$. The oxidation reaction for the two fuels are given by:

$$2 \ C_{16}H_{34} + 49 \ O_2 \xrightarrow{k_{f_1}} 32 \ CO_2 + 34 \ H_2O \tag{4.2}$$

and

$$2 \ C_{12}H_{26} + 37 \ O_2 \xrightarrow{k_{f_1}} 24 \ CO_2 + 26 \ H_2O \tag{4.3}$$
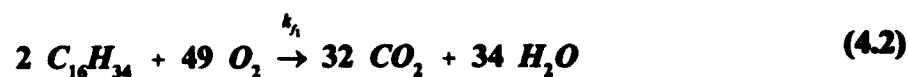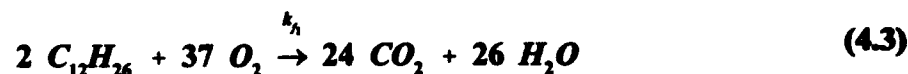
The reaction rate for these oxidation reactions is given by:

$$\omega = k_{f_1} \ [Fuel]^a \ [Oxidizer]^b \tag{4.4}$$

The coefficient, k_{f_1}, is assumed to be of a generalized Arrhenius form,

$$k_{f_1} = A_{f_1} \ T^{\zeta_{f_1}} \exp \ (-E_{f_1}/T) \tag{4.5}$$

where:

A_{f_1} is the Arrhenius coefficient

ζ_{f_1} is the forward temperature exponent

E_{f_1} is the activation temperature, K.

The most common choice of parameters in the global rate expression is a = 1 and b = 1, assuming that the overall reaction is approximately first order with respect to both

fuel and oxidizer. The other parameters, A_{f_1} and E_{f_1} , can be adjusted so that the predicted Pressure-Crank Angle diagram matches the experimental value. It was found in this study that the best agreement with experiments was obtained with values of the fuel exponent $a = 0.25$ and the oxidizer exponent $b = 1.5$ for both hexadecane and dodecane. The best values of the Arrhenius coefficient and activation temperature that gave satisfactory results for both fuels were found to be A_{f_1}-9.0e10 and E_{f_1}-1.5e4 K respectively.

4.4.2 Eddy-Break-Up Model

In diffusion flames, fuel and oxygen occur in separate eddies. Because the chemical reactions in most cases are very fast, it can be assumed that the rate of combustion will be determined by the rate of intermixing of fuel and oxygen eddies on a molecular scale: in other words, by the rate of dissipation of the eddies. Because fuel and oxygen appear as fluctuating intermittent quantities, there will be a relationship between the fluctuations and the mean concentration of the species. Consequently, the rate of dissipation can be expressed by the mean concentration of the reacting species. The EBU model gives a physically based representation of combustion, because it takes into account the effect of turbulence on the mean chemical reaction ratesHx In this study, the model of Magnussen and Hjertager was used [28]. This model relates the rate of combustion to the rate of dissipation of turbulent eddies and expresses the rate of reaction by the mean concentration of a reacting species, the turbulent kinetic energy, and the rate of dissipation of this energy. This model differs from the EBU model of Spalding [34,35] in relating the dissipation of eddies to the mean concentration of intermittent quantities instead of the concentration fluctuations. This is advantageous in view of the uncertainty in determining the concentration fluctuations of the reacting species.

Accordingly, in the case where the adequate presence of fuel is the controlling factor, the rate of combustion of fuel can be expressed by:

$$R_f - A \cdot C_f \cdot \left[\frac{\varepsilon}{k} \right]$$ (4.6)

where:

A is a constant

C_f is the local time-mean fuel concentration

k is the turbulent kinetic energy cm^2/s^2.

ε is the rate of dissipation of turbulent kinetic energy cm^2/s^3

In regions of the flame where the time mean concentration of fuel is high and the oxygen concentration is low, oxygen will be the reacting species that controls the rate of combustion. Accordingly, the rate of combustion in this case can be expressed by:

$$R_f - A \cdot \frac{C_{o_2}}{r_f} \cdot \left[\frac{\varepsilon}{k} \right]$$ (4.7)

where:

C_{o_2} is the local time-mean oxygen concentration

r_f is the stoichiometric oxygen requirement to burn 1 kg fuel.

In premixed turbulent flames, fuel and oxygen will occur in the same eddies. These eddies will be separated by eddies containing hot combustion products. The rate of combustion will, in this case, be determined by the same mechanism described above. However, an extra equation which takes care of the dissipation of the hot eddies must be added in cases where the concentration of hot combustion product is low. The combustion rate can then be expressed by:

$$R_f - A \cdot B \frac{C_p}{1 + r_f} \cdot \left[\frac{\varepsilon}{k} \right]$$ (4.8)

where:

B is a constant

C_p is the local time-mean concentration of reaction products.

Thus, the EBU model is applicable to diffusion as well as to premixed flames. The equation that gives the lowest reaction rate is the one that determines the local rate of combustion. Therefore, combining equations (4.6-4.8), the rate of combustion can be expressed by:

$$R_f - A \cdot \min \left[C_f , \frac{C_{o_2}}{r_f} , \frac{B C_p}{1 + r_f} \right] \left[\frac{\varepsilon}{k} \right]$$ (4.9)

For the model constants, Magnussen suggested the values of $A = 4.0$ and $B = 0.5$, but Gosman [36] used $A = 20$ and $B = 2.5$, while Pinchon [22] used $A = 16$ and $B = 2$ and Varnavas [25] used $A = 0.5$ and $B = 0.5$. It was found in this study that the original values used by Magnussen (A = 4, B = 0.5) gave the best overall agreement with the experimental data.

33

The EBU model has no provision for initiating combustion. To circumvent this problem, the SR chemical kinetic model was employed up to the point of auto-ignition after which the calculation procedure was switched to the EBU model. Switching from the chemical kinetics model to the EBU model depends on whether the ratio of the local turbulent time scale, τ_m, to the local kinetic time scale, τ_r, called the Damkohler number [23] is less than or greater than unity.

When $\tau_m / \tau_r \ll 1$, the process is controlled by chemistry since the chemical reaction time scale is much larger than the turbulent time scale.

When $\tau_m / \tau_r \gg 1$, the process is mixing controlled since the time required for chemical reactions is negligible compared to the time required for mixing.

The two time scales are defined by the relations:

$$\tau_m = \frac{k}{\varepsilon}$$

and

$$\tau_r = A \cdot \rho \, \exp(-E/R_o T)$$

where:

τ_m is the turbulence mixing time scale

τ_r is the chemical reaction time scale

A is the pre-exponential coefficient in the kinetics formula

ρ is the density

E is the activation energy

R_o is the universal gas constant

k is the turbulent kinetic energy

ε is the dissipation rate.

It was decided to switch from the SR to the EBU model of combustion after the ignition delay period when the combustion becomes controlled by mixing. The cylinder gas temperature was used to trigger the switch. A cell gas temperature of 1500 K was choosen to signal the switch to the EBU model. This cell temperature is generally exceeded within one time-step of the onset of combustion. By contrast, the maximum motoring temperature (no combustion) is about 950 K.

Although there is much evidence to support the dependence of the combustion rate on turbulent mixing, it is important to note that the mixing controlled EBU model is inadequate to predict combustion near walls, self-ignition, pollutant formation, and lean and rich flammability limits. These phenomena are controlled by chemical kinetics.

4.4.3 Results of Combustion Modeling

Comparisons of the P-θ diagrams obtained for the baseline engine with both the Eddy-Break-Up model and the single reaction model with experimental results have been made for several different loads and injection timings, and some representative results are presented here. As seen in Figures 4.2 and 4.3 for hexadecane fuel under two different loads for the same timing and engine speed, the cylinder pressure rises faster (rate of heat release is greater) during premixed combustion for the SR Model compared to the EBU Model. Beginning at the point of ignition, the rate of heat release shown by the EBU Model is representative of diffusion combustion. There appears to be no premixed pressure spike. The EBU Model predicts slightly lower peak pressure than the SR Model in all cases examined. A similar trend is noted for dodecane fuel as well, as shown in Figures 4.4 and 4.5.

It is also evident from the P-θ diagrams that the predicted ignition delay is always longer than the experimental value by approximately 3-5 degrees. Recall that the EBU Model has no mechanism for autoignition, and that when using the EBU Model we rely on the Arrhenius SR Model to initiate combustion. We thus see identical ignition delay periods for both models. Ignition delay in the SR model is primarily a function of the activation temperature constant, E_n. The choice of activation temperature that gave the best overall results for the SR Model over a wide range of operating conditions, i.e. $E_n = 1.5*10^4$, resulted in slightly longer ignition delay periods.

Figures 4.6 and 4.7 show the predicted cylinder pressure traces for three different injection timings for the EBU Model and SR Model, respectively. The maximum cylinder pressure increases with advancing injection timing as it should, due to a larger proportion of premixed combustion.

Figure 4.8 shows the predicted cylinder gas temperature versus crank angle for both combustion models. The EBU Model predicts slower gas temperature rise and a lower peak gas temperature than the SR Model, in keeping with the lower peak cylinder pressures.
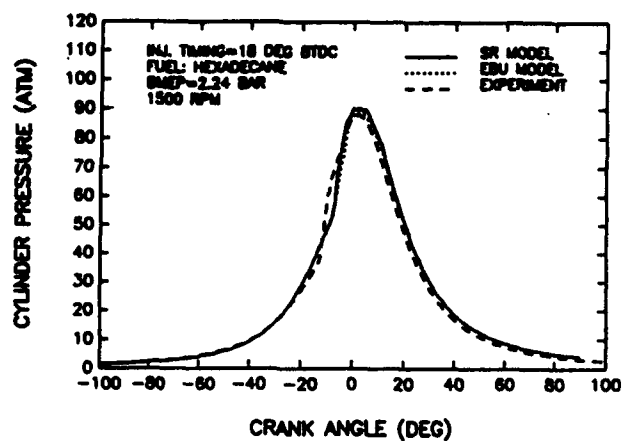
Figure 4.2

Cylinder Pressure Versus Crank Angle For Hexadecane Fuel
1500 RPM, 18 Deg BTDC, 223 KPa BMEP
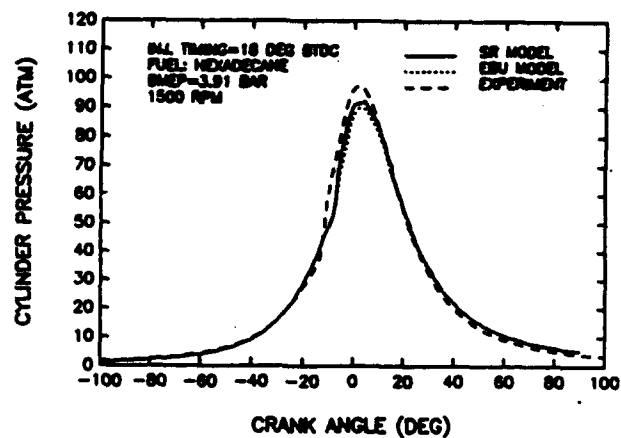
Figure 4.3

Cylinder Pressure Versus Crank Angle for Hexadecane Fuel
1500 RPM, 18 Deg BTDC, 391 KPa BMEP
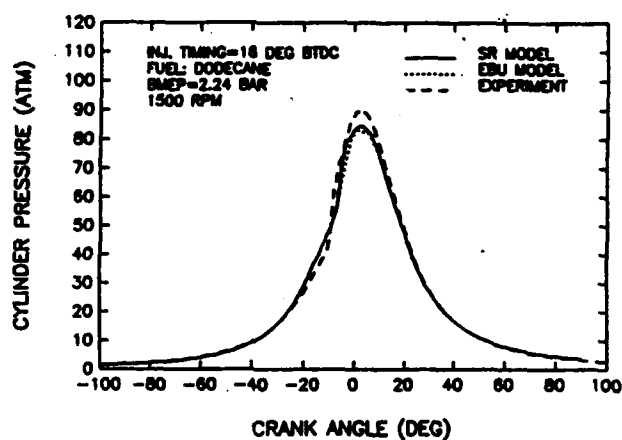
Figure 4.4

Cylinder Pressure Versus Crank Angle For Dodecane Fuel
1500 RPM, 16 Deg BTDC, 223 KPa BMEP
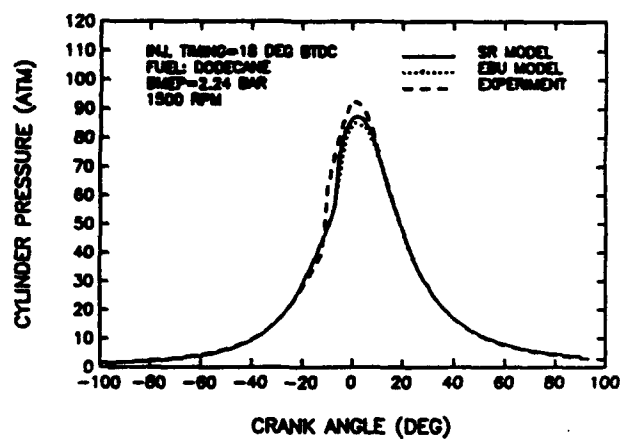
Figure 4.5

Cylinder Pressure Versus Crank Angle for Dodecane Fuel
1500 RPM, 18 Deg BTDC, 223 KPa BMEP

36
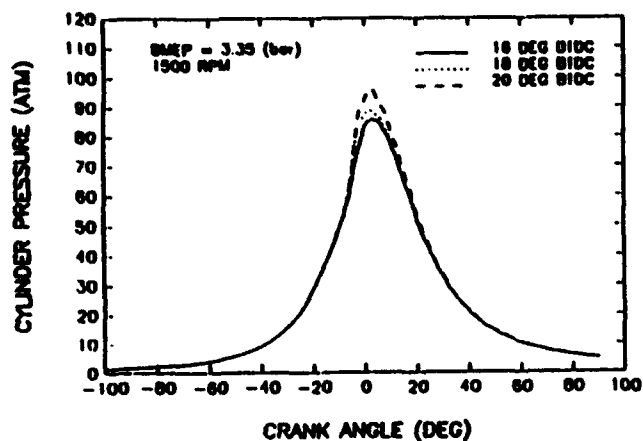
Figure 4.6

Cylinder Pressure Versus Crank Angle For Hexadecane Fuel
EBU Model for Different Injection Timings
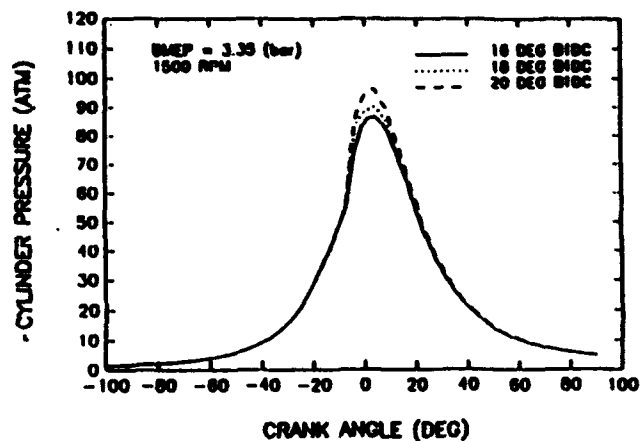
Figure 4.7

Cylinder Pressure Versus Crank Angle for Hexadecane Fuel
SR Model for Different Injection Timings
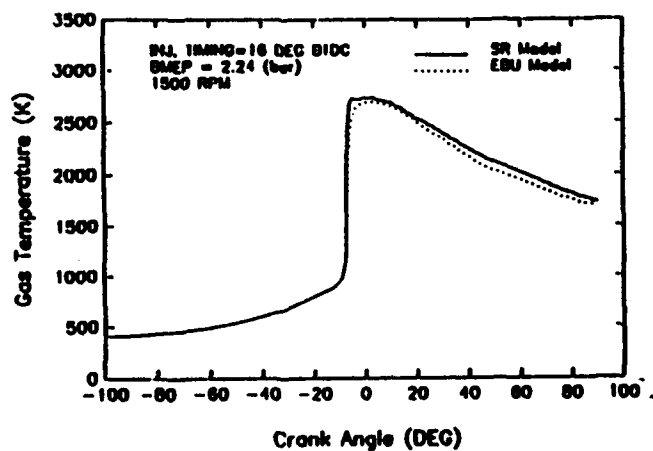
Figure 4.8

Cylinder Temperature Versus Crank Angle For Hexadecane
Single Reaction Model Versus Eddy-Break-Up Model

37

4.5 NITRIC OXIDE MODELING

4.5.1 NO Model

Nitric oxide (NO) is formed in diesel engines by the high temperature oxidation of atmospheric nitrogen. In oxygen-rich (lean) regions, the elementary process for the formation reaction of NO is expressed as:

$$2N_2 + O_2 \underset{k_{b_1}}{\overset{k_{f_1}}{\rightleftharpoons}} 2N + 2NO \tag{4.10}$$

$$2O_2 + N_2 \underset{k_{b_2}}{\overset{k_{f_2}}{\rightleftharpoons}} 2O + 2NO \tag{4.11}$$

In excess-fuel (rich) regions, the oxygen concentration required in equation (4.10) is low, and the reaction of N and OH (which is formed during the decomposition of the fuel) becomes important. This reaction is given by:

$$N_2 + 2OH \underset{k_{b_4}}{\overset{k_{f_4}}{\rightleftharpoons}} 2NO + 2H \tag{4.12}$$

The elementary reaction processes given by equations (4.10) and (4.11) are known as the Zeldovich mechanism [37]. When the elementary reaction process represented by equation (4.12) is further added, the total reaction is called the extended Zeldovich mechanism [38].

Assuming a steady state approximation for the nitrogen atom concentration, the rate expression fits the extended zeldovich mechanism:

$$\frac{d\ [NO]}{dt} - 2\ k_{f_1}\ [O]\ [N_2]\ \left[\frac{1 - [NO]^2\ /\ K\ [O_2]\ [N_2]}{1 + k_{b_1}\ [NO]\ /\ (\ k_{f_3}\ [O_2] + k_{f_4}\ [OH]\ )} \right] \tag{4.13}$$

where:

[ ]   is the species concentration

k_{f_r} is the forward reaction coefficient for the reaction r

k_{b_r} is the backward reaction coefficient for the reaction r

K is the dissociation equilibrium constant = $(\ k_{f_1}\ /\ k_{b_1}\ )(\ k_{f_2}\ /\ k_{b_2}\ )$.

The reaction rate constants used in KIVA-II are [39]:

$$k_{f_2} = 1.5587 *10^{14} \exp(-67627/T)$$

$$k_{b_2} = 7.5 *10^{12}$$

$$k_{f_3} = 2.6484 *10^{10} \exp(-59418/T)$$

$$k_{b_3} = 1.6 *10^{14} \exp(19678/T)$$

$$k_{f_4} = 2.123 *10^{14} \exp(-57020/T)$$

$$k_{b_4} = 0.0$$

The required *OH* concentrations were computed from the following set of equilibrium reactions:

$$H_2 \rightleftarrows 2H$$

$$O_2 \rightleftarrows 2O$$

$$N_2 \rightleftarrows 2N$$

$$H_2 + O_2 \rightleftarrows 2OH$$

$$O_2 + 2H_2O \rightleftarrows 4OH$$

$$2\,CO + O_2 \rightleftarrows 2CO_2$$
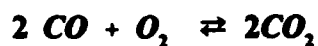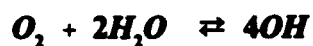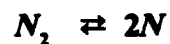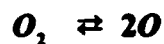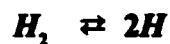
The following relation was used to convert the *NO* values in gm/cycle, as calculated by KIVA, to concentration in particles per million (ppm) for comparison with experiments.

where:

$\dot{m}_{total}$ is the total mass flow rate (air + fuel injected)

rps   is the revolution per second.

4.5.2 Results of NO Modeling

Figures 4.9 and 4.10 compare the NO emission versus crank angle for both models with the experimental values for hexadecane fuel and two different injection timings. The EBU model predicts lower NO emissions than the SR model due to the lower peak cylinder temperature. The values predicted by the SR model are in better agreement with the experimental values, although they are still somewhat below the measured values. Figures 4.11 and 4.12 show similar NO emission results for dodecane fuel. For dodecane, the SR model gives very good agreement with the measured NO values.

Figures 4.13 - 4.15 show the effect of injection timing on NO emission for hexadecane for three different loads, comparing experimental results with both models. th models underpredict NO, but produce the correct trend of increasing NO emission th advanced timing. Figure 4.16 shows similar data for dodecane at low load.
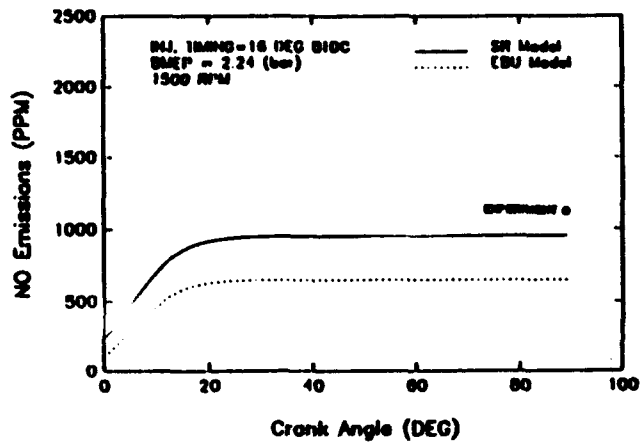
Figure 4.9

NO Emission Versus Crank Angle For Hexadecane Fuel

1500 RPM, 16 Deg BTDC, 223 KPa BMEP
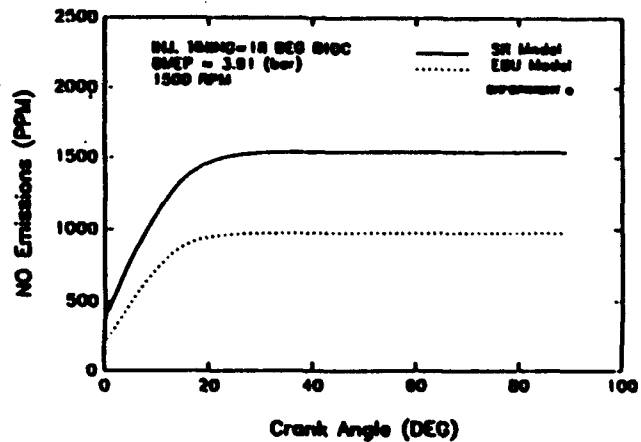
Figure 4.10

NO Emission Versus Crank Angle for Hexadecane Fuel

1500 RPM, 18 Deg BTDC, 391 KPa BMEP
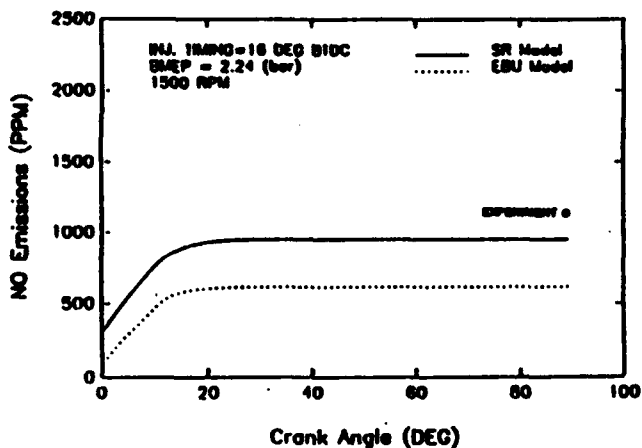
Figure 4.11

NO Emission Versus Crank Angle For Dodecane Fuel

1500 RPM, 16 Deg BTDC, 223 KPa BMEP
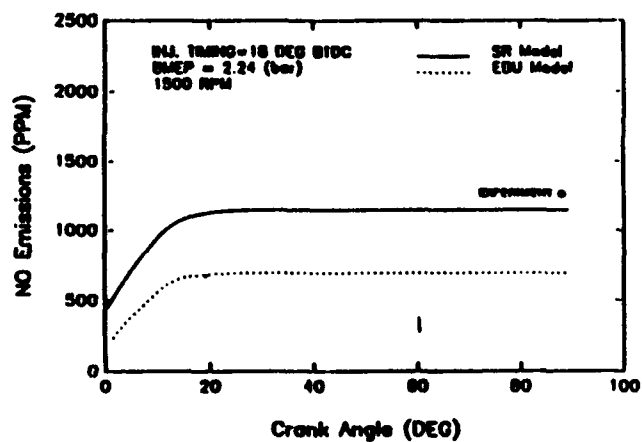
Figure 4.12

NO Emission Versus Crank Angle for Dodecane Fuel

1500 RPM, 18 Deg BTDC, 223 KPa BMEP

41
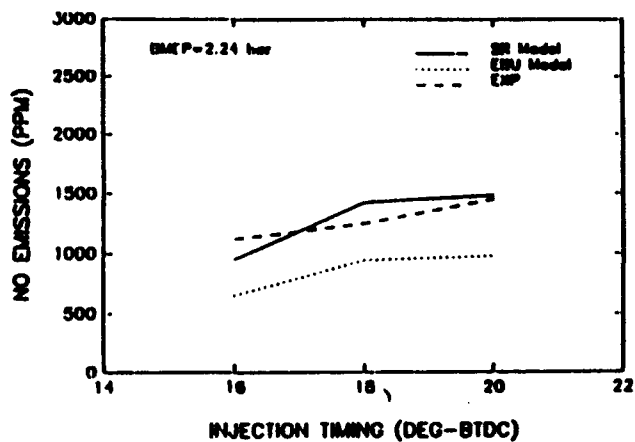
Figure 4.13

NO Emission Versus Injection Timing For Hexadecane Fuel
1500 RPM, 223 KPa BMEP
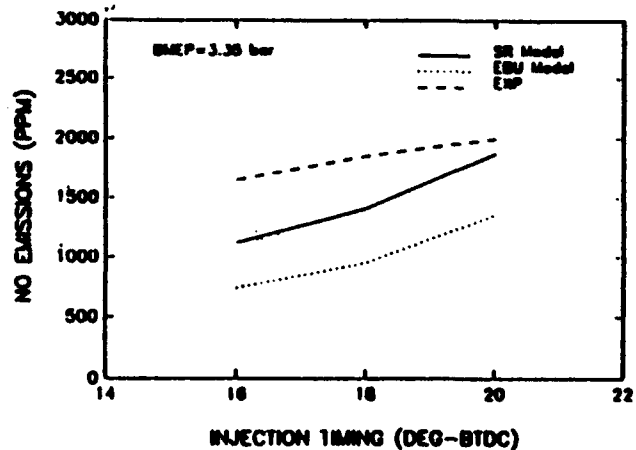
Figure 4.14

NO Emission Versus Injection Timing For Hexadecane Fuel
1500 RPM, 335 KPa BMEP
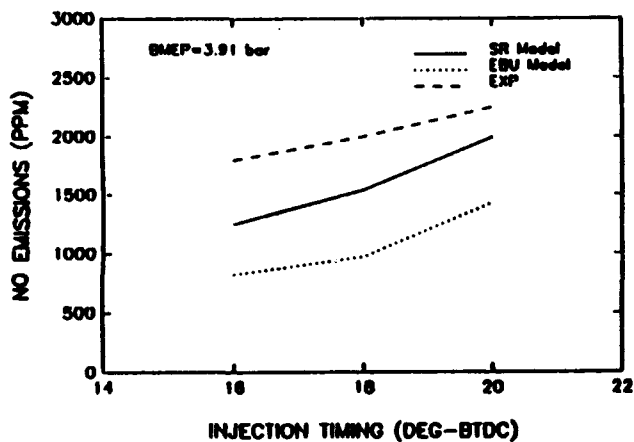
Figure 4.15

NO Emission Versus Injection Timing For Hexadecane Fuel
1500 RPM, 391 KPa BMEP
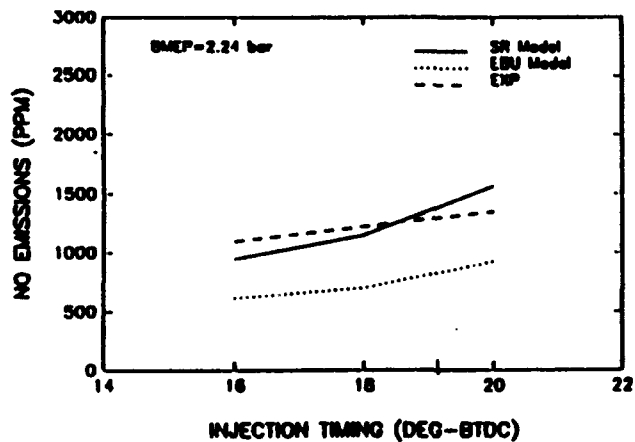
Figure 4.16

NO Emission Versus Injection Timing for Dodecane Fuel
1500 RPM, 223 KPa BMEP

42

4.6 SOOT MODELING

4.6.1 Review of Existing Soot Models

Most models appearing in the literature for the formation and oxidation of soot are empirical and much of the data used in the development of the models are based on laboratory burner flames rather than diesel engines. The literature on soot has been reviewed by several researchers, including Haynes and Wagner [40], and most recently by Morel and Keibar [41]. Although many useful observations have been made, no generally applicable soot emission model has yet been devised.

Khan, et al. [42,43] presented a soot formation correlation based on high pressure diesel engine data. The parameters used in this model are local values of temperature, unburned hydrocarbon concentration, and equivalence ratio. A corresponding soot combustion scheme was not suggested. The rate of soot formation was described as:

$$\frac{ds}{dt} \cong \phi_f^3 P_f \, \exp(-2000/T) \tag{4.15}$$

where:

s is the soot mass
ϕ_f is the equivalence ratio in the formation zone
P_f is the partial pressure of fuel in the formation zone
T is the unburned temperature.

Nagle and Strickland [44] proposed the following relation for the rate of soot oxidation:

$$\frac{ds}{dt} = -\frac{6\,s}{\rho_s\, d_s} P_{O_2} \, f(T, P_{O_2}) \tag{4.16}$$

where:

P_{O_2} is the partial pressure of oxygen

ρ_s is the density of the soot particle
d_s is the diameter of the soot particle

$f(T, P_{O_2})$ is a complex Arrhenius type expression.

Lee [45] proposed the following soot oxidation model:

$$\frac{ds}{dt} = d_s^2 \, P_{O_2} T^{-1/2} \, \exp(-20,000/T) \tag{4.17}$$

Fenimore and Jone's [46] suggested that the rate oHxsoot oxidation is given by:

$$\frac{ds}{dt} = -P_{o_2}^{1/4} \, P_{H_2O}^{1/2} \, T^{-1/2} \, \exp(-19000/T) \qquad (4.18)$$

Hiroyasu and Kadota [47] proposed the following equations for soot formation and oxidation:

$$\frac{dm_{sf}}{dt} = A_f \, m_{fv} \, P^{0.5} \, \exp(-E_{sf}/RT)$$

$$\frac{dm_{sc}}{dt} = A_c \, m_s \, \frac{P_{o_2}}{P} \, P^{1.8} \, \exp(-E_{sc}/RT) \qquad (4.19)$$

$$\frac{dm_s}{dt} = \frac{dm_{sf}}{dt} - \frac{dm_{sc}}{dt}$$

where:

m_{sf} is the mass of formed soot
m_{sc} is the mass of oxidized soot
m_{fv} is the mass of fuel vapor
m_s mass of soot.

E_{sf} and E_{sc} are assumed to be 1.25E+04 Kcal/Kmol and 1.4E+04 Kcal/Kmol respectively. A_f and A_c are constants which are determined so as to match the computed soot with the experimental results.

Morel [41] recommended empirical correlations for soot formation and oxidation directly linked to the combustion model. The soot model incorporates only those variables calculated by the combustion model, i.e., temperature, equivalence ratio, partial pressure of certain species, etc. According to Morel the amount of soot formation is described by

$$\frac{ds}{dt} = A_1 \, \dot{m}_d \, \exp(-A_2/T_f)/(1 + 4.76 \, Y_{o_2})^3 \qquad (4.19)$$

and the subsequent soot oxidation in the burned zone is described by

$$\frac{ds}{dt} = -B_1 s/(\rho_s d_s) \exp(-B_2/T_f) \, P_{o_2}^{1/2} \qquad (4.20)$$

where:

s is the mass of the soot
Y_{o_2} is the mole fraction of available oxygen in the actively burning zone

$\dot{m}_d$ is the rate of fuel burned in the diffusion burning model

A_1 is a constant = 0.38

44

A_2 is a constant = 5000
T_f is the temperature in the formation zone
ρ_s is the soot density = 900 Kg/m^3 (400 - 1500 Kg/m^3)
d_s is the diameter of the elementary soot particle entering the burned zone = 0.012 - 0.032 μm
P_{O_2} is the partial pressure of O_2 in the burned zone

B_1 is a constant = 0.015
B_2 is a constant = 5000.

Tesner [32,33] suggested a kinetic scheme resulting in soot formation based on a chain-type process involving radical nuclei from which soot particles will later grow.

Magnussen and Hjertager [28] used Tesner's soot formation model to analyze a turbulent combustion flow, and added a model of soot oxidation which considers the behavior of soot in turbulent flames. Although there are a number of adjustable parameters in the Tesner model, Magnussen and Hjertager only had to modify Tesner's coefficients slightly to model their measurements of soot formation in turbulent acetylene/air flames. These models are described in more detail below.

4.6.2 Soot Model Adapted to KIVA

It was decided to use the soot formation model developed by Tesner, et al. [32,33] and the sood oxidation model developed by Magnussen and Hjertager [28] due to the fact that they take into consideration the behavior of soot in turbulent flames and, therefore, are suitable for use in conjunction with the eddy-break-up combustion model.

It has been assumed, following Tesner, that soot is formed from a gaseous fuel in two stages, where the first stage represents formation of radical nuclei, and the second stage represents soot particle formation from these nuclei. The rate of formation of radical nuclei is expressed by:

$$R_{nf} - n_o + (f\text{-}g)\, n - g_o . n . N \qquad (\text{part/m}^3\text{/s}) \qquad (4.21)$$

where:

f is a linear branching coefficient
g is a linear termination coefficient
g_o is the coefficient of linear termination of soot particles
n is the concentration of radical nuclei (part/m^3)
N is the concentration of soot particles (part/m^3)
n_o is the rate of spontaneous formation of radical nuclei.

n_o is expressed by:

$$n_o - a_o . c_f . e^{(-E/RT)} \qquad (\text{part/m}^3\text{/s}) \qquad (4.22)$$

45

where:

a_o is a constant

c_f is the mass concentration of fuel (Hx/m^3)

E is the activation temperature (K)

T is the absolute temperature (K)

R is the universal gas constant.

The rate of soot particle formation is expressed by:

$$R_{s,f} = m_p \, (a - b N) \, n \qquad (kg/m^3/s) \qquad\qquad (4.23)$$

where:

a & b are constants

m_p is the mass of the soot particle (Kg/part). It is calculated assuming soot particles to be spherical and having an average diameter d_s = 200 Å and density ρ_s = 2000 Kg/m³.

In this model, the soot formation is limited to regions of unburnt fuel.

Soot oxidation occurs when soot particles come into contact with oxygen. The soot combustion model developed by Magnussen and Hjertager takes into account the behavior of soot in turbulent flames.

For regions where the local mean soot concentration is low compared to the oxygen concentration, the rate of soot combustion can be expressed as:

$$R_{s,c} = A \cdot C_s \left[\frac{\varepsilon}{k} \right] \qquad (kg/m^3/s) \qquad\qquad (4.24)$$

where:

A is a constant

C_s is the local mean soot concentration (kg/m³)

k is the turbulent kinetic energy cm^2/s^2

ε is the rate of dissipation of turbulent kinetic energy cm^2/s^3.

In regions where the oxygen concentration is low, the oxygen will limit the rate of soot combustion. The soot must also compete for oxygen with the unburned fuel. In this case, the rate of soot combustion is given by:

$$R_{s,c} = A \left[\frac{C_{o_2}}{r_s} \right] \left[\frac{\varepsilon}{k} \right] \left[\frac{C_s \, r_s}{C_s \, r_s + C_f \, r_f} \right] \qquad (kg/m^3/s) \qquad\qquad (4.25)$$

where:

r_s is the stoichiometric oxygen requirement to burn 1 kg soot

r_f is the stoichiometric oxygen requirement to burn 1 kg fuel

C_{o_2} is the local time mean oxygen concentration (kg/m³)

C_f is the local time mean fuel concentration (kg/m³).

The equation that gives the lower reaction rate determines the local rate of soot combustion. Thus, combining equations (4.24) and (4.25) leads to the expression:

$$R_{s,c} = A \frac{\varepsilon}{k} \min \left[C_s , \left[\frac{C_{o_2}}{r_s} \right] \left[\frac{C_s r_s}{C_s r_s + C_f r_f} \right] \right] \quad (kg/m^3/s) \quad (4.26)$$

The local number of radical nuclei can be assumed to be reduced by combustion according to:

$$R_{n,c} = R_{s,c} \left[\frac{n}{C_s} \right] \quad (part/m^3/s) \quad (4.27)$$

The concentration rate of soot particles is given by the difference of the soot formation rate and the oxidation rate, i.e.

$$\frac{dN}{dt} = R_{s,f} - R_{s,c} \quad (part/m^3/s) \quad (4.28)$$

Similarly, The concentration rate of radical nuclei is given by:

$$\frac{dn}{dt} = R_{n,f} - R_{n,c} \quad (part/m^3/s) \quad (4.29)$$

The simultaneous solution of the above two differential equations is obtained using a fourth order Runge-Kutta method.

4.6.3 Soot Model Parameters

Referring to studies on soot formation in atmospheric flames and shock tubes showed that the conditions under which soot formation occurs, as well as the quantity of soot formed, vary little for most hydrocarbons. Therefore, the constants appearing in the soot formation equation recommended by Tesner et al. for acetylene-oxygen flames have been used in this investigation along with the constants recommended by Magnussen [28] for the soot oxidation equations. The values of these constants are given below:

a = 1.6e5	/s
f-g = 100	/s
g_o = 1.0e-15	m^3/part/s
b = 8e-14	m^3/part/s
a_o = 7.254e30	part/kg/s

47

$E/R = 9e4$ K

$\rho_s = 2$ g/cm^3

d_s (the soot particle mean diameter) = 200 Å

The local mean soot concentration, C_s (kg/m^3), is defined as:

$$C_s = \rho_s \ (kg/m^3) \ \ vol_s \ (m^3/part) \ \ N \ (part/m^3)$$

where:

    ρ_s is the density of the soot particle (kg/m^3)

    vol_s is the volume of a soot particle (m^3/part)

    N   is the concentration of soot particles (part/m^3).

The mass of a soot particle, m_p (kg/part), is defined as:

$$
\begin{aligned}
m_p \quad &= \rho_s \ (kg/m^3) \ \ vol_s \ (m^3/part) \\
&= 2000 \ (kg/m^3) \ \ (4/3)\pi \ (d_s/2)^3 \ (m^3/part) \\
&= 8.37758e\text{-}21 \ (kg/part)
\end{aligned}
$$

Therefore, the local mean soot concentration, C_s (kg/m^3), is given by:

$$C_s \quad = 8.37758e\text{-}21 \ (kg/part) \ \ N \ (part/m^3)$$

The stoichiometric oxygen requirement to burn 1 kg of soot, r_s, is calculated from the following chemical reaction [48]:

$$Soot + O_2 \rightarrow CO_2$$
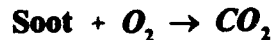
Therefore, r_s is given by:

$$r_s - 32/12 - 2.66667$$

The soot model calculates the soot concentration in (kg/m^3). The calculation stops at 90 degree crank angle ATDC where the calculated average cylinder gas temperature is 990 K, and the average cylinder pressure is 4.98 atm. For comparison with the experimental data, this value is converted to exhaust gas conditions using the following relation, assuming ideal gas conditions.

$$C_s \ (at \ STP) = C_s \ (at \ 90° \ ATDC) \ast \ \frac{T_{cyl}}{T_{exh}} \ \frac{P_{exh}}{P_{cyl}} \ \ (kg/m^3) \qquad (4.30)$$

Appendix F lists the soot model FORTRAN source code, and Appendix G shows the modifications made to the KIVA-II subroutine NEWCYC, and subroutine GLOBAL associated with the soot model.

4.6.4 Results of Soot Modeling

Figures 4.17 and 4.18 show the computed soot formation, soot oxidation, and the soot concentration, which is the different between the formation and oxidation, for hexadecane and dodecane at 1500 RPM, 18 DBTDC and a load of 3.91 bar BMEP. Figures 4.19 and 4.20 show the computed soot concentration versus crank angle for hexadecane and dodecane at three different BMEP of 2.24, 3.35, and 3.91 bar at 1500 RPM and an injection timing of 18 DBTDC. The model produces the correct trend of increasing soot concentration with increasing load.

The rate of soot concentration versus crank angle can be divided into three regions. First, soot begins to form in the fuel rich mixture at the beginning of combustion and during the injection process where the fuel-air ratio at the inner zone of the spray is high. Then the compression stroke continues until the piston reaches TDC, and the expansion stroke begins. During this period, the air motion (swirl) is low and the rate of soot formation is higher than the rate of soot oxidation. This continues to about 20 degrees ATDC and the soot concentration rises sharply. At 20 degrees ATDC, the air motion continues increasing at a higher rate as the piston continues moving to about 40 degrees ATDC. This results in increasing the rate of soot oxidation. It is observed that the maximum soot concentration occurs at about 40 degrees crank angle ATDC. After 40 degrees crank angle ATDC, the air motion continues to increase at a higher rate and the small amount of remaining fuel continues to burn. On the other hand, the soot formed earlier comes in contact with oxygen, resulting in a high oxidation rate, and, as seen from the figures, the rate of soot concentration continues to decrease to about 60 degrees ATDC. Finally, the mixture reaches equilibrium and the amount of soot concentration remains constant until the end of the expansion stroke.

Figures 4.21 and 4.22 compare the experimental soot emission for the baseline engine with the computed results. The Figures show the effect of load on the soot emission at STP condition (T=289 K, P=1 atm) for hexadecane and dodecane respectively. The soot model produces the correct trend of increasing soot concentration with increasing load. As shown in the figures, the model gives fair agreement with the measured soot values.
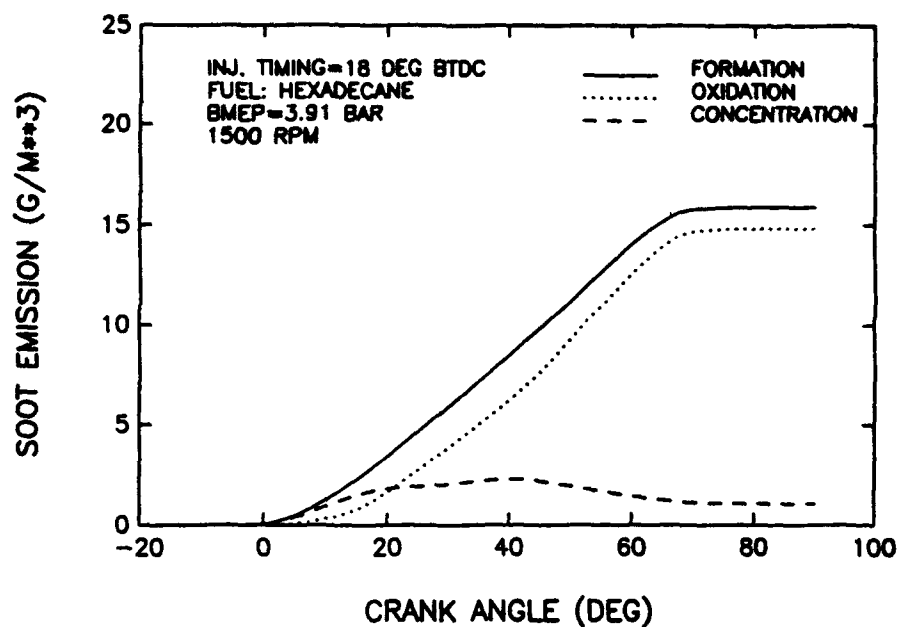
Figure 4.17

Soot Formation and Oxidation Versus Crank Angle for Hexadecane
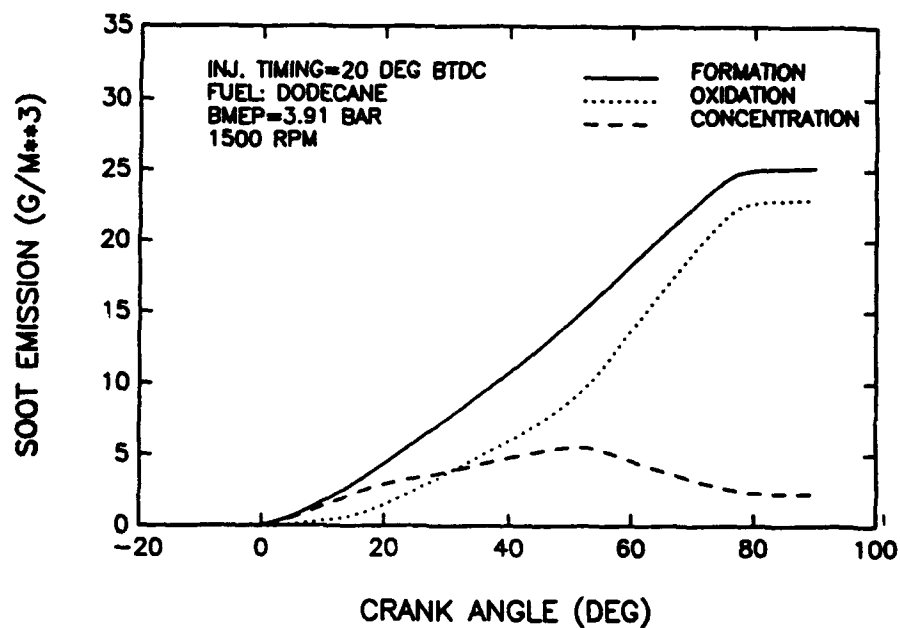
Figure 4.18

Soot Formation and Oxidation Versus Crank Angle for Dodecane

50
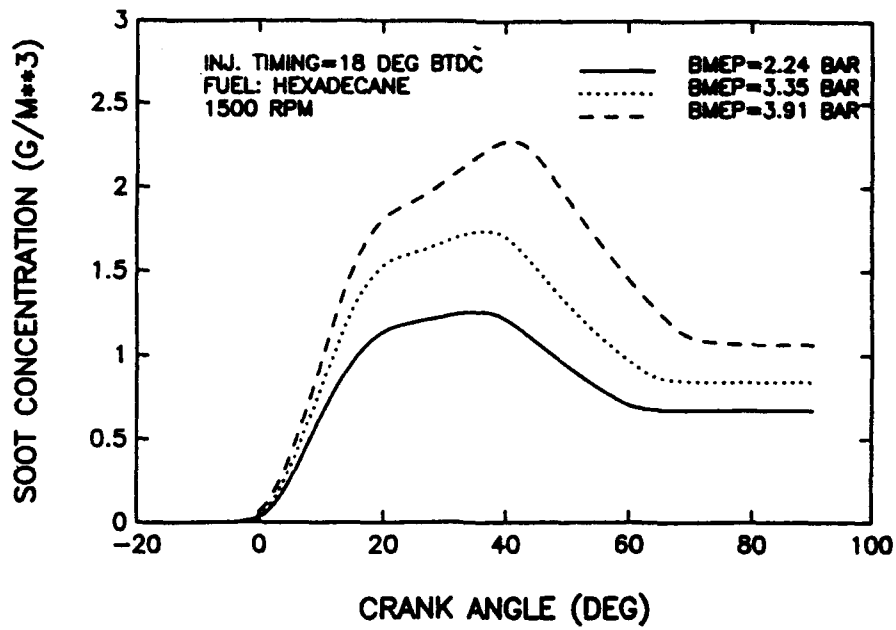
Figure 4.19

Soot Concentration Versus Crank Angle for Hexadecane
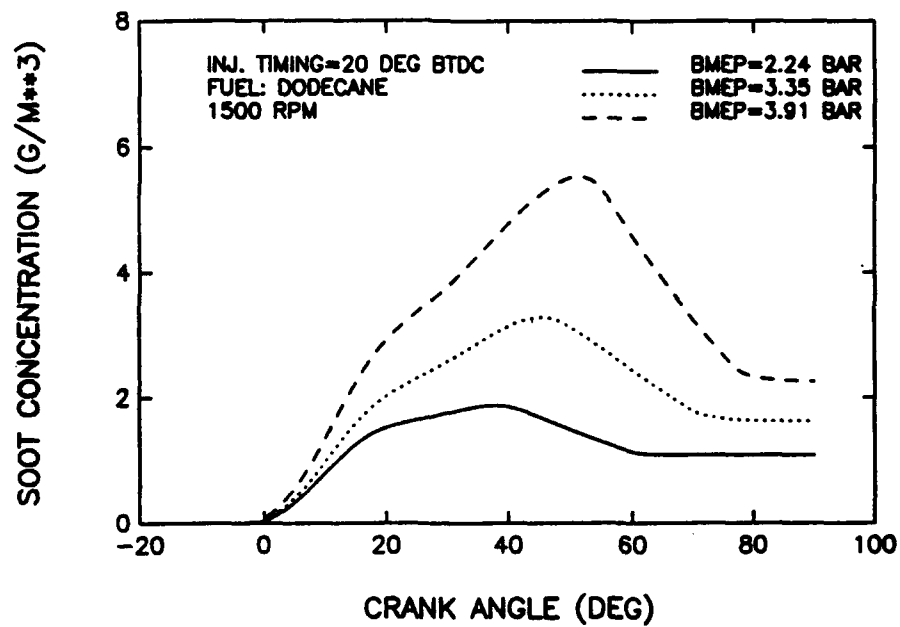
Figure 4.20

Soot Concentration Versus Crank Angle for Dodecane

51
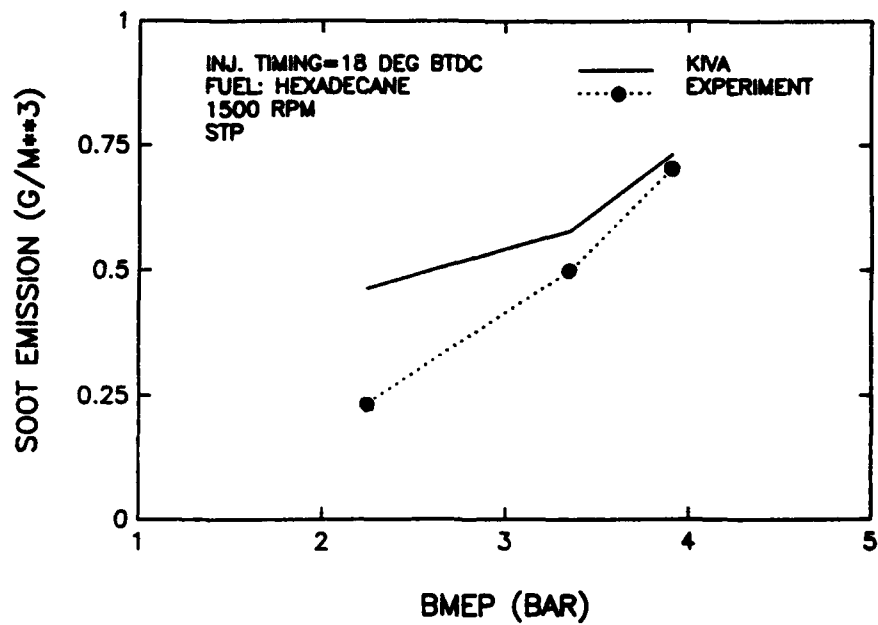
Figure 4.21
Soot Emission Versus Load for Hexadecane
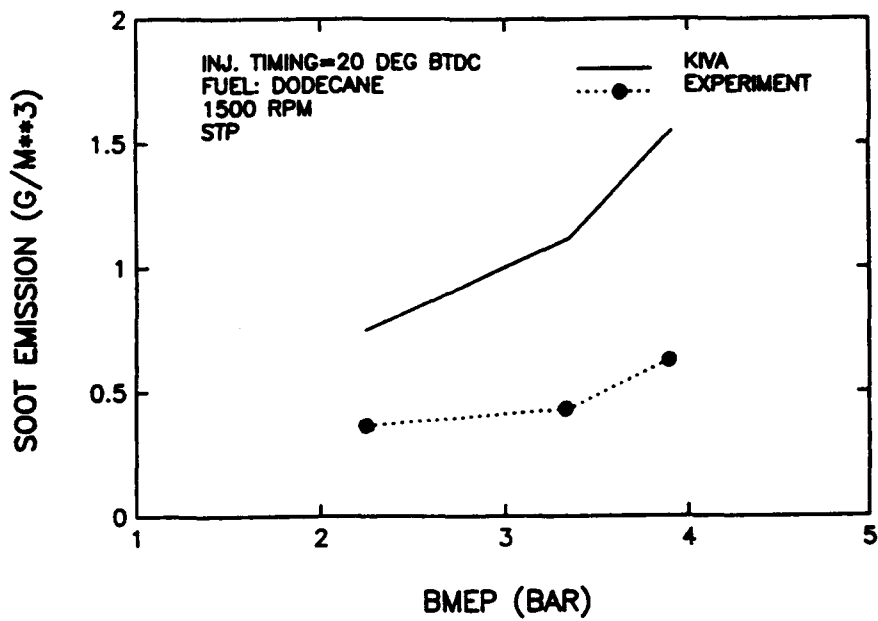
Figure 4.22
Soot Emission Versus Load for Dodecane

4.7 THERMAL MODELING OF CERAMIC COATINGS

Two of the input parameters required for KIVA-II are the surface temperature of the combustion chamber walls and the intake air temperature. For the baseline case, the temperature of all surfaces was assumed constant and uniform at 425 K, and the intake air temperature was assumed to be 315 K. The effect of applying a thin ceramic coating to combustion chamber surface is to increase both the average surface temperature and the variation in surface temperature relative to the baseline metallic surface. To model this effect, the coated surfaces were assumed to have a cyclic temperature profile, as depicted in Figure 4.23, consisting of a 100 K variation centered on an average value of 475 K. This temperature profile is based on results of experimental and analytical studies related to ceramic coated surface temperatures as cited in references 3, 6, and 7. The uncoated surfaces of the combustion chamber were kept at the same value as for the baseline model, i.e. 425 K, following a study by Smavik [8] who observed negligible temperature rise in the uninsulated components. The intake air temperature at the start of compression was also increased to account for both the mixing with higher exhaust gas temperature residuals caused by insulated surfaces and heat transfer from the higher temperature surfaces to the intake air. For the coated-piston case and the all-surface-coated case, 325 K was assumed for the intake air, while for the coated-head case, 320 K was assumed. These values were based on the experimental volumetric efficiency data.

4.8 THERMAL MODELING RESULTS

KIVA results are presented in Figures 4.24-4.27 for four different sets of operating conditions. All results shown are for hexadecane fuel at 1500 RPM. Figure 4.24 is for a load of 8 NM (223 KPa BMEP) and a timing of 22 DBTDC. Figure 4.25 is for a load of 12 NM (335 KPa BMEP) and a timing of 20 DBTDC. Figure 4.26 is for a load of 12 NM (335 KPa BMEP) and a timing of 22 DBTDC. Figure 4.27 is for a load of 14 NM (391 KPa BMEP) and a timing of 22 DBTDC. Each figure includes plots of cylinder pressure, cylinder gas temperature, mass of burnt fuel and NO concentration for the specified load and injection timing. Each plot compares the three ceramic coated cases with the baseline case. The effect of the various insulation schemes on pressure, temperature, rate of fuel combustion and NO emission is discussed in the following sections.

4.8.1 Cylinder Gas Pressure

The P-θ diagrams in Figures 4.24(a)- 4.27(a) are simulations from KIVA for the baseline case and the three insulated engines. In each case the peak cylinder pressure is highest for the baseline engine, followed by the coated-head case, the all-surface-coated case and the coated-piston case. The coated-piston case always produces the lowest peak cylinder pressure. These KIVA results agree well with the experimental P-θ diagrams shown in Figure 3.1. In general, the peak cylinder pressure is a function of the ratio t_p/t_d (premixed combustion duration/diffusion combustion duration). The higher the ratio, the higher the peak cylinder pressure, and vice versa. This leads to the conclusion that selective insulation of the combustion chamber walls can modify the combustion characteristics of the engine, causing the peak cylinder pressure to vary accordingly. It also implies that the ignition delay for the coated-piston engine is the shortest and the ignition delay for the baseline engine is the longest of the four engine builds investigated. This is substantiated by the experimental data in some cases but not in others, as discussed in Section 3.5.

4.8.2 Cylinder Gas Temperature

KIVA-II calculates the gas temperature in each computational cell at each time step. Relations were added in this study to further calculate the mass average temperature of the entire cylinder contents based on an energy balance at each time step. Figures 4.24(b) - 4.27(b) compare the calculated average gas temperature versus crank angle for the baseline and three selective insulation schemes. The following general observations can be made from these figures: 1) During compression, the cylinder gas temperature is higher for the coated cases than for the baseline, 2) the gas temperature for the various ceramic coated cases begins to rise earlier but at a slower rate than the baseline case, 3) the maximum average cylinder gas temperature is lowest for the coated-piston case and highest for the baseline case, with the coated-head and totally insulated cases lying in between.

These observations may be attributed to the effect of the selective coating schemes on the ignition delay period. The initial higher gas temperature is due to the higher surface temperature of the ceramic surfaces. The earlier rising temperature is indicative of a shorter ignition delay which results in a smaller premixed combustion fraction and a longer diffusion combustion period resulting in a lower average peak cylinder temperature and a higher gas temperature during the expansion stroke. The results discussed above for peak cylinder pressure are also in support of this reasoning.

54

4.8.3 Mass of Burnt Fuel

Figures 4.24(c) - 4.27(c) depict the mass of fuel burnt during the combustion process. In general, it can be noted that the rapid rate of combustion associated with the premixed combustion phase occurs earlier and consumes less fuel for all of the coated cases relative to the baseline case, indicative of shortened ignition delay and decreased t_r/t_d. This is in keeping with the lower cylinder pressure and temperature predictions. Typically it is the coated-piston case that displays the lowest rate of combustion.

4.8.4 Nitric Oxide Emission

The rate of NO formation during combustion for the baseline and three selective insulation schemes is shown in Figures 4.24(d) - 4.27(d). It is noted that the coated-piston case typically produces the lowest NO emission consistent with the lowest rate of combustion and cylinder temperature. The baseline engine typically produces the highest NO emission except for the case shown in Figure 4.27(d) for 14 NM (391 KPa BMEP) load and 22 DBTDC. In this case the coated head produced a higher NO value than did the baseline. The experimental values of NO for these cases are indicated by the data points shown along the right side Y-axis. Reasonable agreement between experimental and predicted values is shown in most cases and the correct relative values of the coated cases versus baseline are obtained except for the low load condition shown in Figure 4.24(d) where agreement is not obtained for the insulated head case. Figures 4.28 and 4.29 further illustrate reasonable agreement between experimental values of NO and those predicted with KIVA, especially at higher values of load. At low loads KIVA underpredicted NO by about 25 percent.
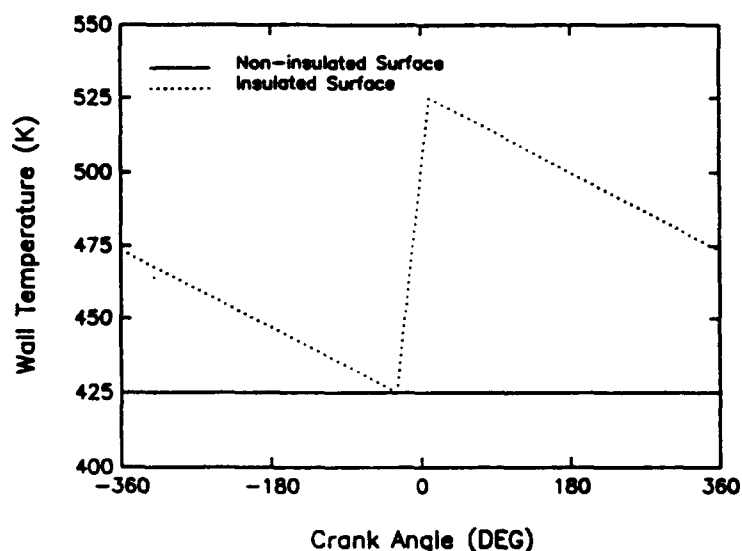
Figure 4.23 Assumed Coated Surface Temperature Versus Crank Angle Profile
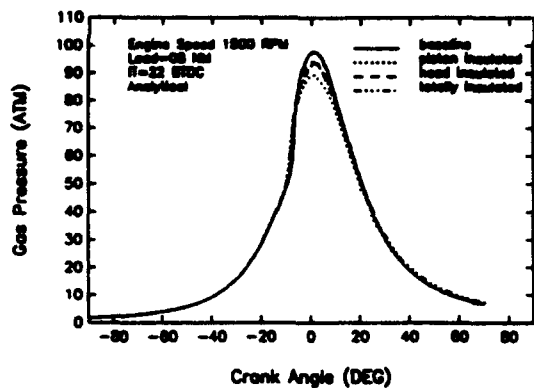
Figure 4.24(a)

Cylinder Gas Pressure Versus Crank Angle
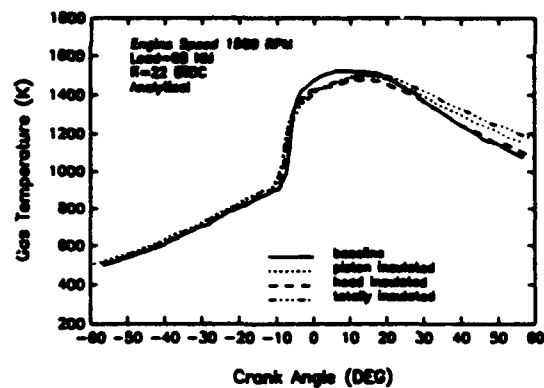
Figure 4.24(b)

Cylinder Gas Temperature Versus Crank Angle
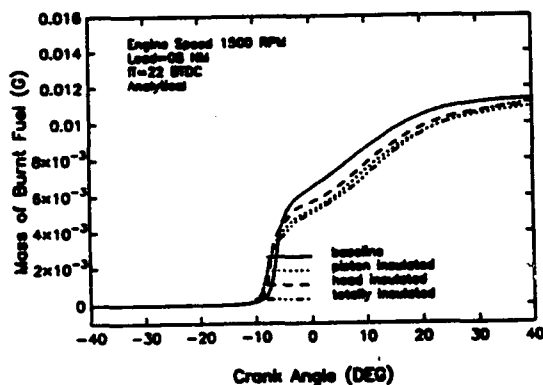
Figure 4.24(c)

Mass of Fuel Burnt Versus Crank Angle
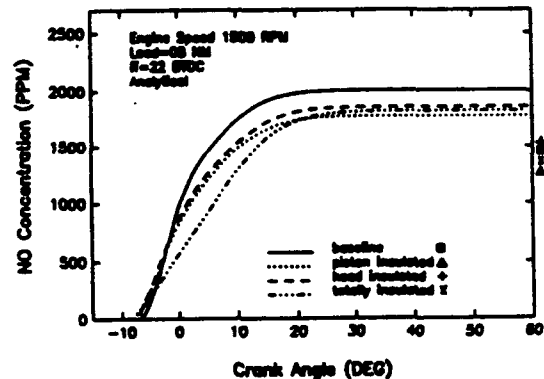
Figure 4.24(d)

Nitric Oxide Concentration Versus Crank Angle

Figure 4.24

KIVA Results for 1500 RPM, 22 DBTDC and 223 KPa BMEP Load (8 NM Torque)
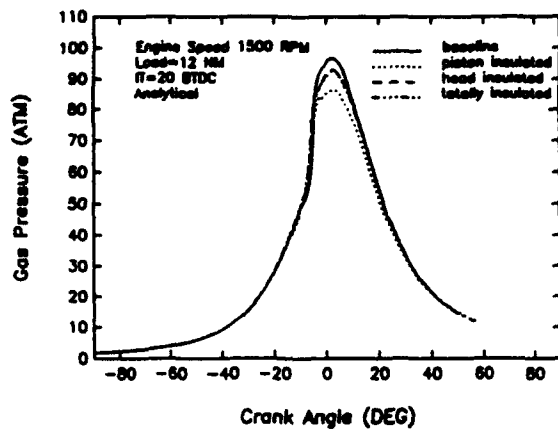
Figure 4.25(a)

Cylinder Gas Pressure Versus Crank Angle
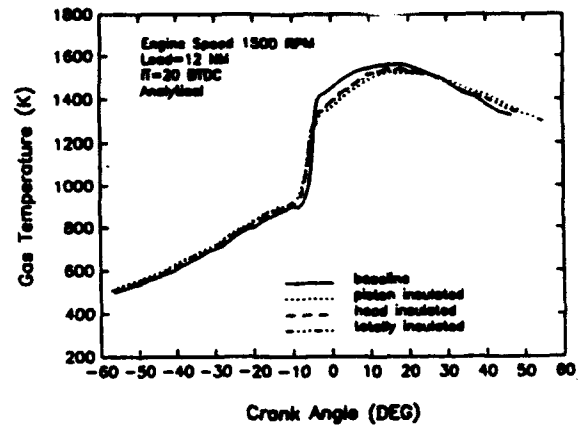
Figure 4.25(b)

Cylinder Gas Temperature Versus Crank Angle
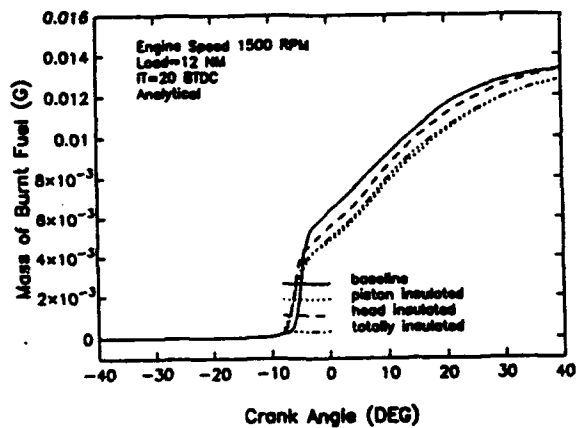
Figure 4.25(c)

Mass of Fuel Burnt Versus Crank Angle
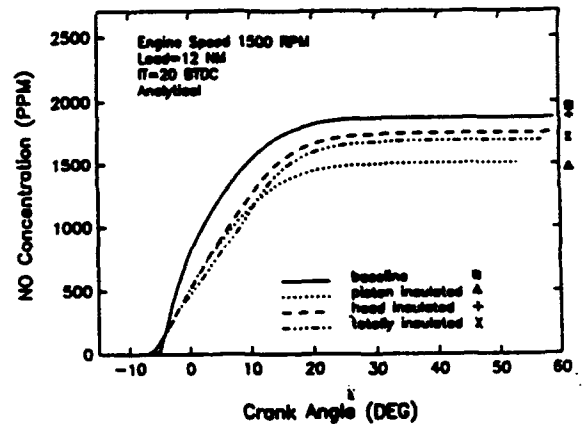
Figure 4.25(d)

Nitric Oxide Concentration Versus Crank Angle

Figure 4.25

KIVA Results for 1500 RPM, 20 DBTDC and 335 KPa BMEP Load (12 NM Torque)
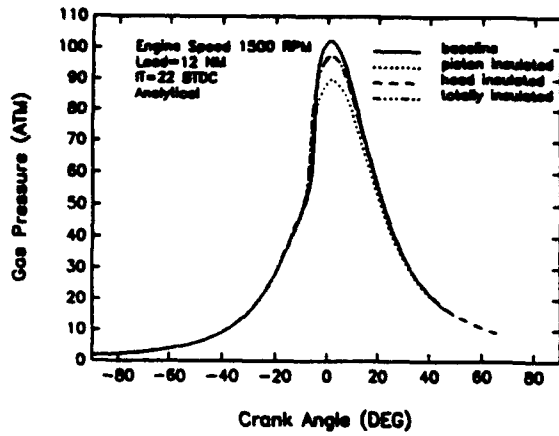
Figure 4.26(a)

Cylinder Gas Pressure Versus Crank Angle
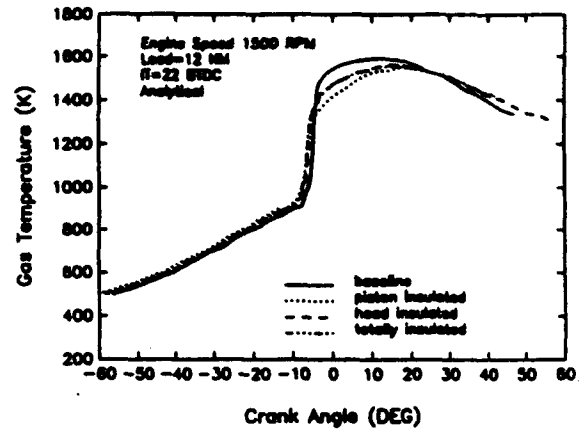
Figure 4.26(b)

Cylinder Gas Temperature Versus Crank Angle
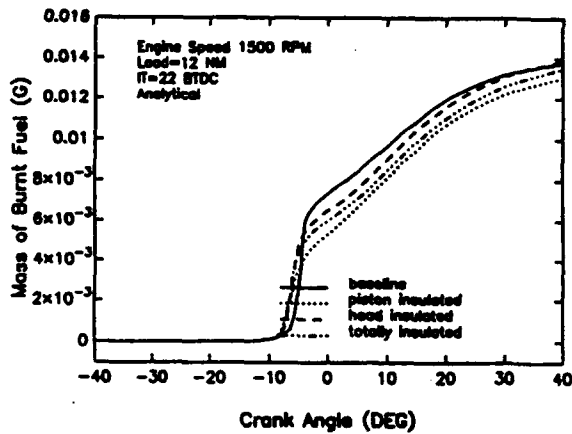
Figure 4.26(c)

Mass of Fuel Burnt Versus Crank Angle
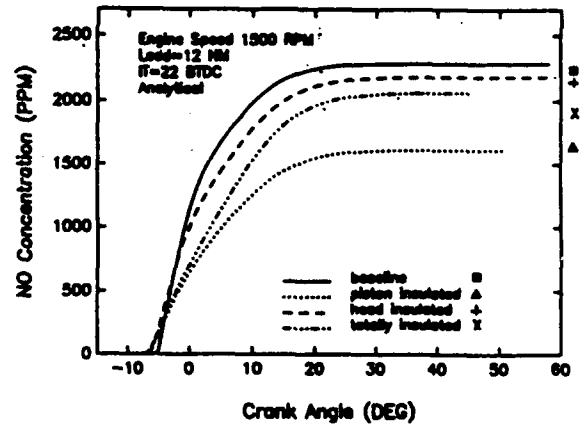
Figure 4.26(d)

Nitric Oxide Concentration Versus Crank Angle

Figure 4.26

KIVA Results for 1500 RPM, 22 DBTDC and 335 KPa BMEP Load (12 NM Torque)
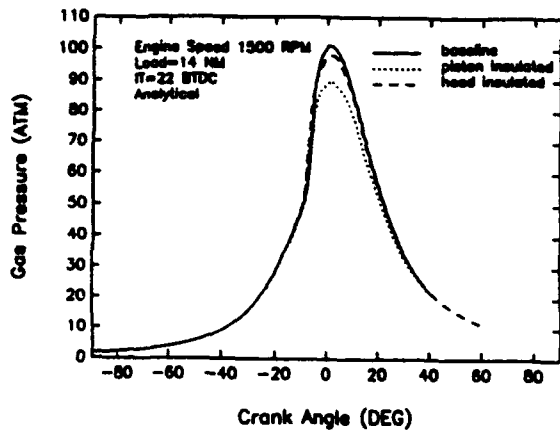
Figure 4.27(a)

Cylinder Gas Pressure Versus Crank Angle
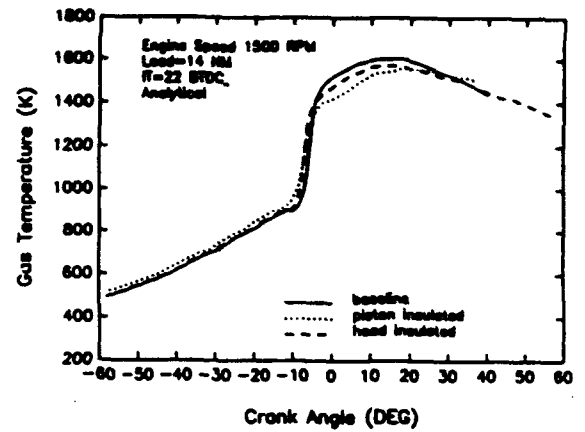
Figure 4.27(b)

Cylinder Gas Temperature Versus Crank Angle
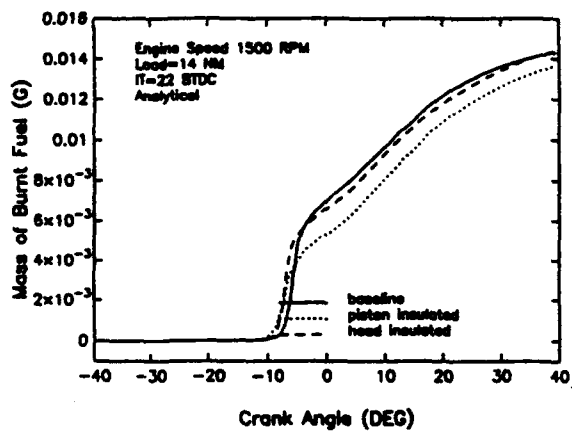
Figure 4.27(c)

Mass of Fuel Burnt Versus Crank Angle
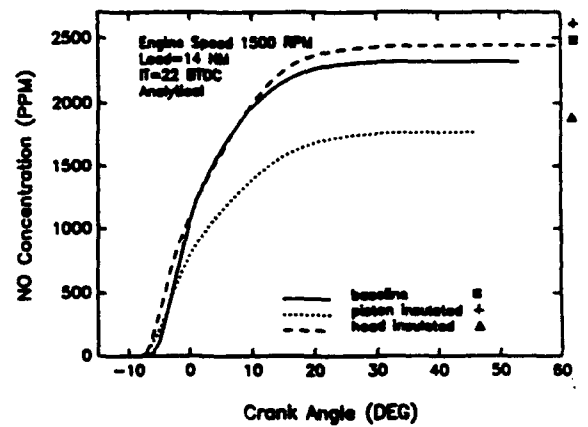
Figure 4.27(d)

Nitric Oxide Concentration Versus Crank Angle

Figure 4.27

KIVA Results for 1500 RPM, 22 DBTDC and 391 KPa BMEP Load (14 NM Torque)
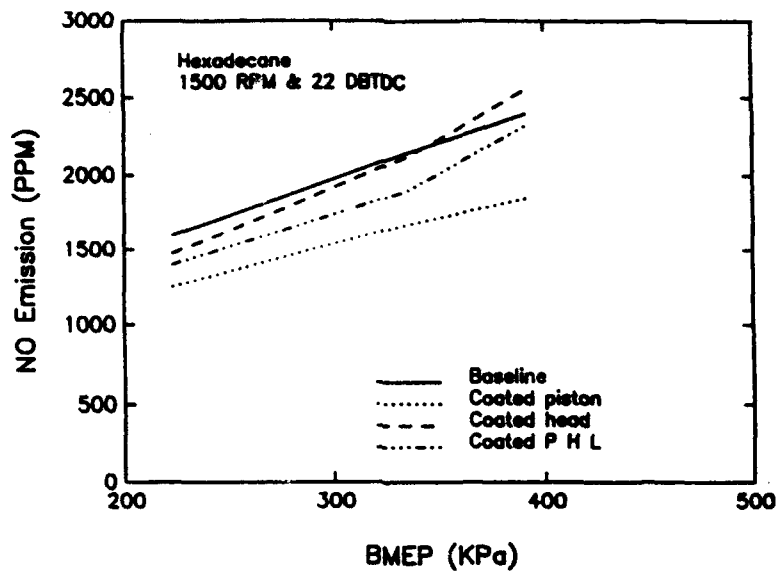
Figure 4.28

Experimental Results For NO Emission Versus Load
For Hexadecane at 1500 RPM and 22 DBTDC Injection Timing
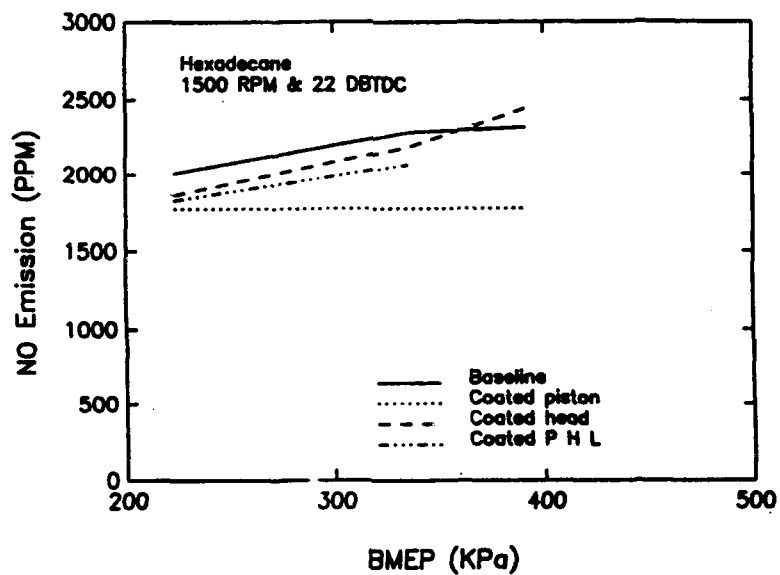
Figure 4.29

KIVA Results For NO Emission Versus Load
For Hexadecane at 1500 RPM and 22 DBTDC Injection Timing

REFERENCES

1. Dickey, D. W., "The Effect of Insulated Combustion Chamber Surfaces on DI Diesel Engine Performance, Emissions, and Combustion", SAE Paper 890292, 1989.

2. Assanis, D., et. al, "The Effect of Ceramic Coatings on Diesel Engine Performance and Exhaust Emissions", SAE Paper 910460, 1991.

3. Miyairi, Y., et. al, "Selective Heat Insulation of Combustion Chamber Walls for a DI Diesel Engine With Monolithic Ceramics", SAE Paper 890141, 1989.

4. Alkidas, A.C., "Performance and Emissions Achievements with an Uncooled Heavy Duty Single Cylinder Diesel Engine", SAE Paper 890144, 1989.

5. Thring, R.H., "Low Heat Rejection Engines", SAE Paper 860314, 1986.

6. Kamo, R., Assanis, D.N. and Bryzik, W., "Thin Thermal Barrier Coatings for Engines", SAE Paper 890143, 1989.

7. Kamo, R. and Bryzik W., "Cummins/ TACOM Advanced Adiabatic Engines", SAE Paper 840428, 1984.

8. Smavik, B.M. "Thermal Barrier Influence on Performance and Heat Transfer of a Medium Speed Two-Stroke Diesel Engine", SAE Paper 880435, 1988.

9. Heywood, J.B., *Internal Combustion Engines Fundamentals*", McGraw Hill Book Company, NY, 1988.

10. Daby, E.E., Garwin, I.J., Havstad, P.H. and Hunter, C.E., "Research Program on Reduced Combustion Chamber Heat Loss Effects on Alternative Fuel Combustion", Oak Ridge National Laboratory Report, ORNL/Sub/87-95918/1, Oak Ridge, TN, 1988.

11. "Diesel Engine Smoke Measurement", SAE Information Report, SAE J255a, 1978.

12. Morel, T., Fort, E.F. and Blumberg, P.N., "Effect of Insulation Strategy and Design Parameters on Diesel Engine Heat Rejection and Performance", SAE Paper 850506, 1985.

13. Amsden, A.A., O'Rourke, P.J., and Butler, T.D., "KIVA-II: A Computer Program for Chemically Reactive Flows with Sprays", Los Alamos National Laboratory Report LA-11560-MS, May, 1989.

14. Amsden, A.A., Ramshaw, J.D., O'Rourke, P.J., and Dukowicz, J.K., "KIVA: A Computer Program for Two-and-Three-Dimensional Fluid Flows With Chemical Reactions and Fuel Sprays", Los Alamos National Laboratory report LA-10245-MS, February, 1985.

15. Amsden, A.A., Ramshaw, J.D., Cloutman, L.D., and O'Rourke, P.J., "Improvements and Extensions to the KIVA Computer Program", Los Alamos National Laboratory report LA-10534-MS, October, 1985.

16. Amsden, A.A., Butler, T.D., O'Rourke, P.J., and Ramshaw, J.D., "KIVA - A Comprehensive Model for 2-D and 3-D Engine Simulations", SAE Paper 850554, 1985.

17. O'Rourke, P.J., and Amsden, A.A., "Three Dimensional Numerical Simulations of the UPS-292 Stratified Charge Engine", SAE 870597, 1987.

18. Gentry, R.A., Daly, B.J. and Amsden, A.A., "KIVA-COAL: A Modified Version of the KIVA Program for Calculating the Combustion Dynamics of a Coal-Water Slurry in a Diesel Engine Cylinder", Los Alamos National Laboratory report LA-11045-MS, 1987.

19. Naber, J.D. and Reitz, R.D., "Modeling Engine Spray/Wall Impingement", SAE Paper 880107, 1988.

20. Kuo, T.W. and Reitz, R.D., "Computation of Premixed-Charge Combustion in Pancake and Pent-Roof Engine", SAE Paper 890670, 1989.

21. Reitz, R.D., and Diwakar, R., "Structure of High-Pressure Fuel Sprays", SAE Paper 870598, 1987.

22. Pinchon, P., "Three Dimensional Modeling of Combustion in a Prechamber Diesel Engine", SAE Paper 890666, 1989.

23. Zellat, M., Rolland, Th. and Poplow, F., "Three Dimensional Modeling of Combustion and Soot Formation in an Indirect Injection Diesel Engine", SAE Paper 900254, 1990.

24. Gibson, D.H., Mahaffey III, W.A. and Mukerjee, T., "In Cylinder Flow and Combustion Modeling of 1.7 Caterpillar Engine", SAE Paper 900253, 1990.

25. Varnavas, C.A., and Assanis, D.N., "Combustion Studies in a Diesel Engine Using a Multidimensional Engine Simulation", ASME 91-ICE-2, 1991.

26. Ramos, J.I., "*Internal Combustion Engine Modeling*", Hemisphere Publishing Co., 1989.

27. Markatos, N. C., "*Computer Simulation for Fluid Flow, Heat and Mass Transfer, and Combustion in Reciprocating Engines*", Hemisphere Publishing Corporation, 1989.

28. Magnussen, B.F. and Hjertager, B.H., "On Mathematical Modeling of Turbulent Combustion with Special Emphasis on Soot Formation and Combustion", 16th Symposium (International) on Combustion, pp. 719-729, The Combustion Institute, Pittsburgh, 1979.

29. Magnussen, B.F., "The Rate of Combustion of Soot in Turbulent Flames", 13th Symposium (International) on Combustion, pp. 869-877, The Combustion Institute, Pittsburgh, 1971.

30. Magnussen, B.F., Hjertager, B.H., Olsen, J.G. and Bhaduri, D., "Effect of Turbulent Structure and Local Concentrations on Soot Formation and Combustion in C_2H_2 Diffusion Flames", 17th Sympos. (Internat'l) on Combustion, pp. 1383-1393, The Combustion Institute, Pittsburgh, 1979.

31. Magnussen, B.F., "An Investigation Into the Behavior of Soot in Turbulent Free Jet C_2H_2 - Flame", 15th Sympos. (Int.) on Combustion, p. 1415, The Combust. Inst., Pittsburgh, 1975.

32. Tesner, P.A., Snegiriova, T.D., and Knorre, V.G., "Kinetics of Dispersed Carbon Formation", Combustion and Flame, Vol 17, 253-260, 1971.

33. Tesner, P.A., Tsygankova, E.I., Guilazetdinov, L.P., Zuyev, V.P. and Loshakova, G.V., "The Formation of Soot From Aromatic Hydrocarbon-Hydrogen Mixtures", Combustion and Flame, vol 17, 279-285, 1971.

34. Spalding, D.B., "Development of the Eddy-Break-Up Model of Turbulent Combustion", 16th Symposium (International) on Combustion, pp. 1659-1663, The Combustion Institute, 1977.

35. Spalding, D.B., "Mixing and Chemical Reaction in Steady Confined Turbulent Flames", 13th Symposium (Int.) on Combustion, The Combustion Institute, pp. 649-657, 1971.

36. Gosman, A.D., and Harvey, P.S., "Computer Analysis of Fuel Air Mixing and Combustion in an Axisymmetric D.I. Diesel Engine", SAE Paper 820036, 1982.

37. Zeldovich, Y.B. et. al, "Oxidation of Nitrogen in Combustion", Academy of Sciences of USSR, Institute of Chemical Physics, Moscow-Leningrad, 1974.

38. Lavoie, G.A., Heywood, J.B. and Keck, J.C., Combust. Sci. Technol., Vol. 1, p. 313, 1970.

39. Diwakar, R., "Multidimensional Modeling Applied to the Direct Injection Stratified-Charge Engine-Calculation Versus Experiment", SAE Paper 810225, 1981.

40. Haynes, B. S. and Wagner, H. G., "Soot Formation", Prog. Energy Combust. Sci., Vol 4, pp. 229-273, 1981.

41. Morel, T. and Keibar, R., "Heat Radiation in D.I Diesel engines", SAE Paper 860445, 1986.

42. Khan, I.M., Wang, C.H.T. and Langridge, B.E., "Coagulation and Combustion of Soot Particles in Diesel Engines", Comb. Flame, 17, 409-419, 1971.

43. Khan, I.M., Greeves, G. and Wang, C.H.T., "Factors Affecting Smoke and Gaseous Emissions from Direct Injection Diesel Engine and Method of Calculation", SAE 730163, 1973.

44. Nagle, J. and Strickland-Constable, R.F., "Oxidation of Carbon Between 1000-2000°C", Proc. of the Fifth Conference on Carbon, pp. 154-164, Pergamon Press, London 1962.

45. Lee, K.B., Thring, M.W., and Beer, J.M., "On the Rate of Combustion of Soot in Laminar Flames", Combustion and Flame, Vol. 6, 137-145, 1962.

46. Fenimore, C.P. and Jones, G.W., "Coagulation of Soot to Smoke in Hydrocarbon Flames", Combustion and Flame, 13, 303-310, 1969.

47. Hiroyasu, H., and Kadota, T., "Models for Combustion and Formation of Nitric Oxide and Soot in Diesel Engines", SAE Paper 760129, 1976.

48. Farmer, R., Edelman, R. and Wong, E., "Modeling Soot Emission in Combustion Systems", Proceedings of an International Symposium on Particulate Carbon: Formation During Combustion, General Motors Research Laboratories, Warren Michigan, October 15-16, 1980.

APPENDIX A

BSFC Data Plots
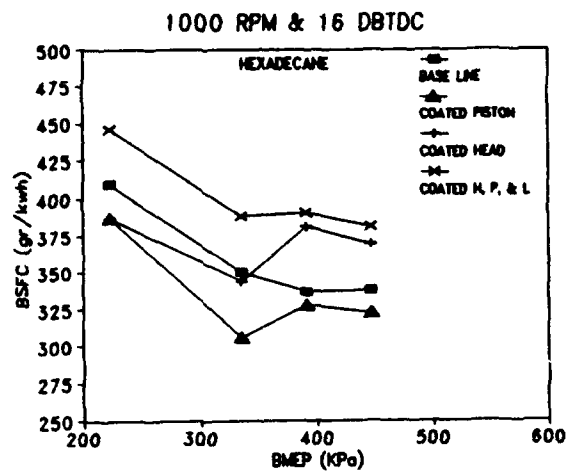
Fig A1(a)
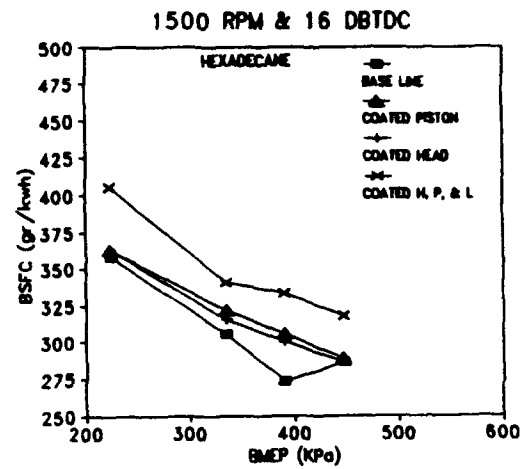
Fig A1(b)
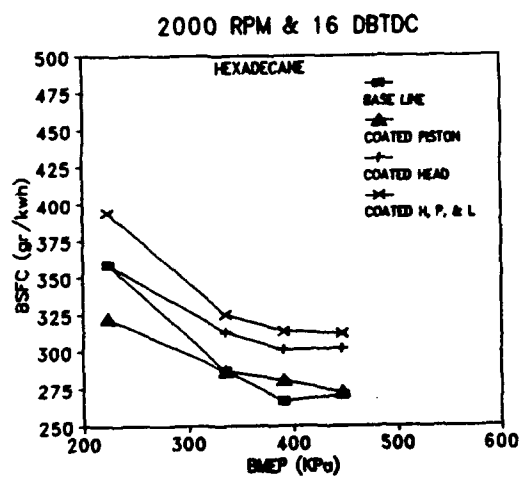
Fig A1(c)
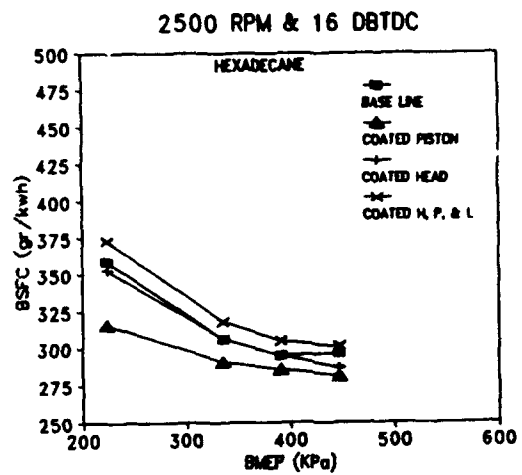
Fig A1(d)

Figure A1

BSFC Versus Load for Hexadecane Fuel at 16 Degrees BTDC
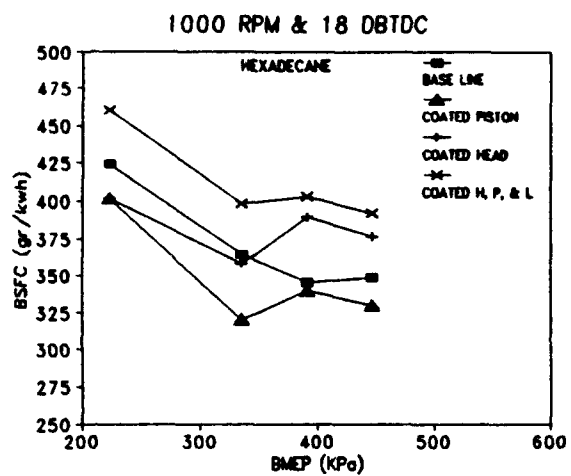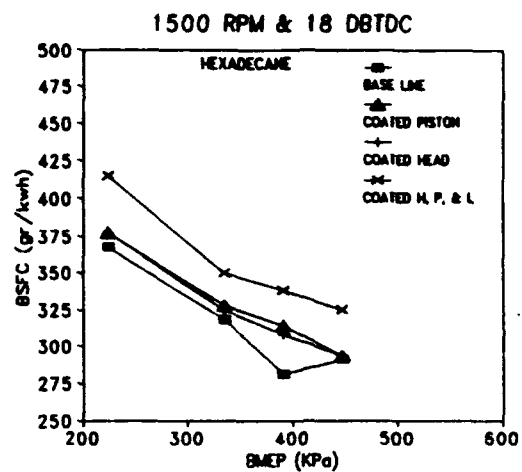
Fig A2(a) Fig A2(b)
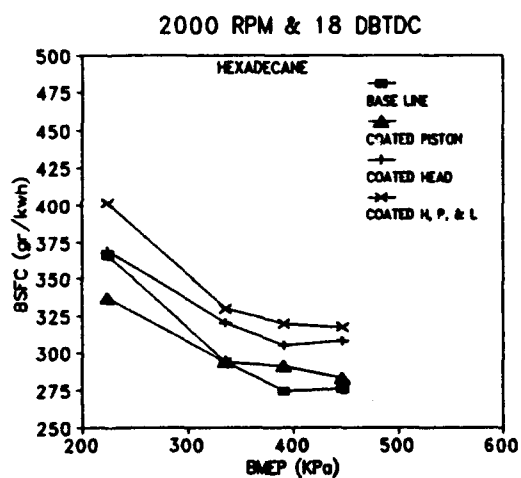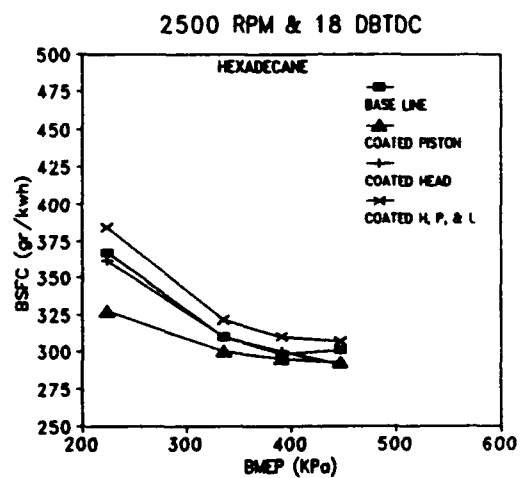
Fig A2(c) Fig A2(d)

Figure A2

BSFC Versus Load for Hexadecane Fuel at 18 Degrees BTDC
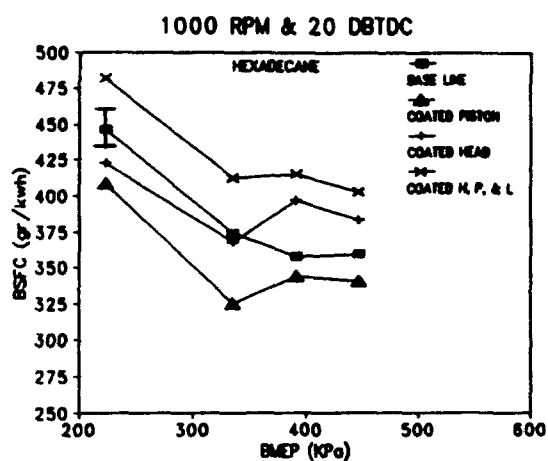
Fig A3(a)
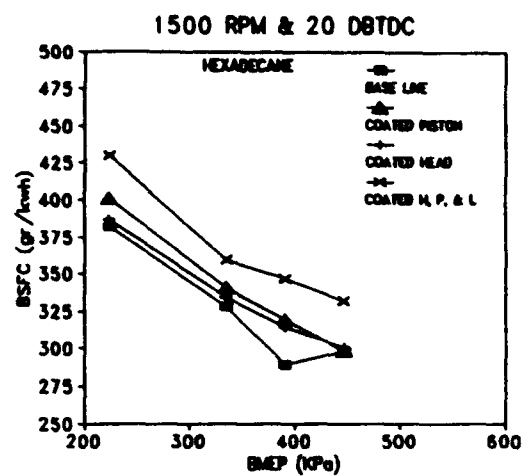
Fig A3(b)
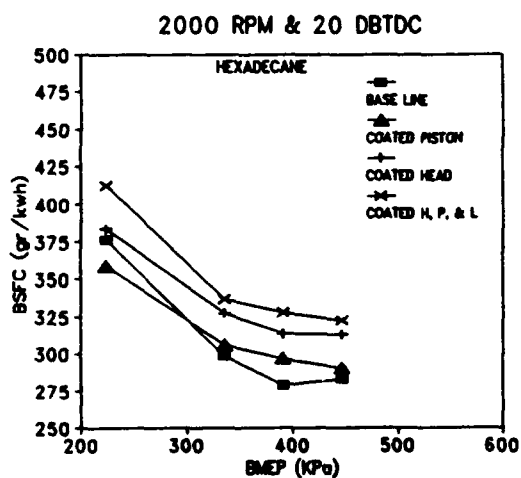
Fig A3(c)
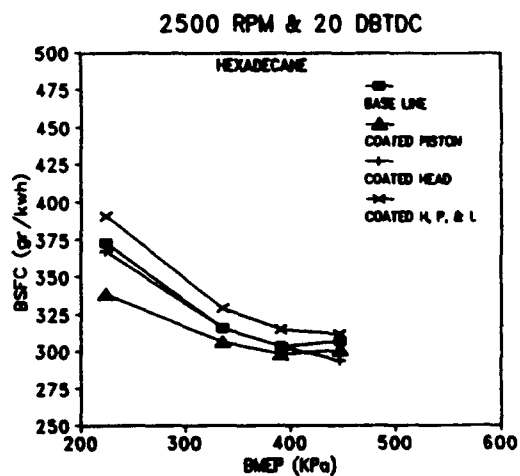
Fig A3(d)

Figure A3

BSFC Versus Load for Hexadecane Fuel at 20 Degrees BTDC

68
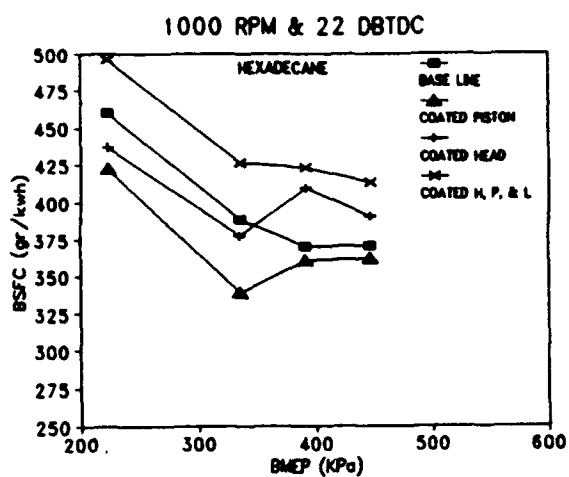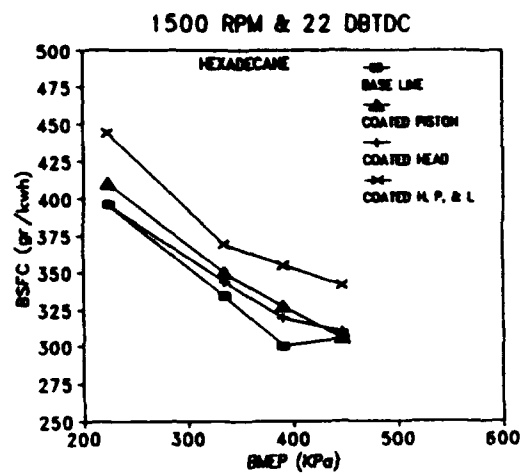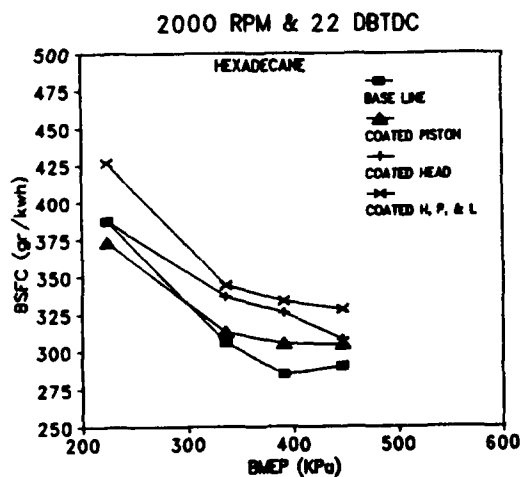
Fig A4(a)

Fig A4(b)

Fig A4(c)
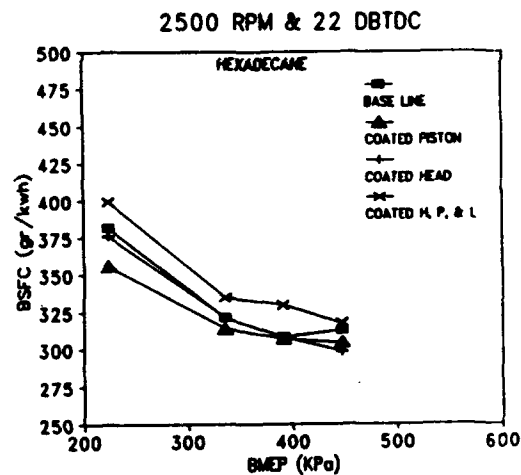
Fig A4(d)

Figure A4

BSFC Versus Load for Hexadecane Fuel at 22 Degrees BTDC
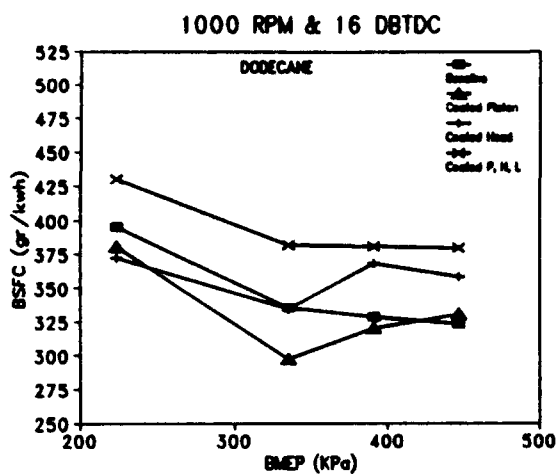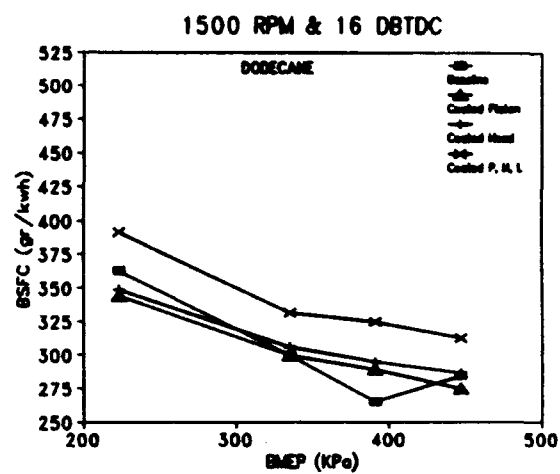
Fig A5(a)   Fig A5(b)
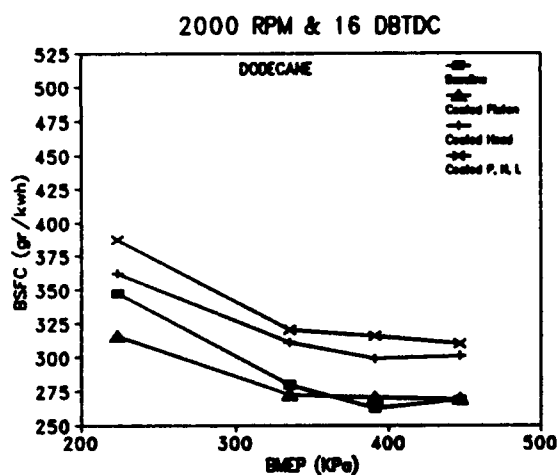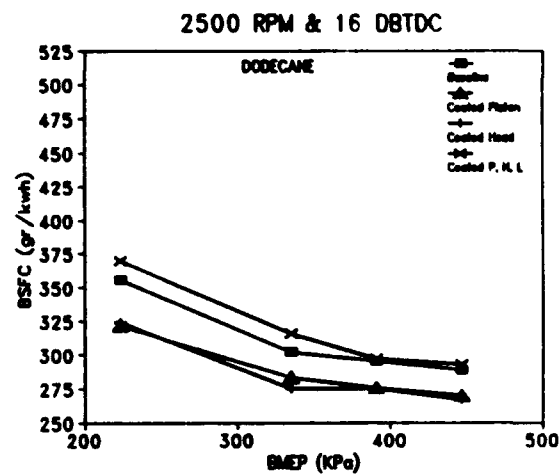

Fig A5(c)   Fig A5(d)

Figure A5

BSFC Versus Load for Dodecane Fuel at 16 Degrees BTDC
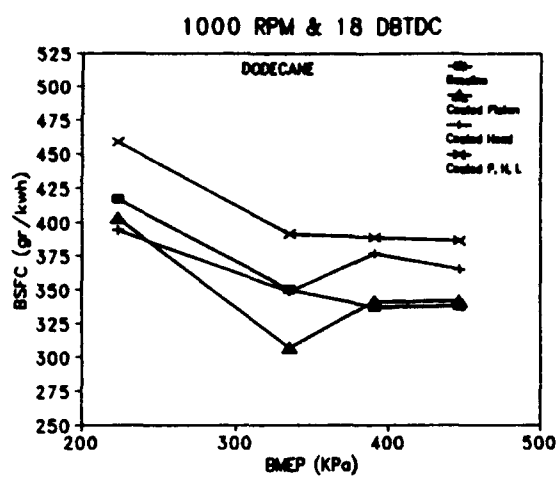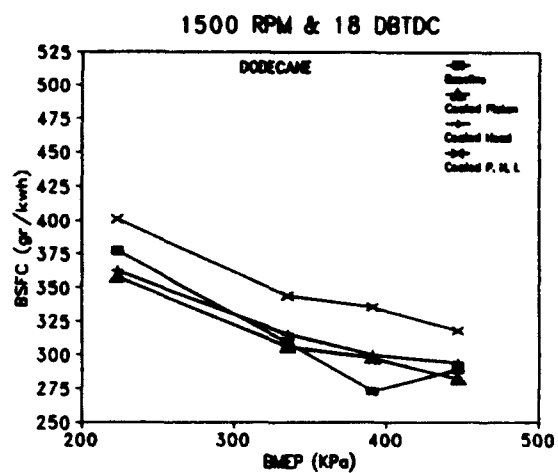
Fig A6(a)   Fig A6(b)
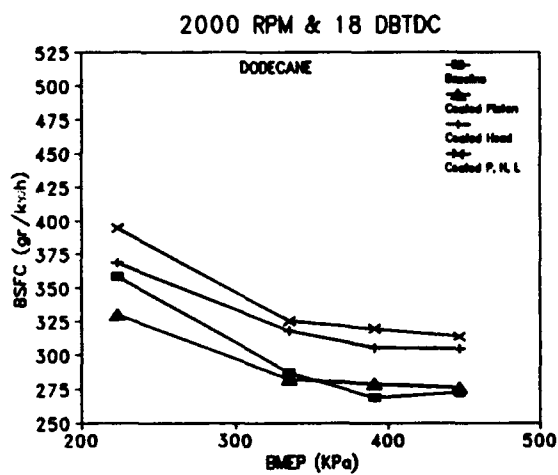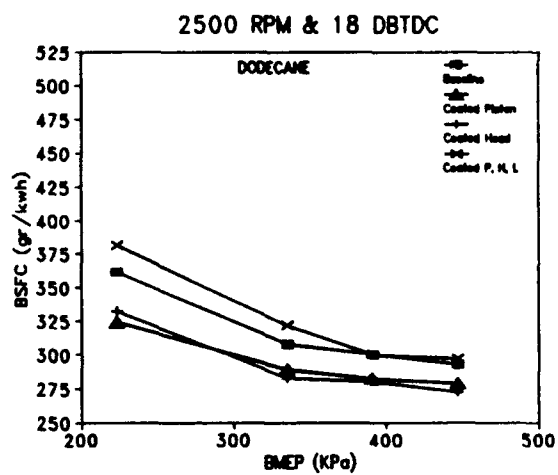
Fig A6(c)   Fig A6(d)

Figure A6

BSFC Versus Load for Dodecane Fuel at 18 Degrees BTDC

71
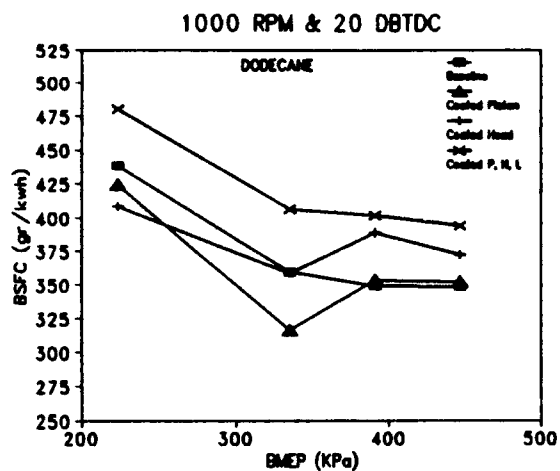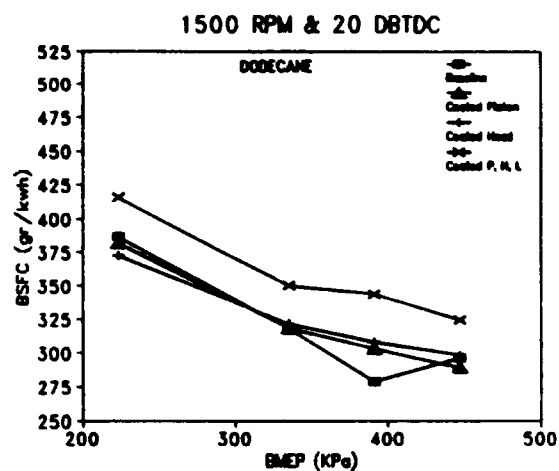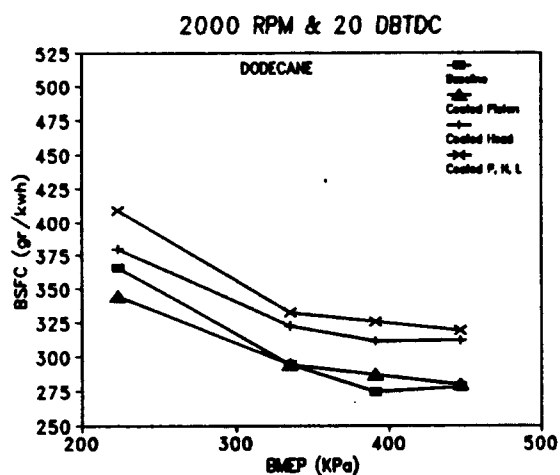
Fig A7(a)

Fig A7(b)

Fig A7(c)
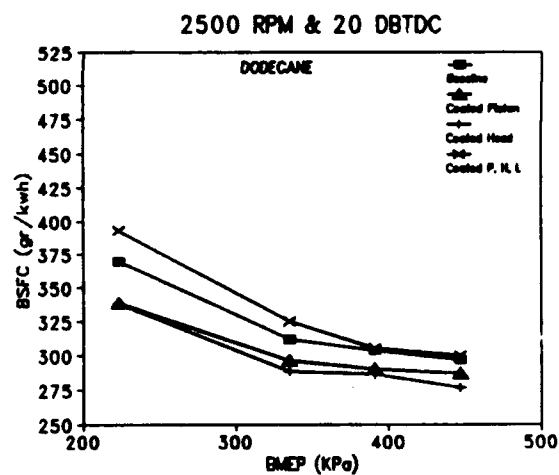
Fig A7(d)

Figure A7

BSFC Versus Load for Dodecane Fuel at 20 Degrees BTDC
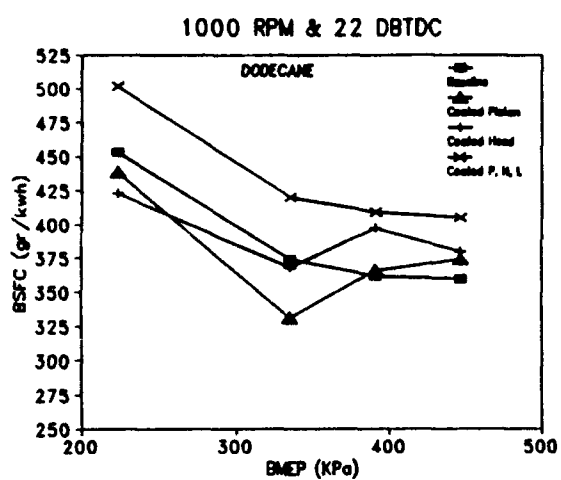
Fig A8(a)
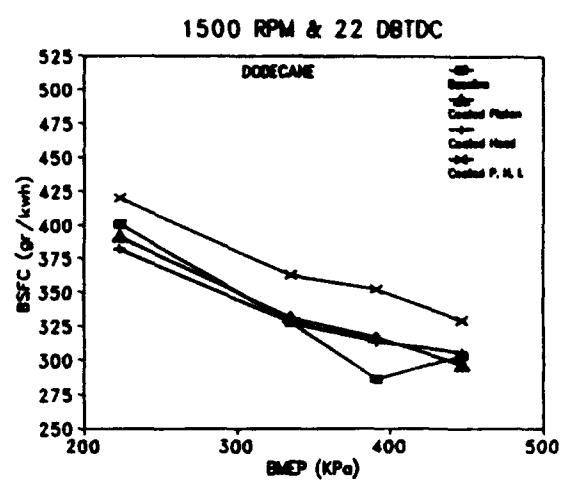
Fig A8(b)
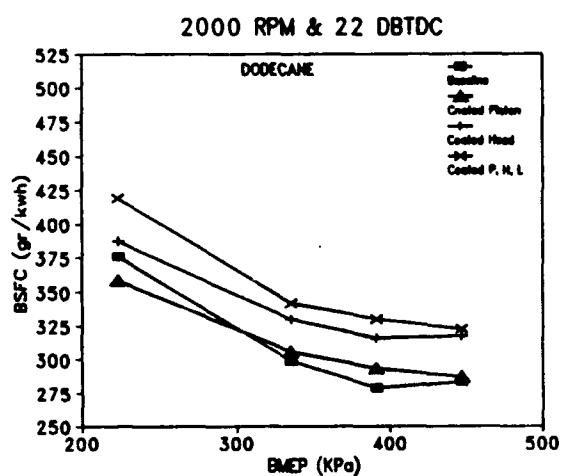
Fig A8(c)
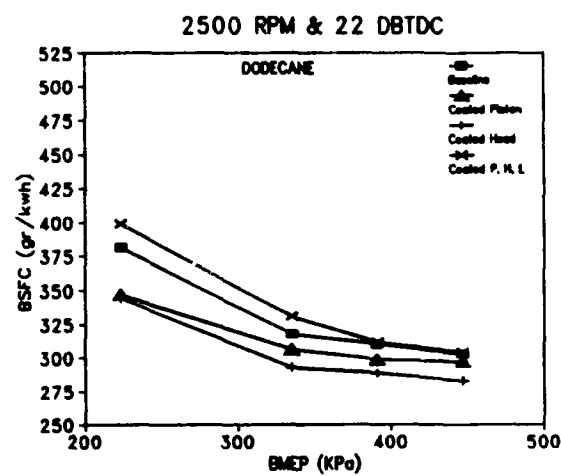
Fig A8(d)

Figure A8

BSFC Versus Load for Dodecane Fuel at 22 Degrees BTDC

73

APPENDIX B

NOx Data Plots
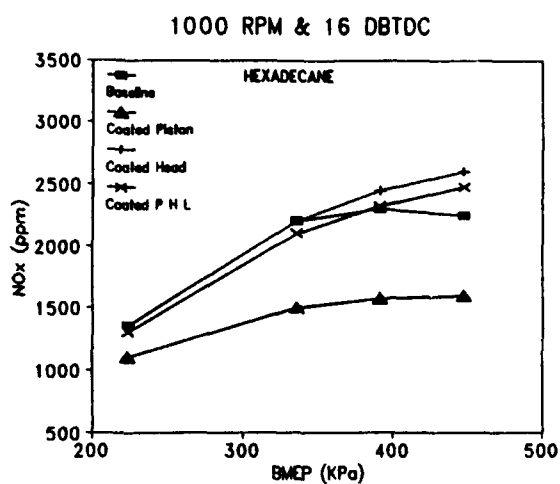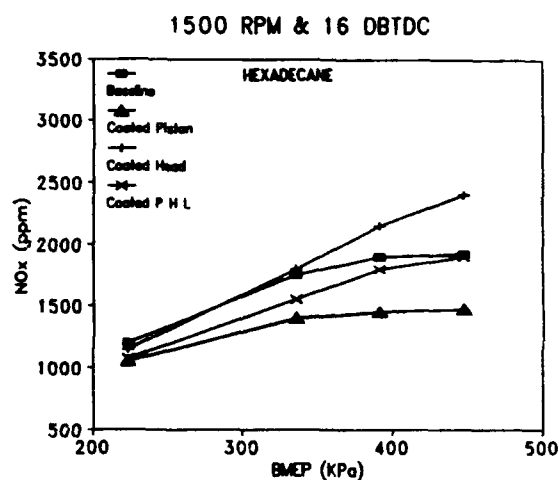
Fig B1(a)   Fig B1(b)
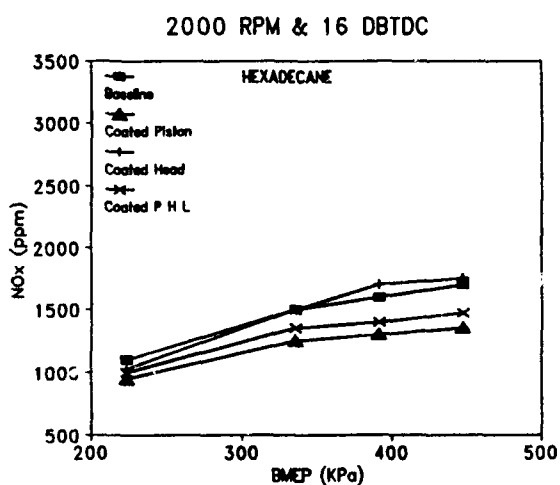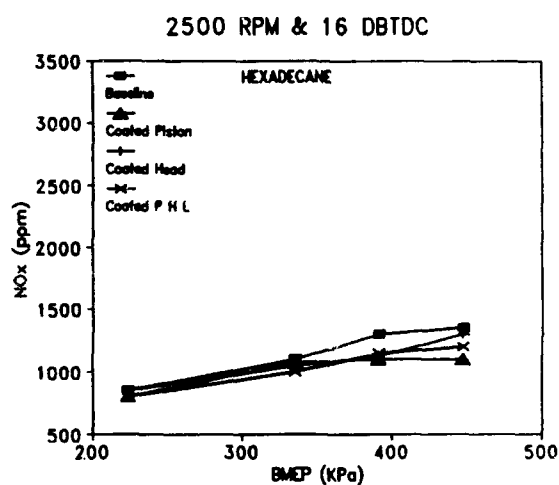
Fig B1(c)   Fig B1(d)

Figure B1

NOx Versus Load for Hexadecane Fuel at 16 Degrees BTDC
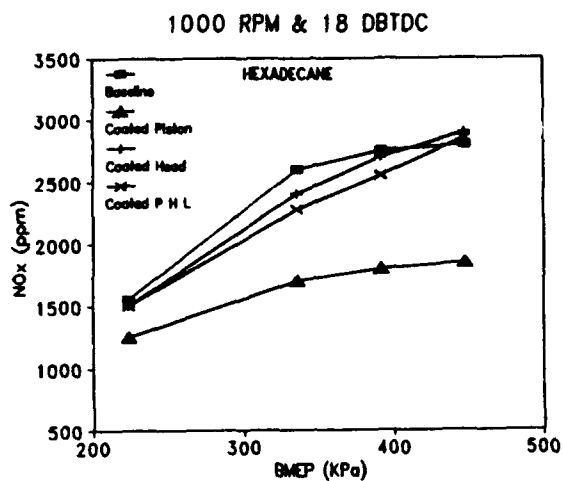
Fig B2(a)
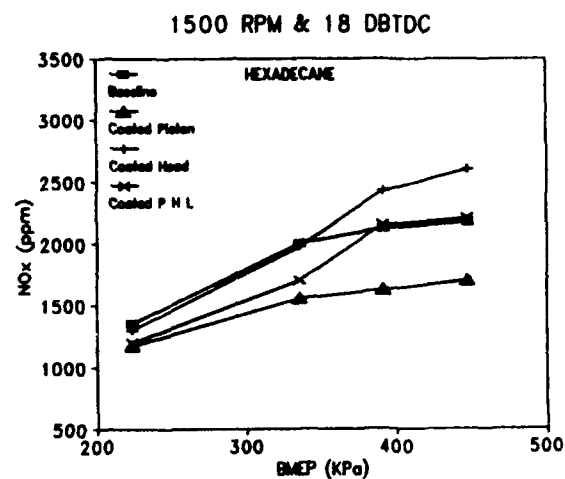
Fig B2(b)
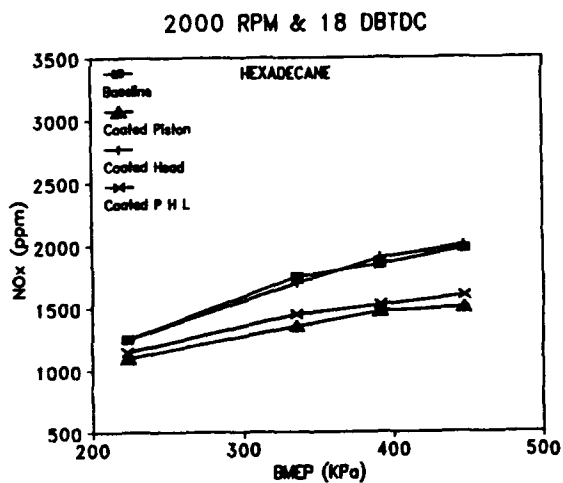
Fig B2(c)
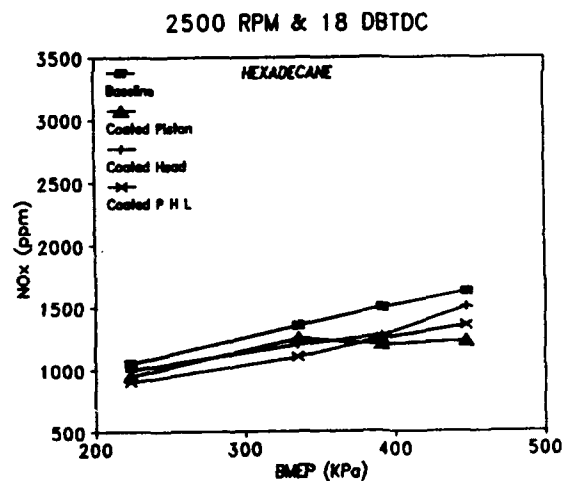
Fig B2(d)

Figure B2

NOx Versus Load for Hexadecane Fuel at 18 Degrees BTDC

76
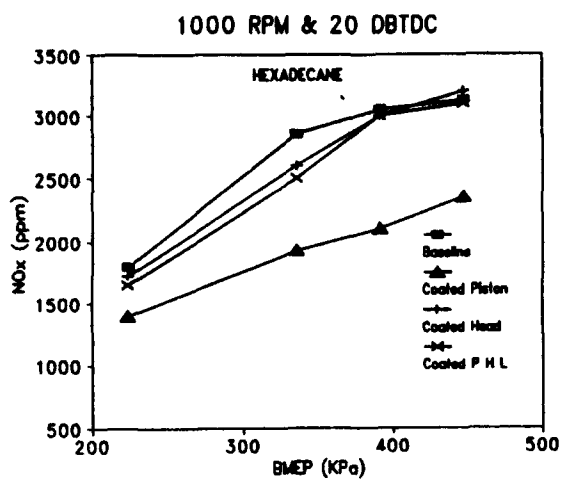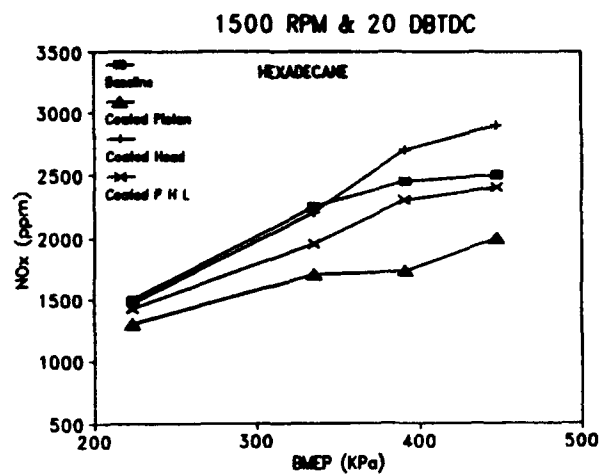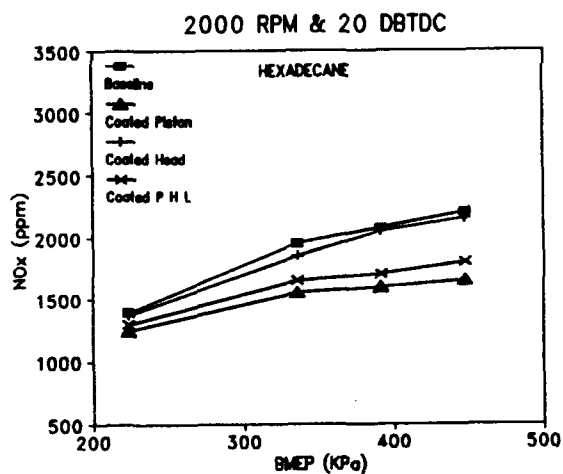
Fig B3(a)

Fig B3(b)

Fig B3(c)
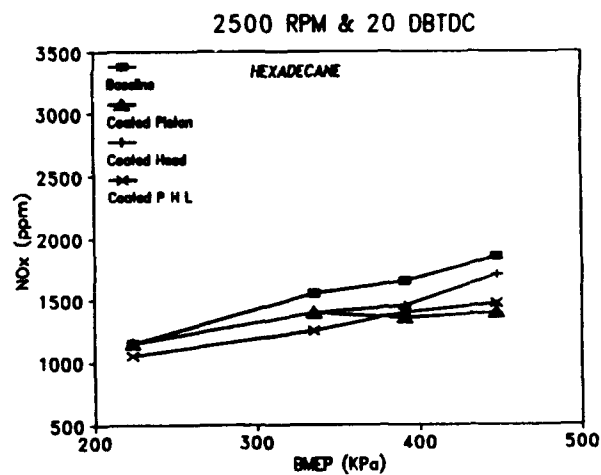
Fig B3(d)

Figure B3

NOx Versus Load for Hexadecane Fuel at 20 Degrees BTDC
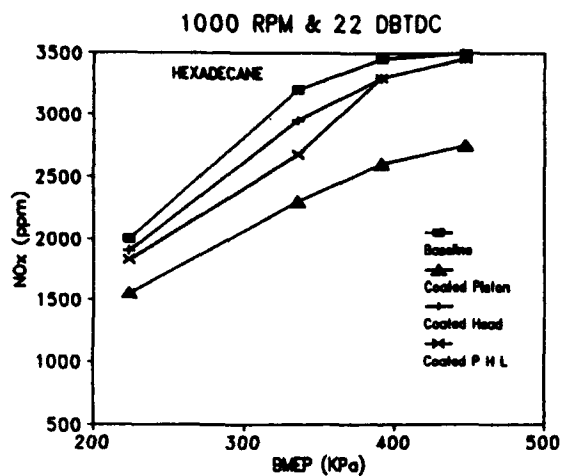
Fig B4(a)
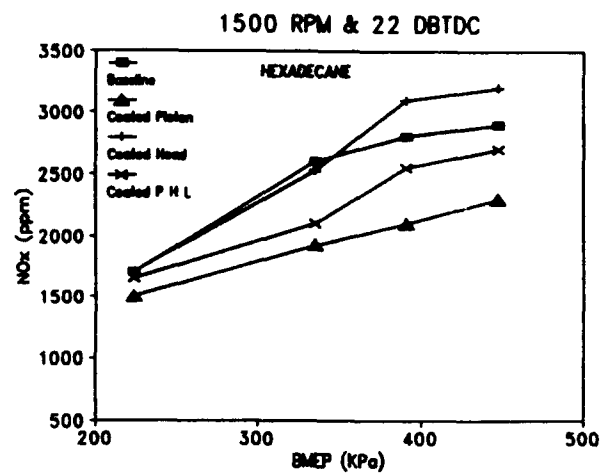
Fig B4(b)
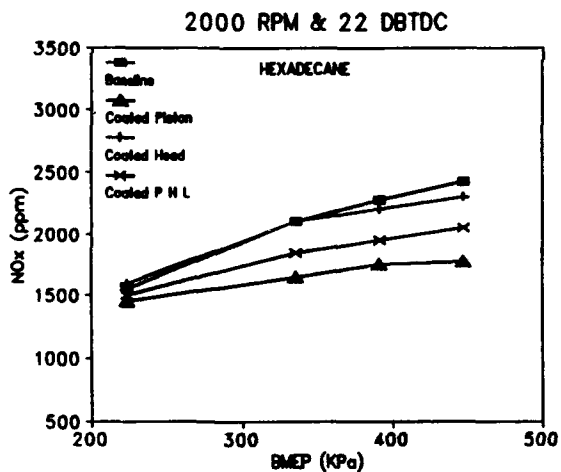
Fig B4(c)
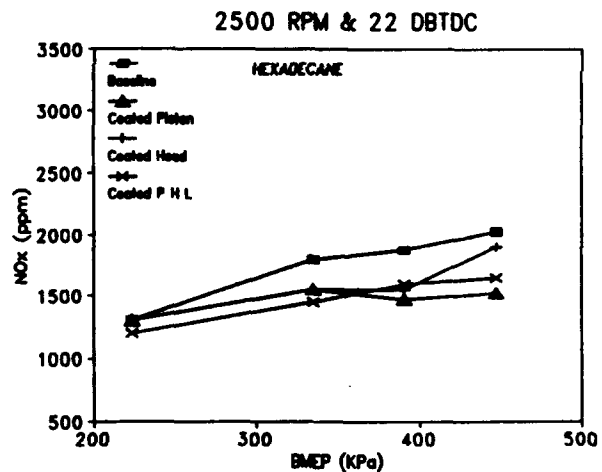
Fig B4(d)

Figure B4

NOx Versus Load for Hexadecane Fuel at 22 Degrees BTDC
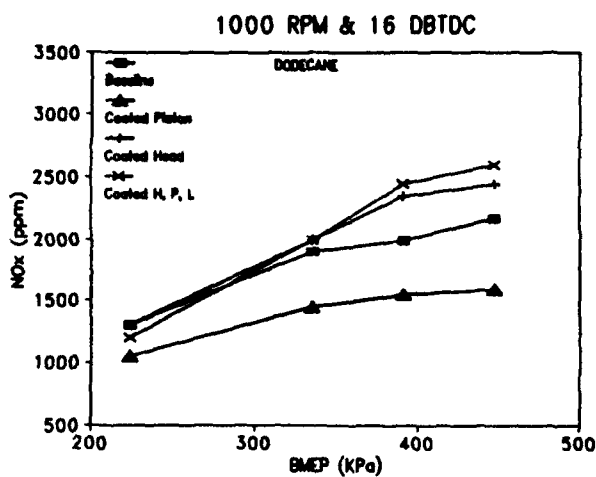
Fig B5(a)
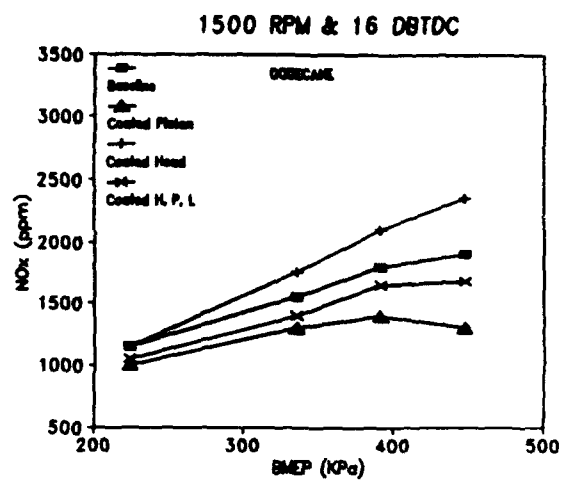
Fig B5(b)
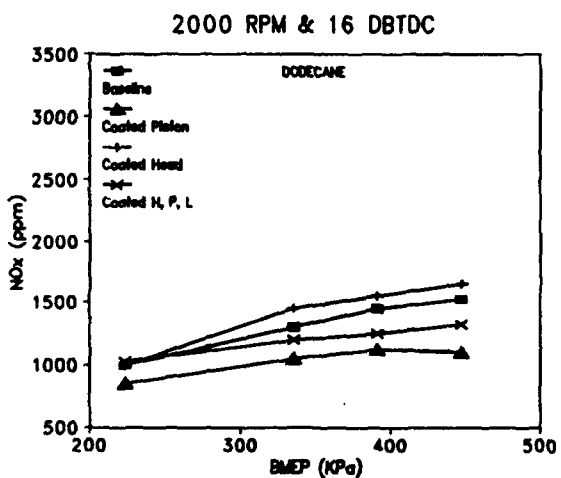
Fig B5(c)
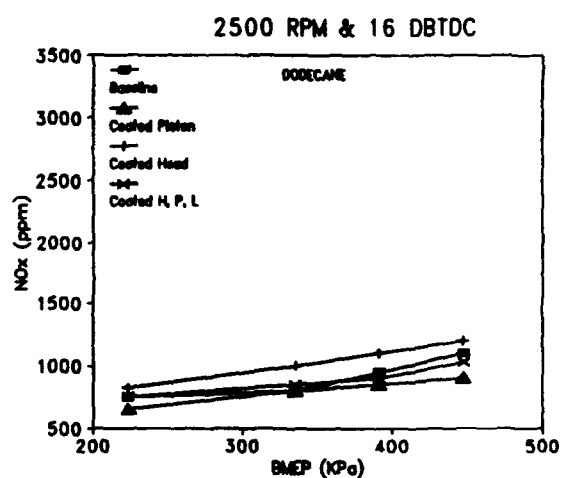
Fig B5(d)

Figure B5

NOx Versus Load for Dodecane Fuel at 16 Degrees BTDC

1000 RPM & 18 DBTDC

DODECANE

Baseline
Coated Piston
Coated Head
Coated H, P, L

NOx (ppm)

3500
3000
2500
2000
1500
1000
500

200   300   400   500

BMEP (KPa)

Fig B6(a)

1500 RPM & 18 DBTDC

DODECANE

Baseline
Coated Piston
Coated Head
Coated H, P, L

NOx (ppm)

3500
3000
2500
2000
1500
1000
500

200   300   400   500

BMEP (KPa)

Fig B6(b)

2000 RPM & 18 DBTDC

DODECANE

Baseline
Coated Piston
Coated Head
Coated H, P, L

NOx (ppm)

3500
3000
2500
2000
1500
1000
500

200   300   400   500

BMEP (KPa)

Fig B6(c)

2500 RPM & 18 DBTDC

DODECANE

Baseline
Coated Piston
Coated Head
Coated H, P, L

NOx (ppm)

3500
3000
2500
2000
1500
1000
500

200   300   400   500

BMEP (KPa)

Fig B6(d)

Figure B6

NOx Versus Load for Dodecane Fuel at 18 Degrees BTDC
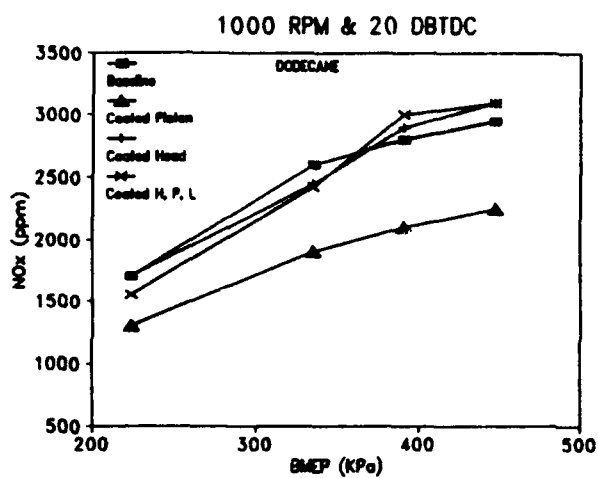
Fig B7(a)
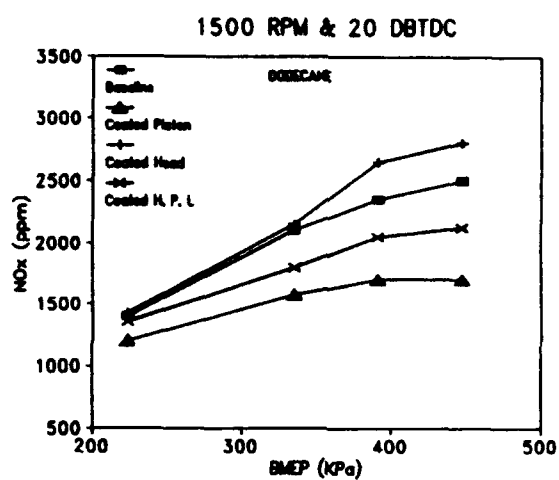
Fig B7(b)
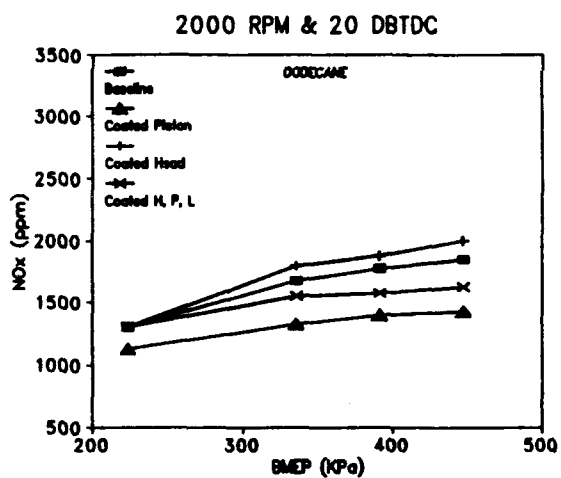
Fig B7(c)
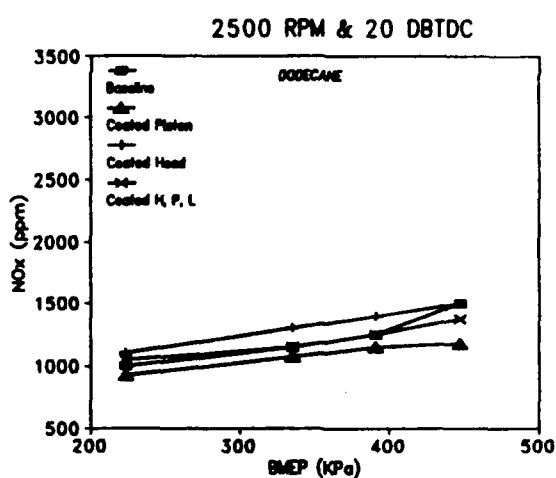
Fig B7(d)

Figure B7

NOx Versus Load for Dodecane Fuel at 20 Degrees BTDC
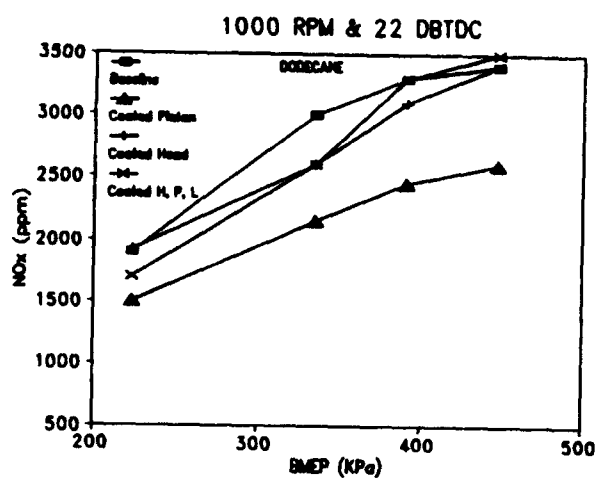
Fig B8(a)
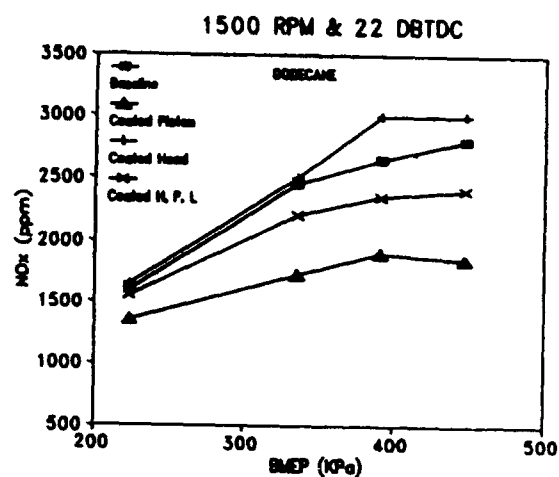
Fig B8(b)
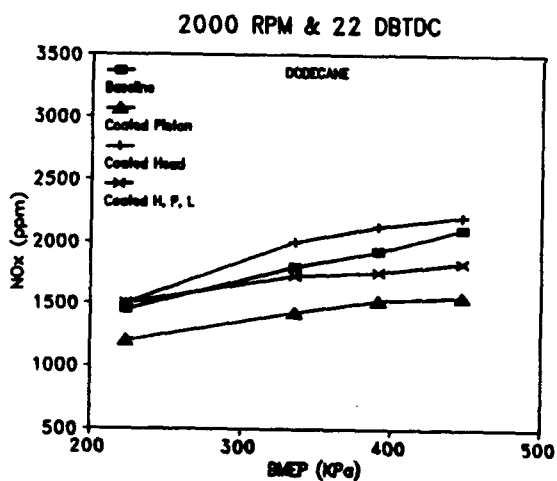
Fig B8(c)
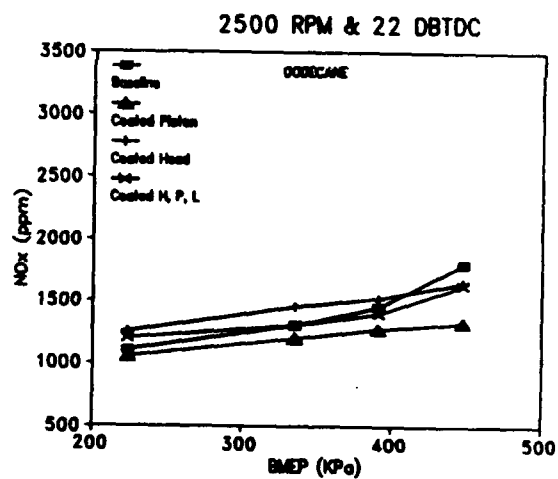
Fig B8(d)

Figure B8

NOx Versus Load for Dodecane Fuel at 22 Degrees BTDC

APPENDIX C

Ignition Delay Data Plots
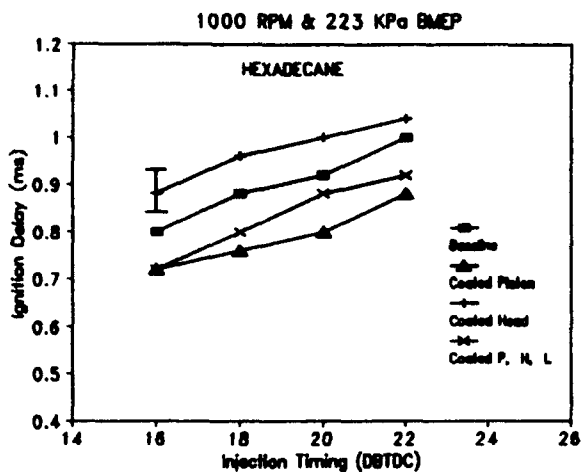
Fig C1(a)
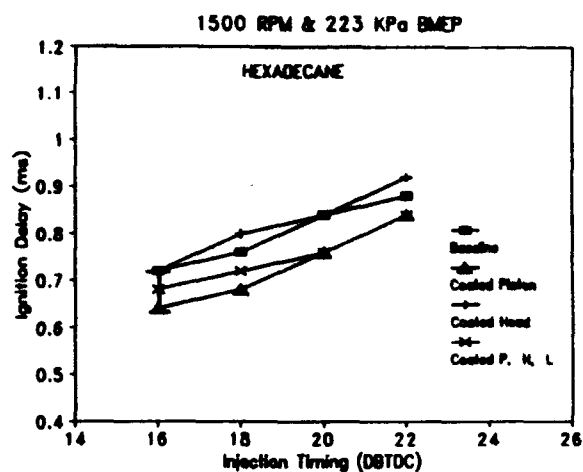
Fig C1(b)
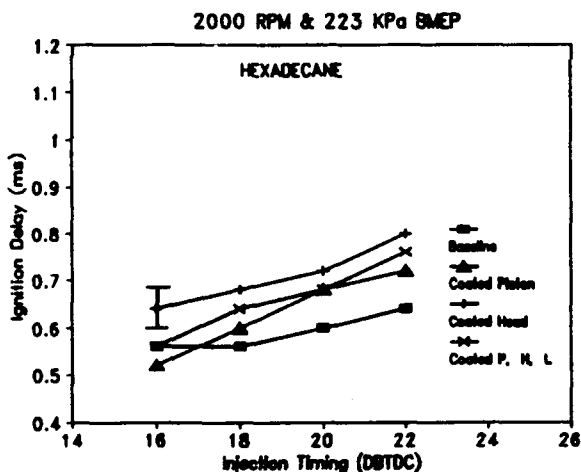
Fig C1(c)
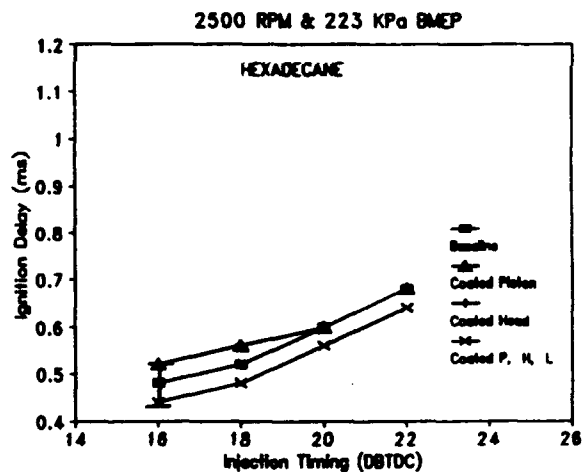
Fig C1(d)

Figure C1

Ignition Delay Versus Timing for Hexadecane Fuel at 223 KPa BMEP
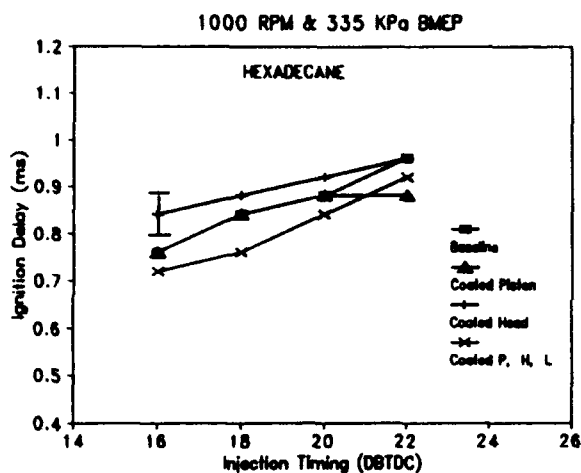
Fig C2(a)
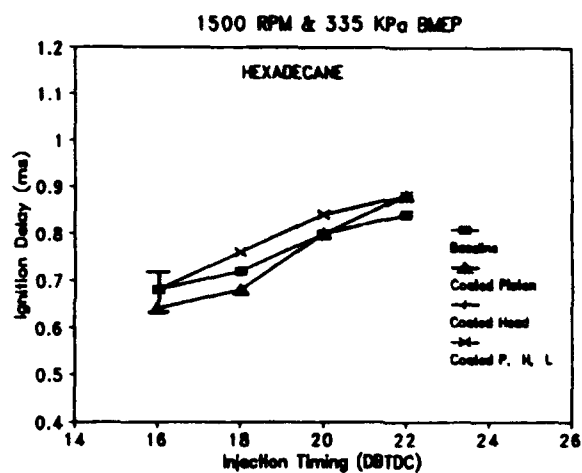
Fig C2(b)
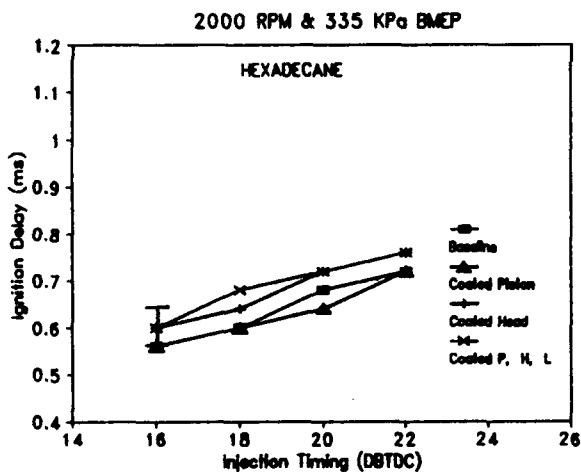
Fig C2(c)
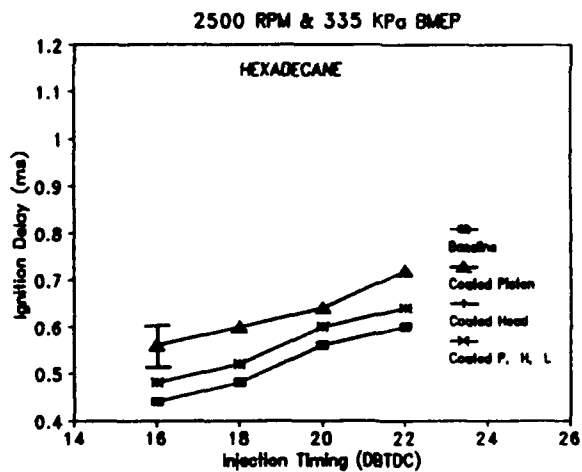
Fig C2(d)

Figure C2

Ignition Delay Versus Timing for Hexadecane Fuel at 335 KPa BMEP
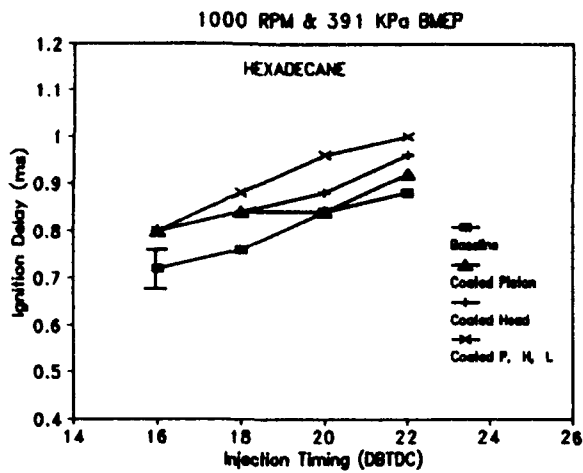
Fig C3(a)
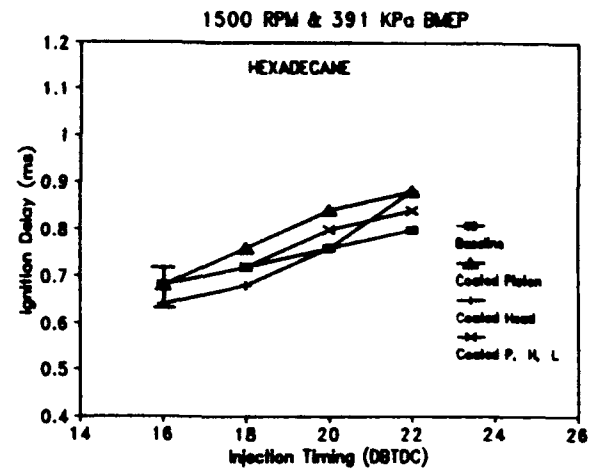
Fig C3(b)
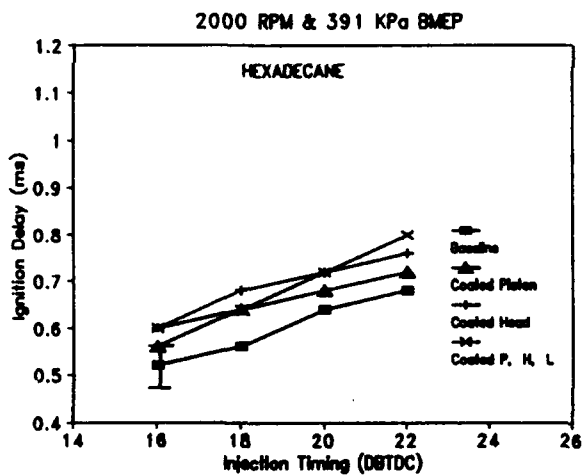
Fig C3(c)
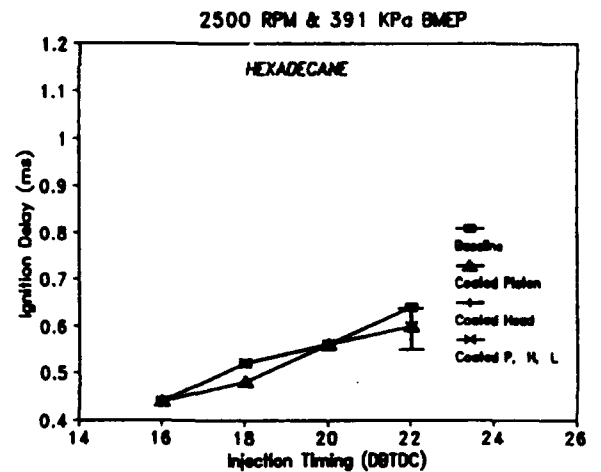
Fig C3(d)

Figure C3

Ignition Delay Versus Timing for Hexadecane Fuel at 391 KPa BMEP
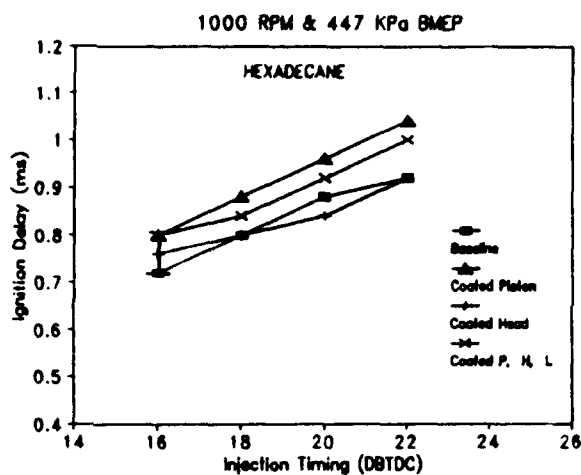
Fig C4(a)
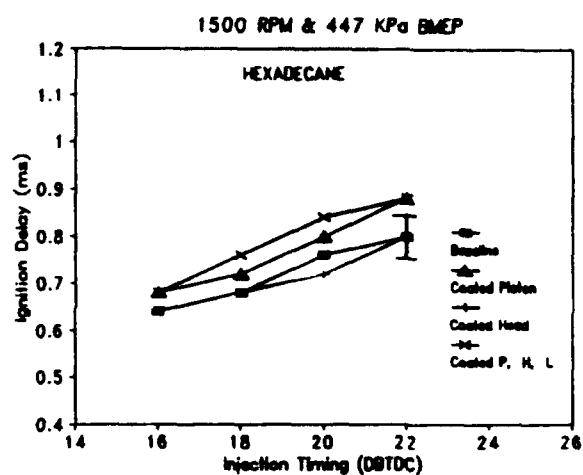
Fig C4(b)
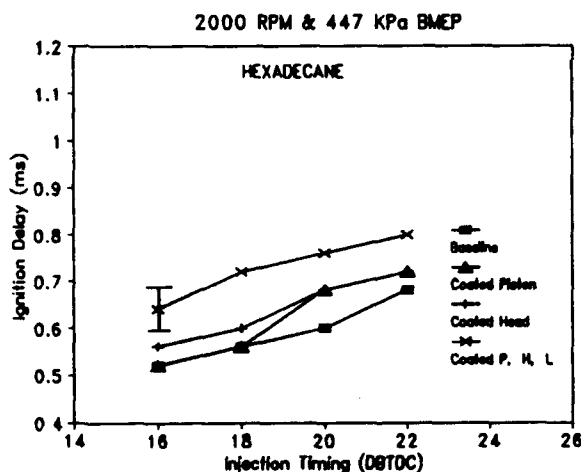
Fig C4(c)
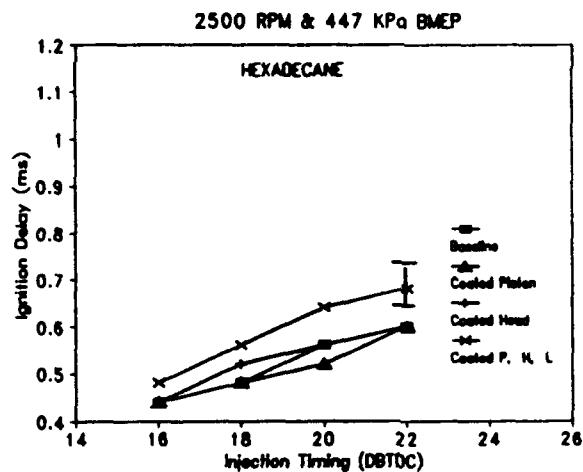
Fig C4(d)

Figure C4

Ignition Delay Versus Timing for Hexadecane Fuel at 447 KPa BMEP

1000 RPM & 223 KPa BMEP

1500 RPM & 223 KPa BMEP

Fig C5(a)

Fig C5(b)

2000 RPM & 223 KPa BMEP

2500 RPM & 223 KPa BMEP
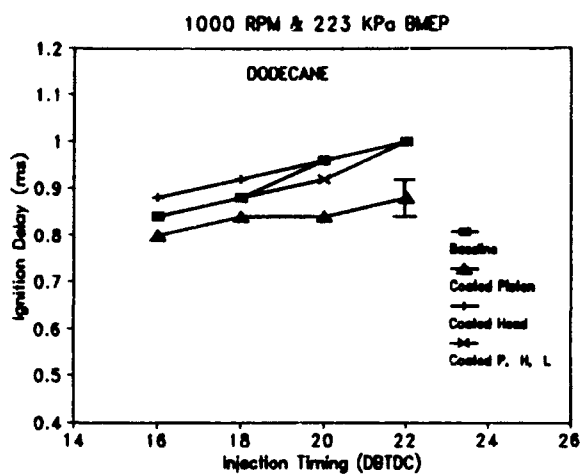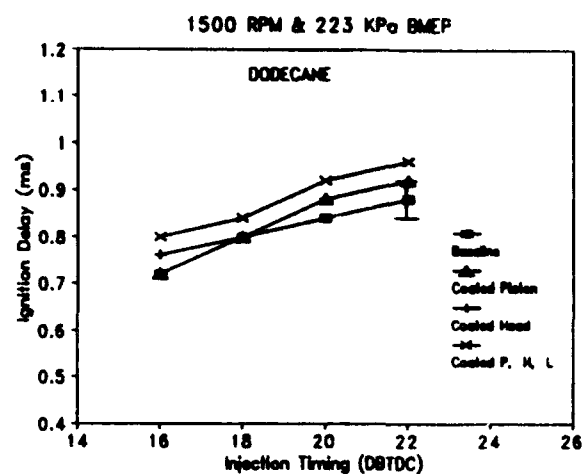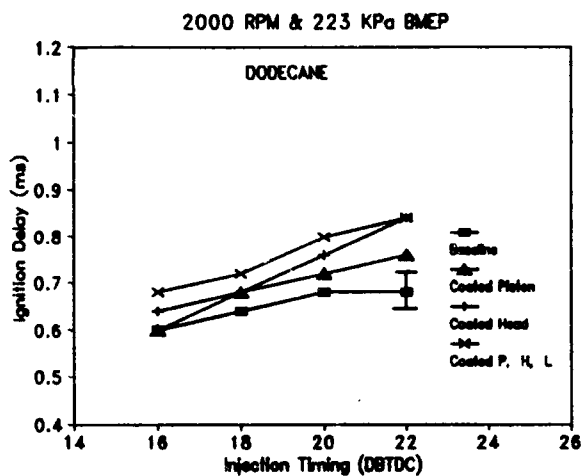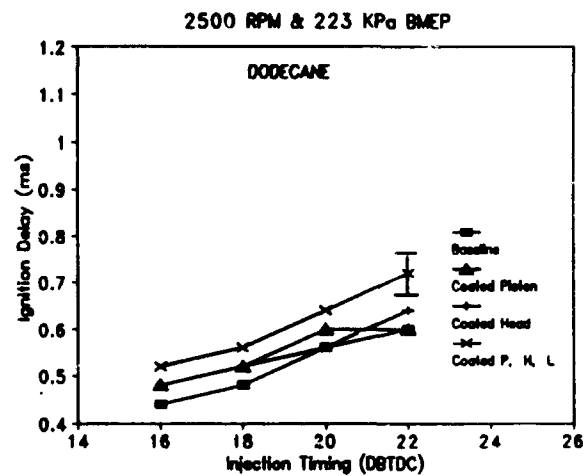
Fig C5(c)

Fig C5(d)

Figure C5

Ignition Delay Versus Timing for Dodecane Fuel at 223 KPa BMEP
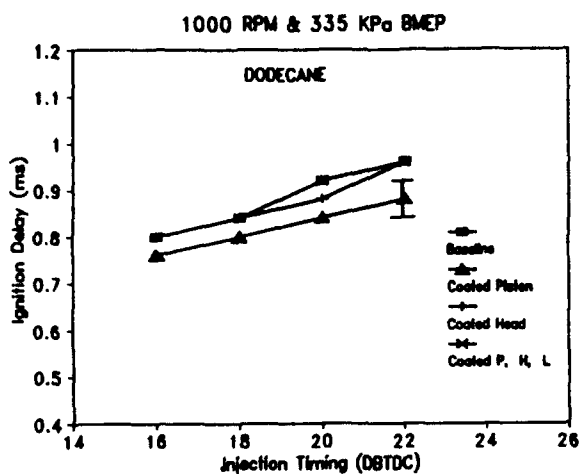
Fig C6(a)
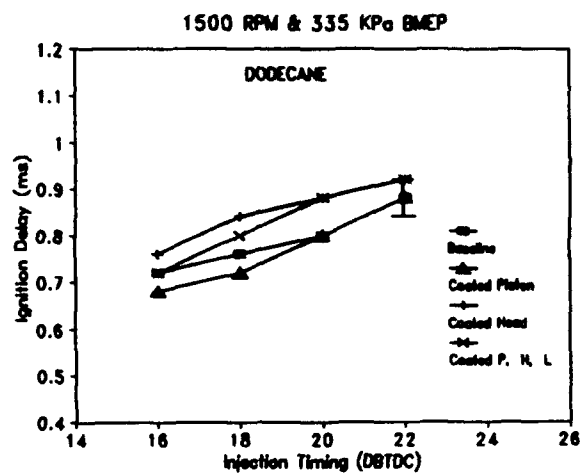
Fig C6(b)
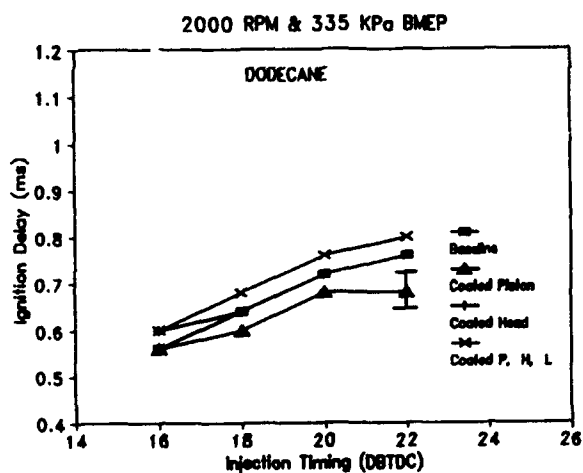
Fig C6(c)
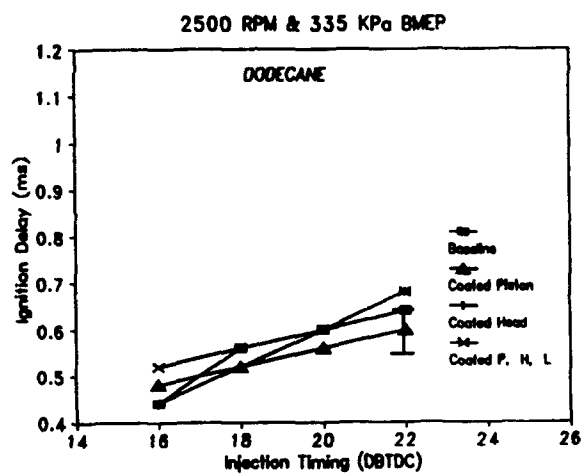
Fig C6(d)

Figure C6

Ignition Delay Versus Timing for Dodecane Fuel at 335 KPa BMEP
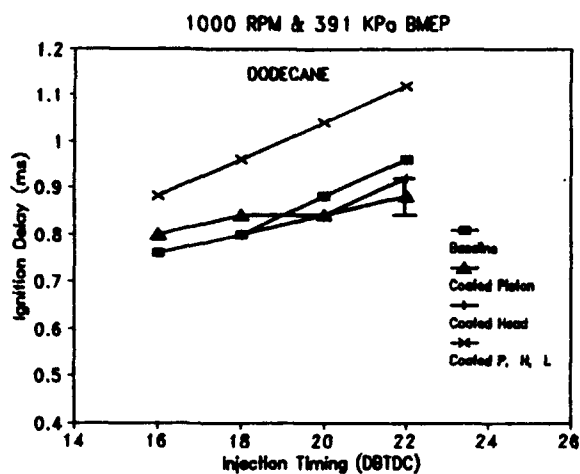
Fig C7(a)
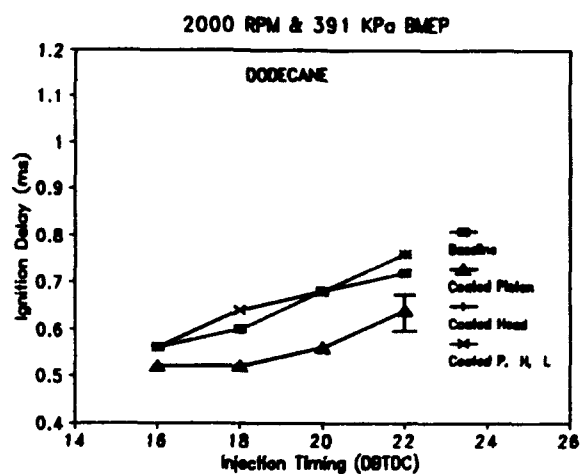
Fig C7(b)
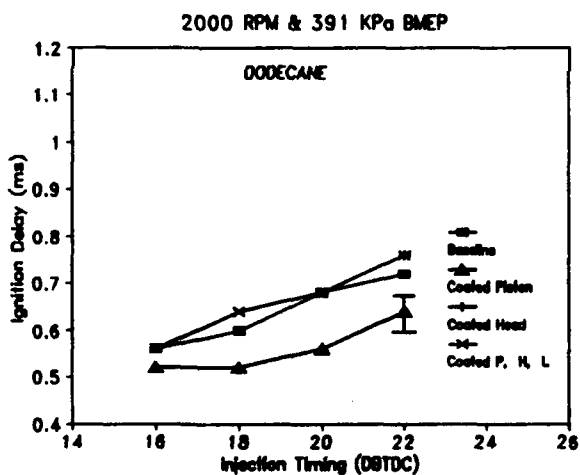
Fig C7(c)
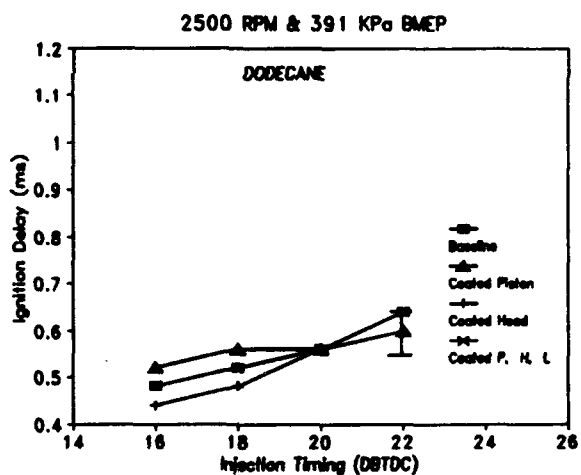
Fig C7(d)

Figure C7

Ignition Delay Versus Timing for Dodecane Fuel at 391 KPa BMEP

90
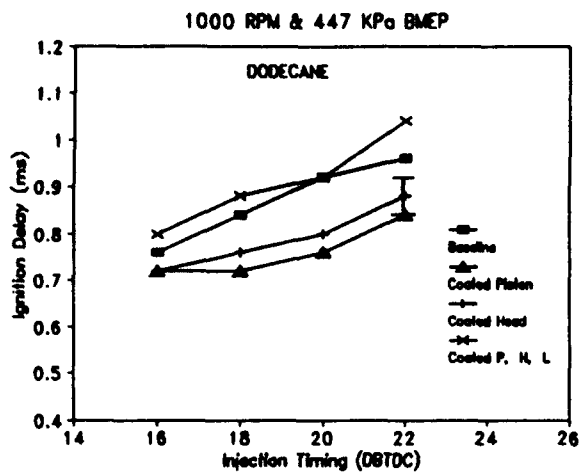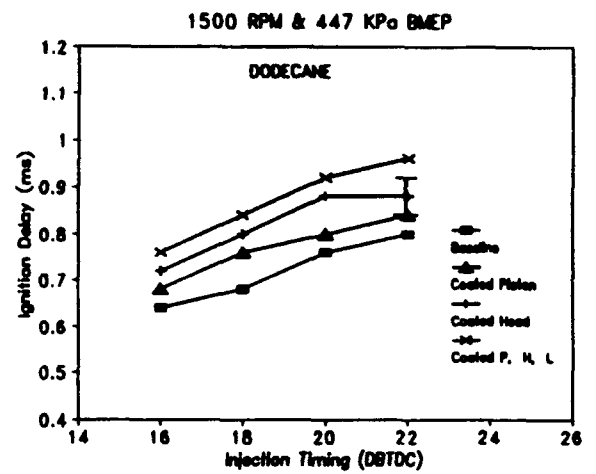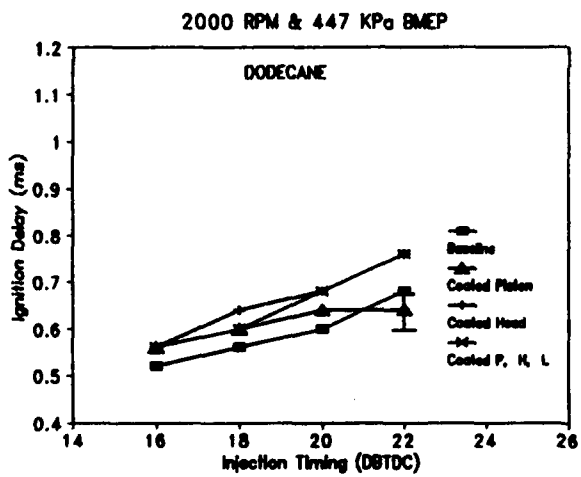
Fig C8(a)

Fig C8(b)

Fig C8(c)
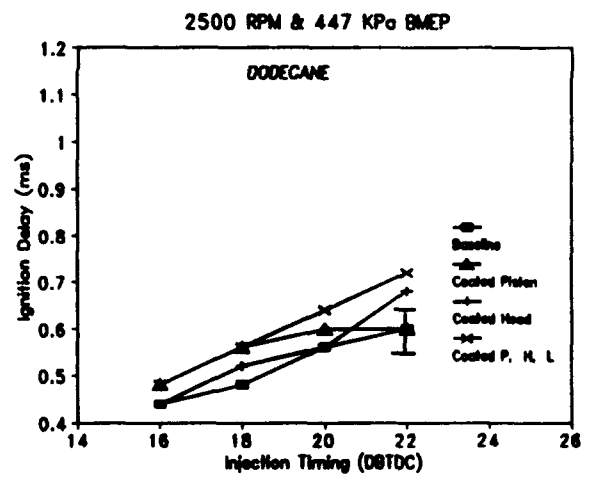
Fig C8(d)

Figure C8

Ignition Delay Versus Timing for Dodecane Fuel at 447 KPa BMEP

APPENDIX D

Soot Concentration Data Plots
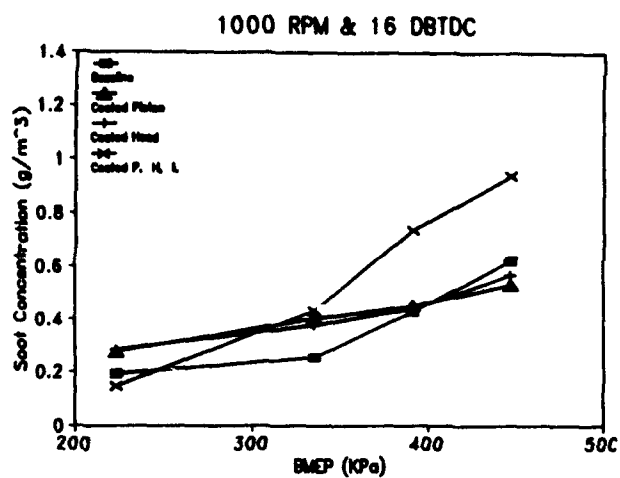
Fig D1(a)
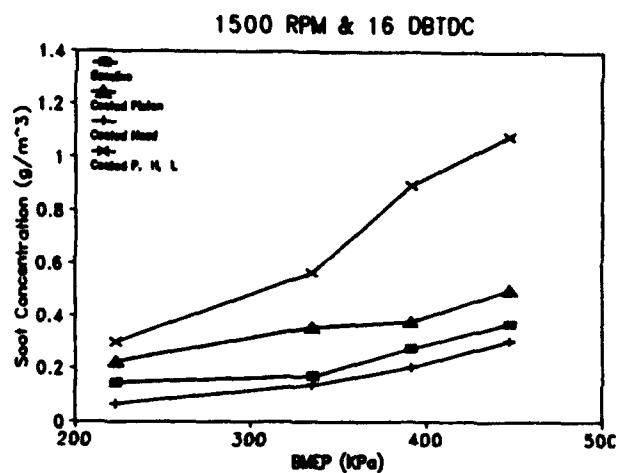
Fig D1(b)
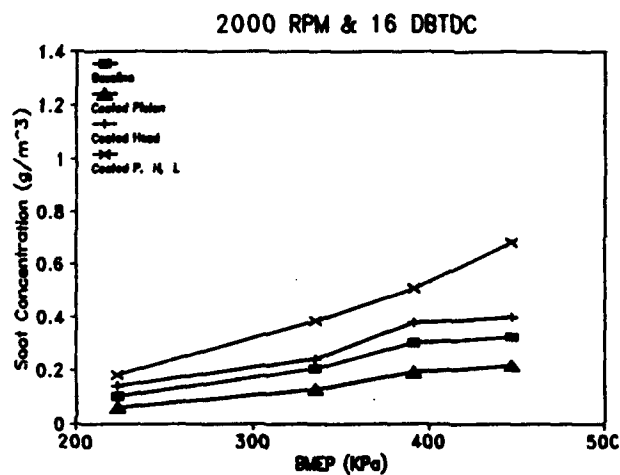
Fig D1(c)
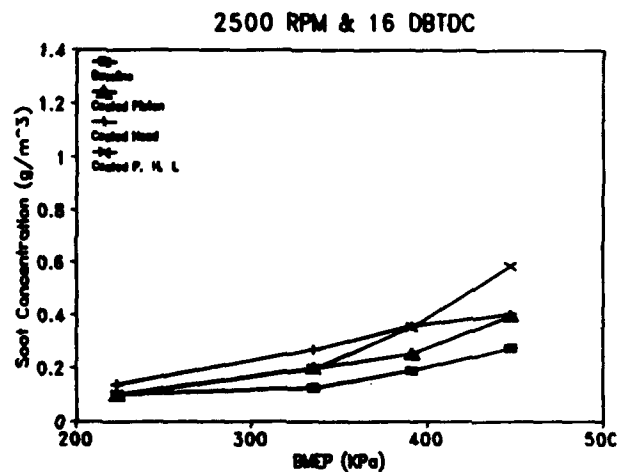
Fig D1(d)

Figure D1

Soot Concentration Versus Load for Hexadecane at 16 DBTDC
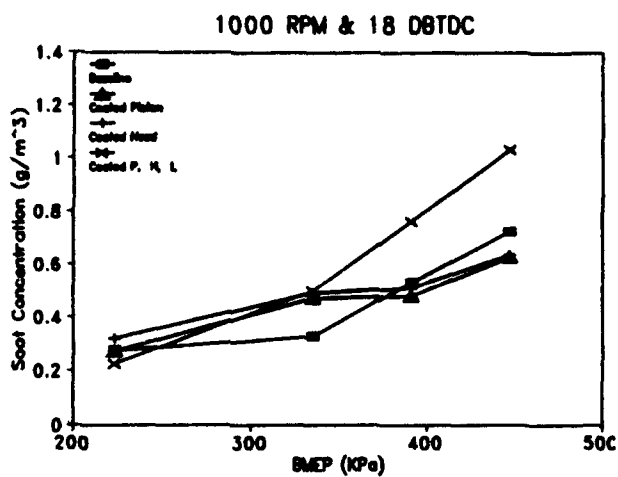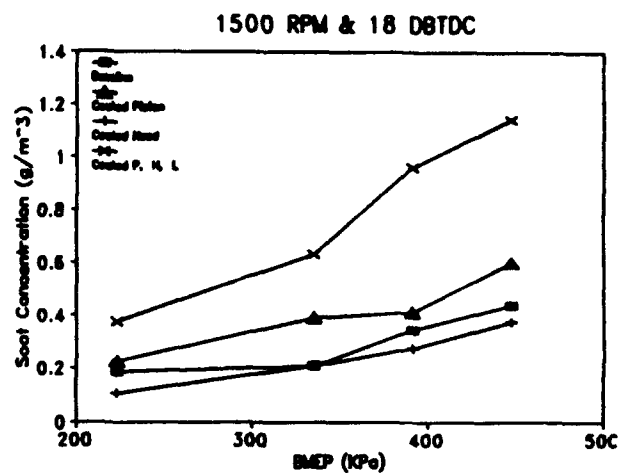
Fig D2(a)   Fig D2(b)
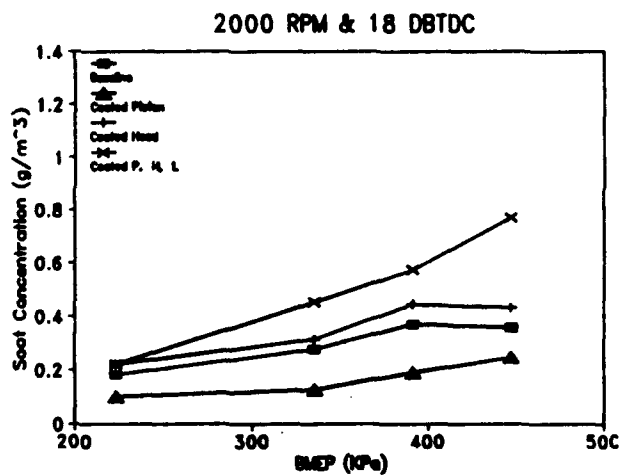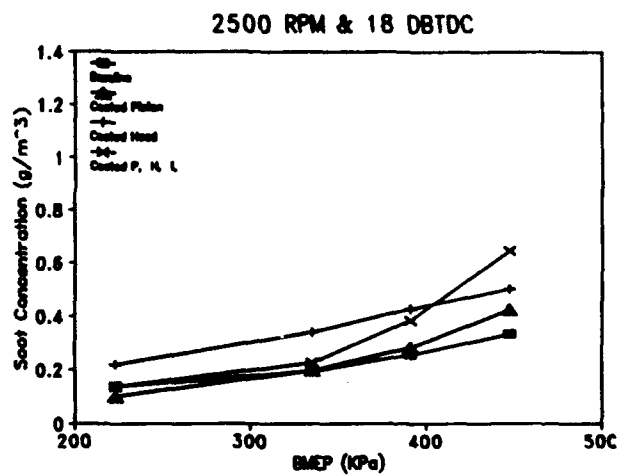
Fig D2(c)   Fig D2(d)

Figure D2

Soot Concentration Versus Load for Hexadecane at 18 DBTDC

94
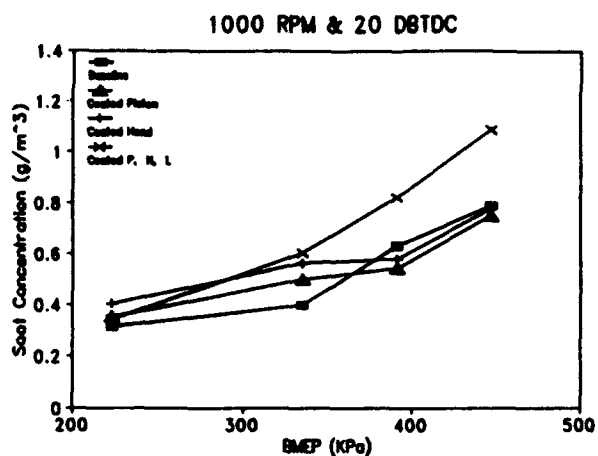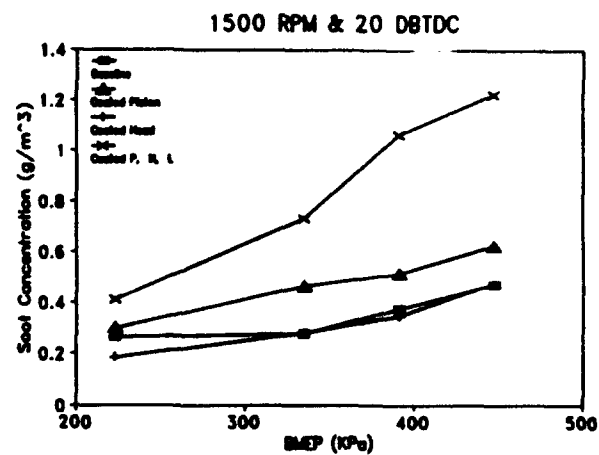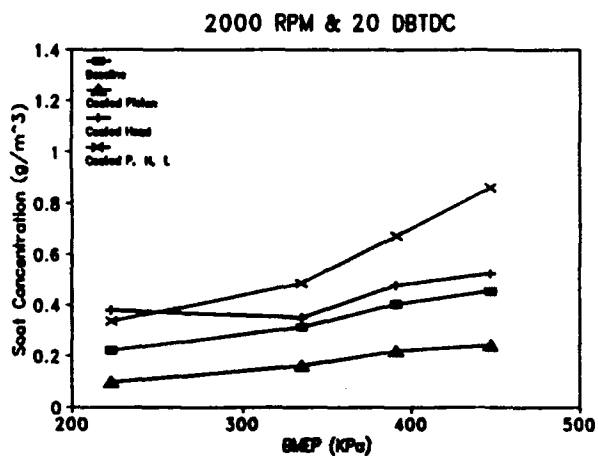
Fig D3(a)

Fig D3(b)

Fig D3(c)
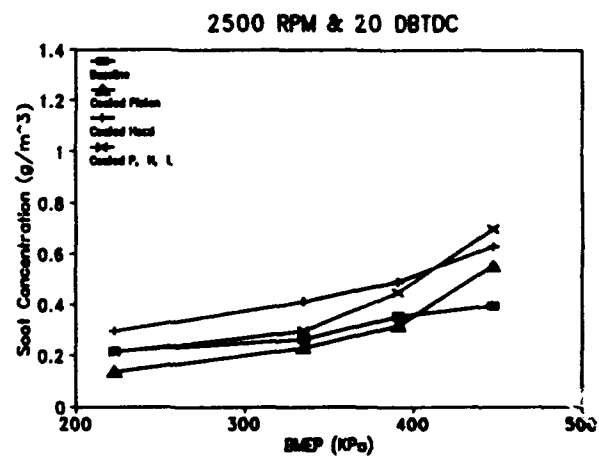
Fig D3(d)

Figure D3

Soot Concentration Versus Load for Hexadecane at 20 DBTDC
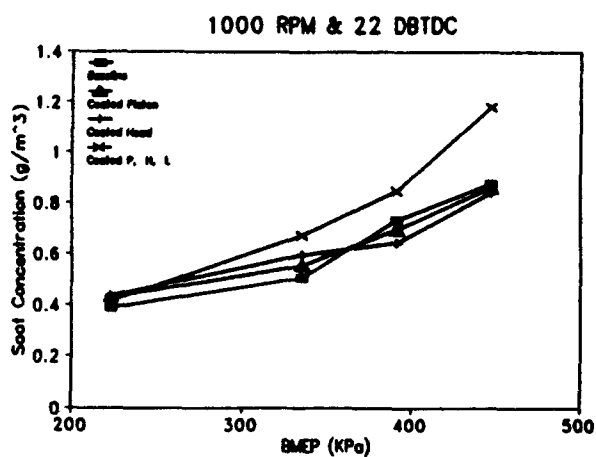
Fig D4(a)
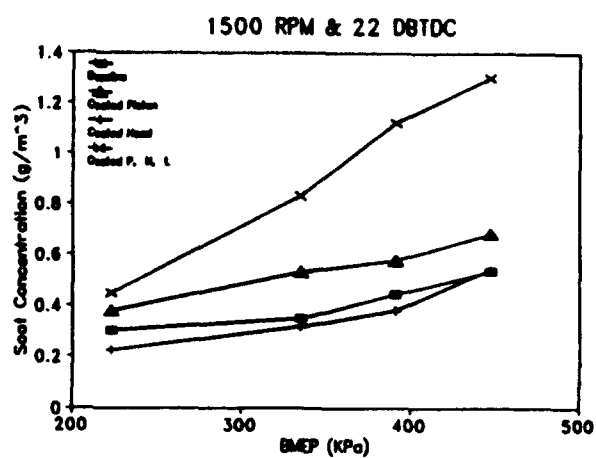
Fig D4(b)
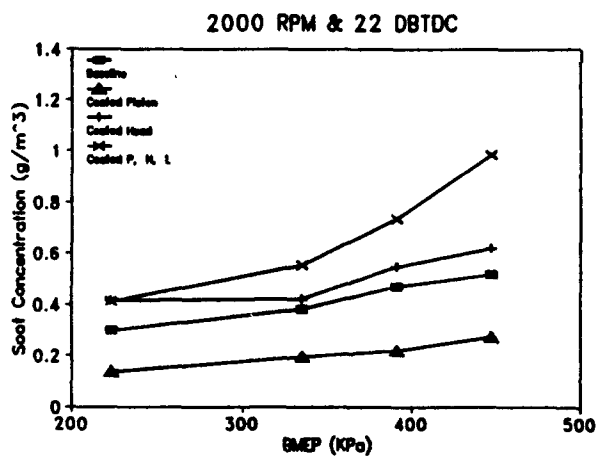
Fig D4(c)
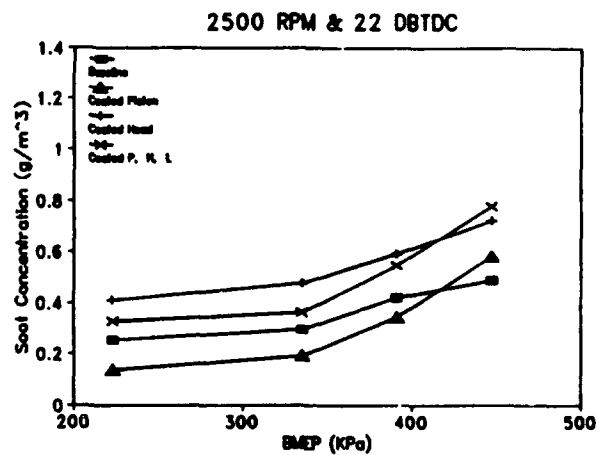
Fig D4(d)

Figure D4

Soot Concentration Versus Load for Hexadecane at 22 DBTDC
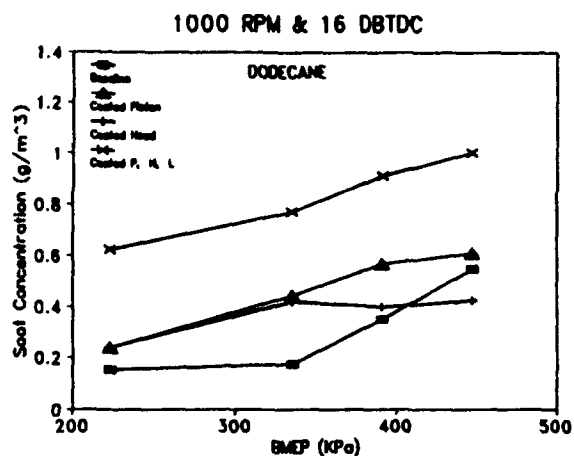
Fig D5(a)
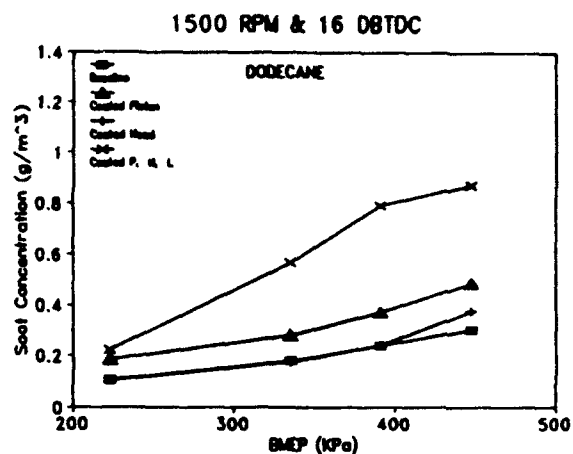
Fig D5(b)
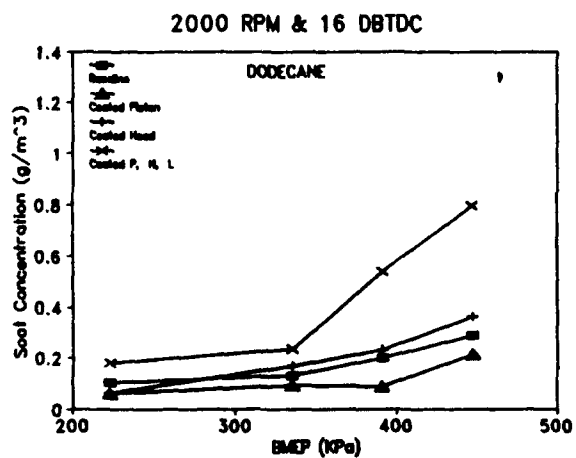
Fig D5(c)
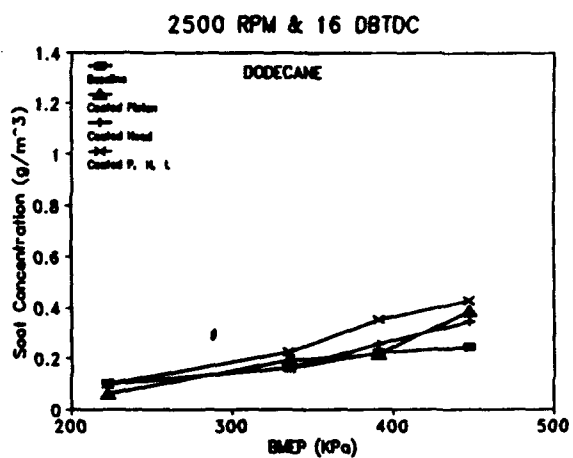
Fig D5(d)

Figure D5

Soot Concentration Versus Load for Dodecane at 16 DBTDC
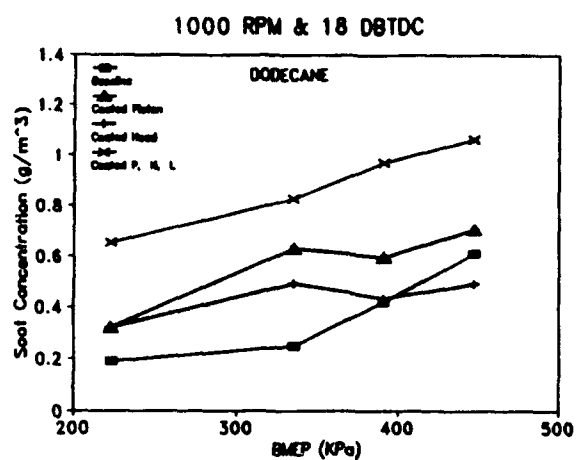
Fig D6(a)
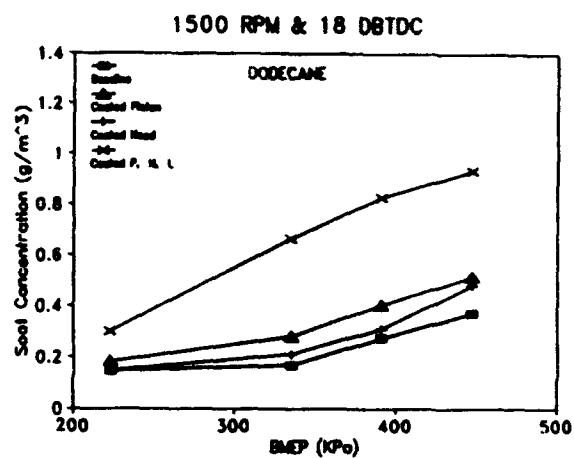
Fig D6(b)
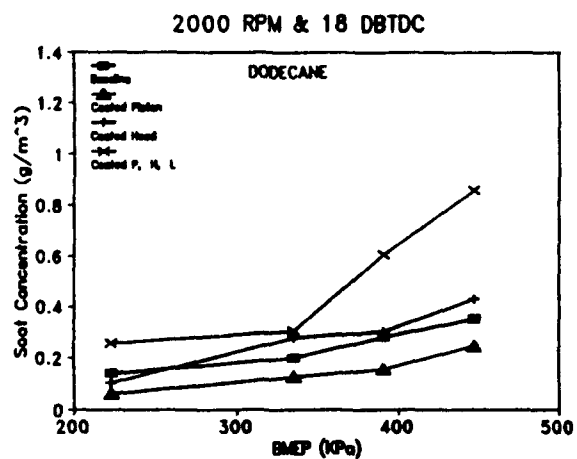
Fig D6(c)
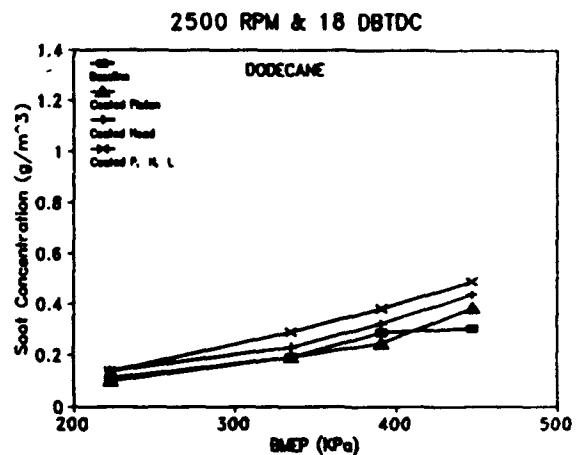
Fig D6(d)

Figure D6

Soot Concentration Versus Load for Dodecane at 18 DBTDC

98
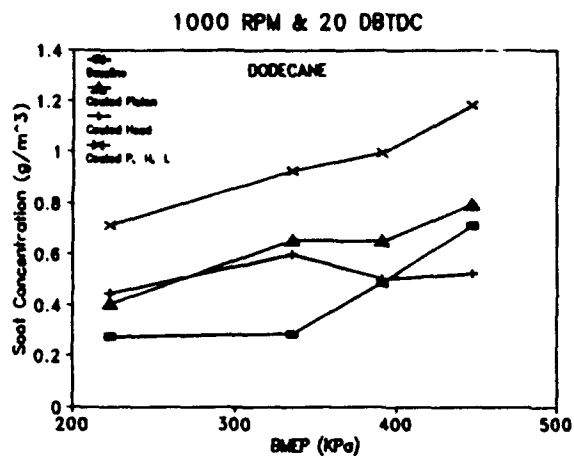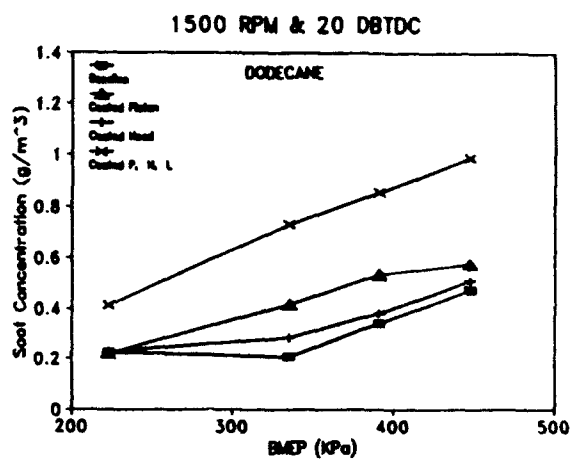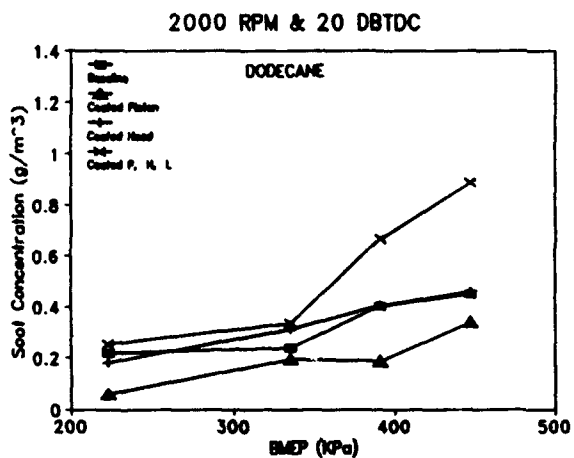
Fig D7(a)

Fig D7(b)

Fig D7(c)
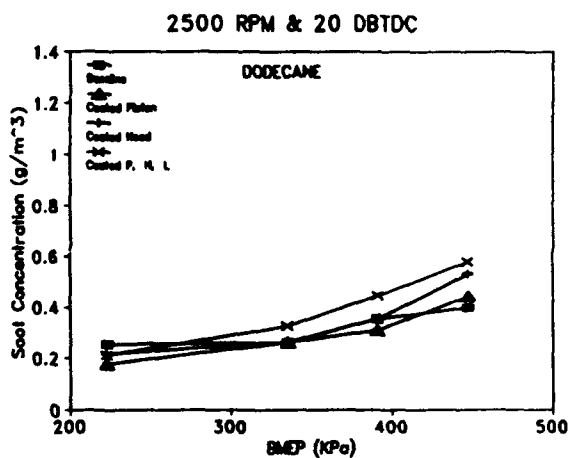
Fig D7(d)

Figure D7

Soot Concentration Versus Load for Dodecane at 20 DBTDC

99
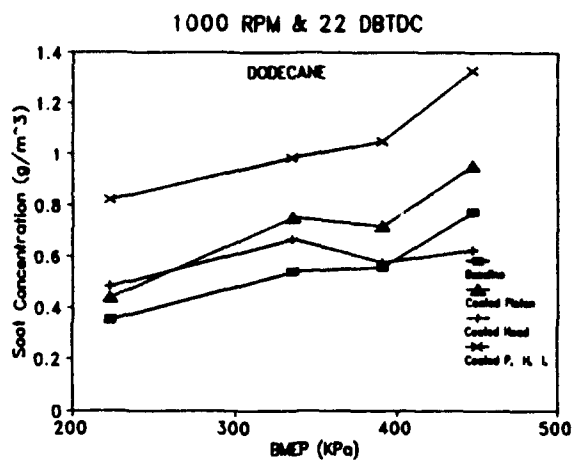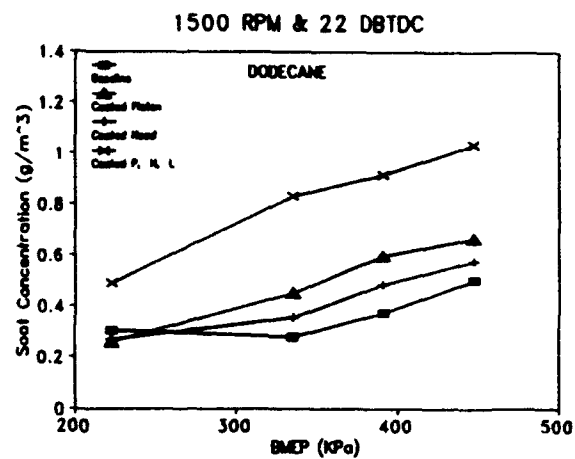
Fig D8(a) Fig D8(b)
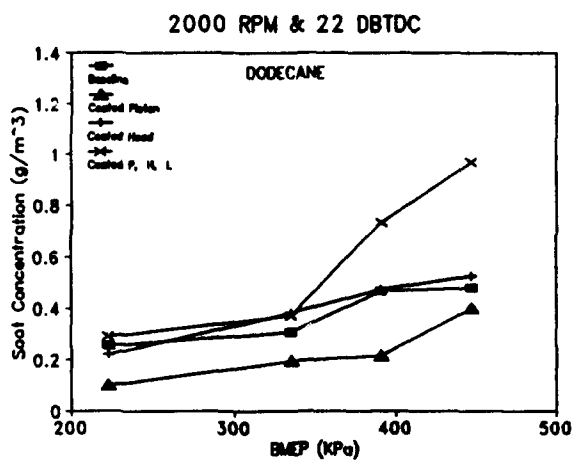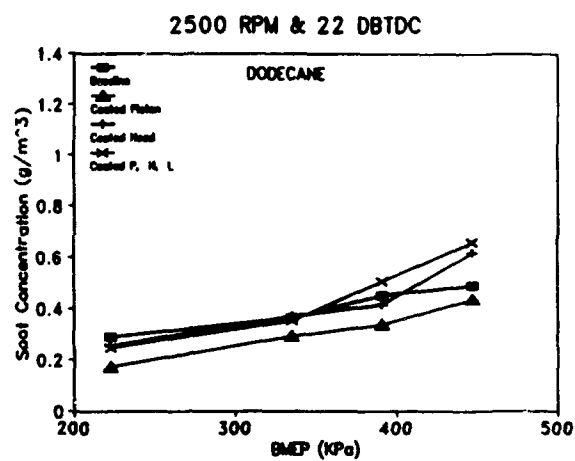
Fig D8(c) Fig D8(d)

Figure D8

Soot Concentration Versus Load for Dodecane at 22 DBTDC

100

APPENDIX E

Exhaust Gas Temperature Data Plots
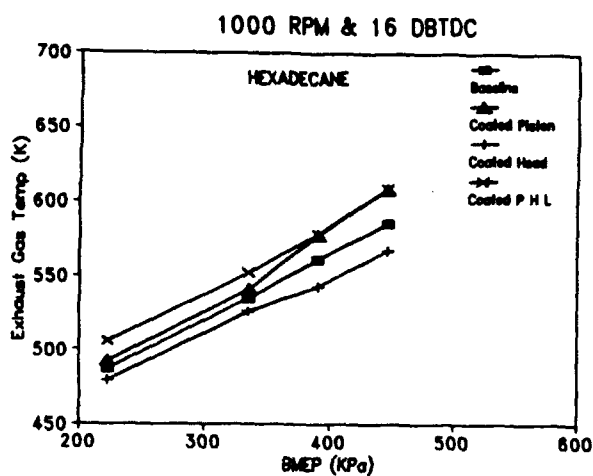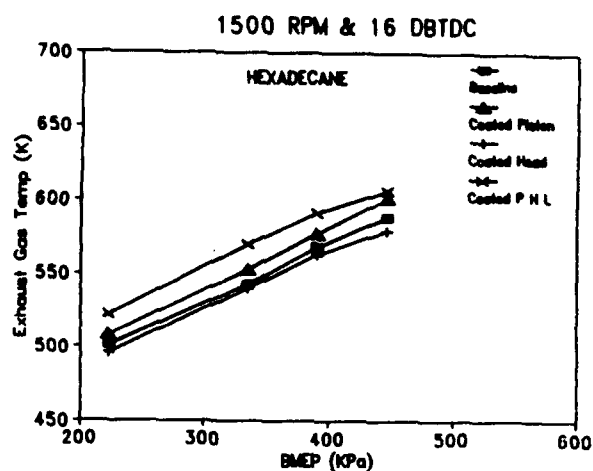
Fig E1(a)   Fig E1(b)
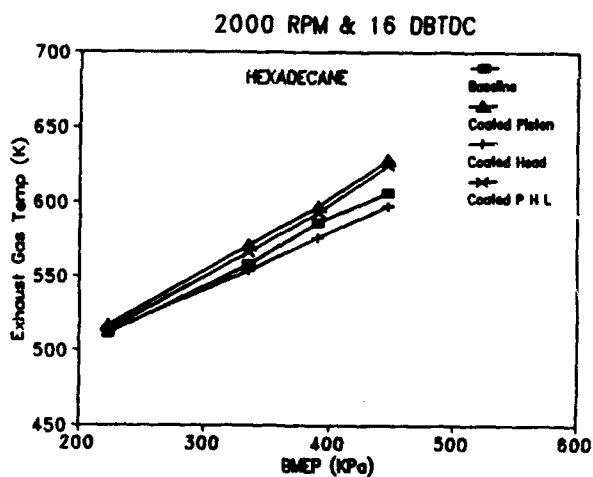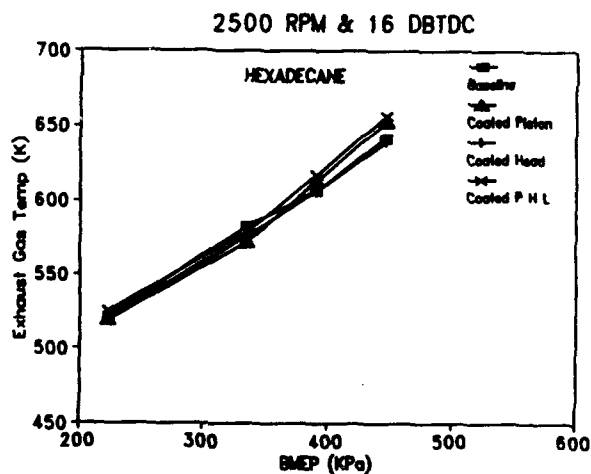
Fig E1(c)   Fig E1(d)

Figure E1

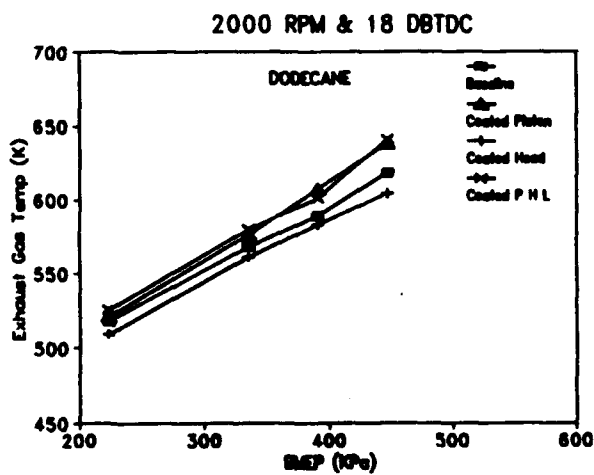Exhaust Gas Temperature Versus Load for Hexadecane at 16 DBTDC

102
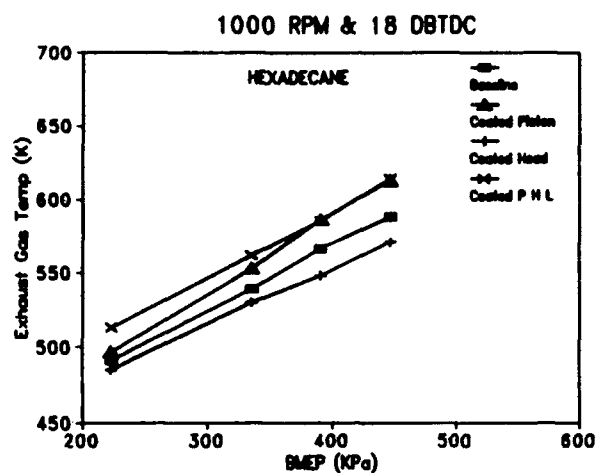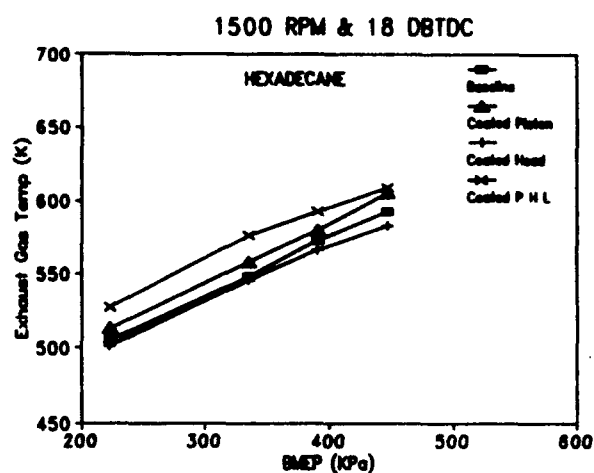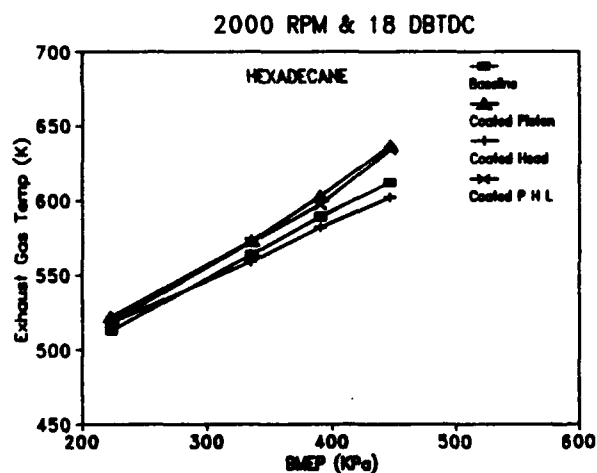
Fig E2(a)

Fig E2(b)

Fig E2(c)
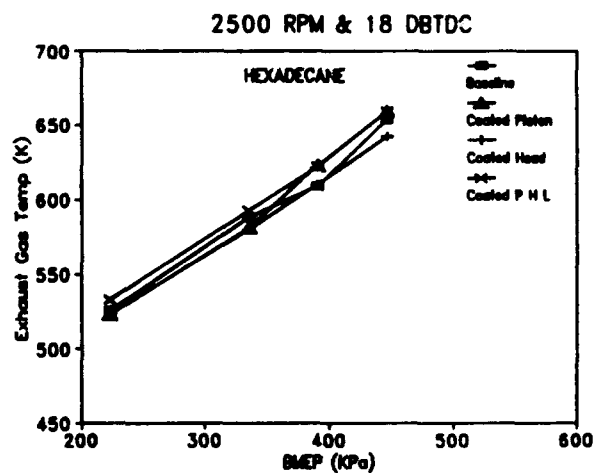
Fig E2(d)

Figure E2

Exhaust Gas Temperature Versus Load for Hexadecane at 18 DBTDC

103
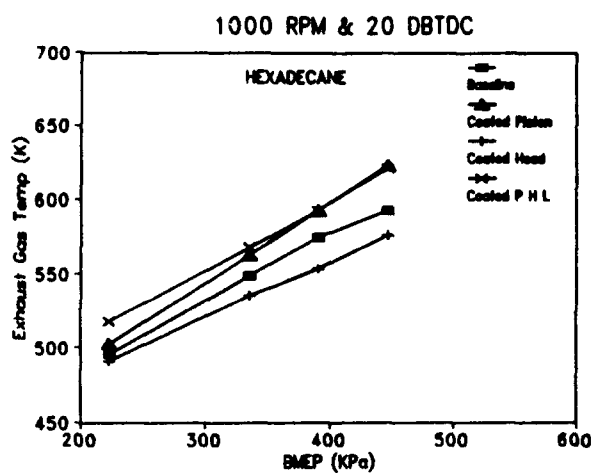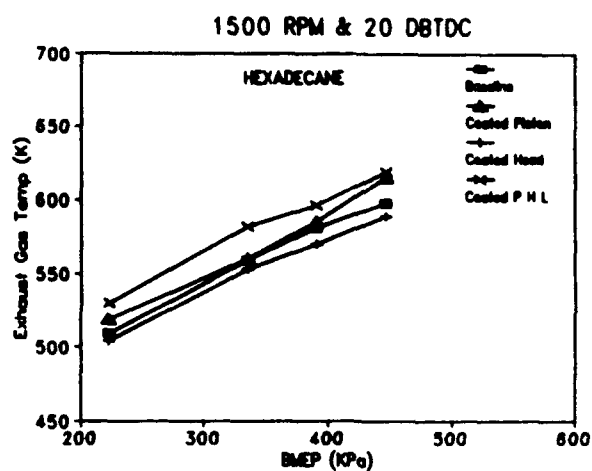
Fig E3(a) Fig E3(b)
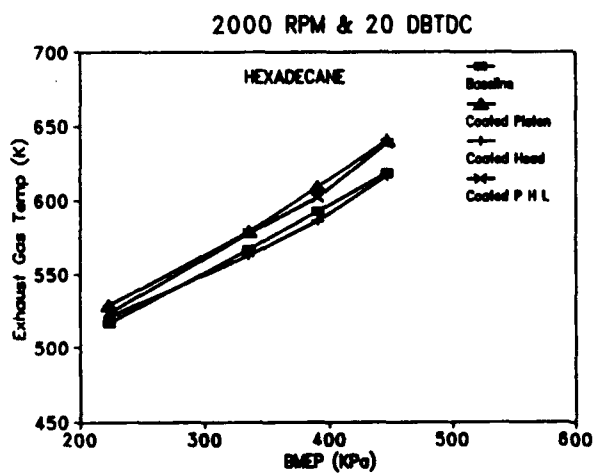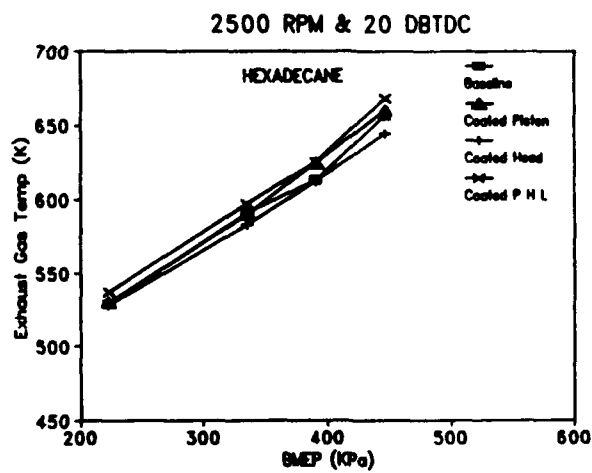
Fig E3(c) Fig E3(d)

Figure E3

Exhaust Gas Temperature Versus Load for Hexadecane at 20 DBTDC

104
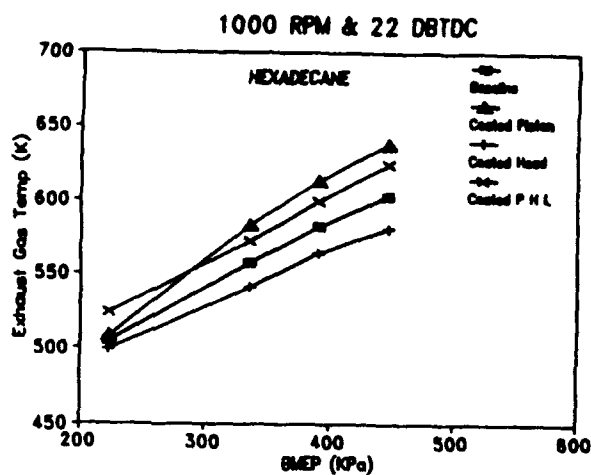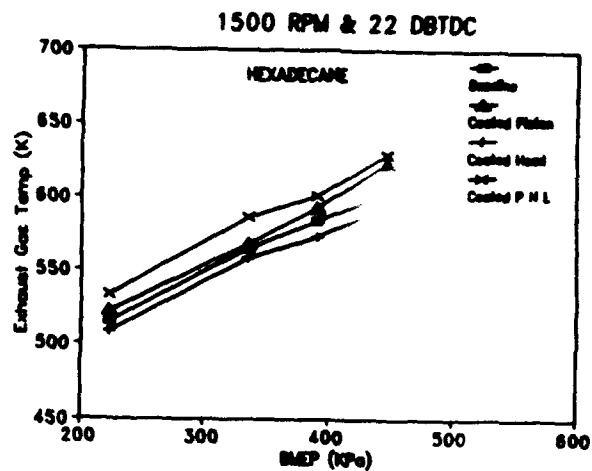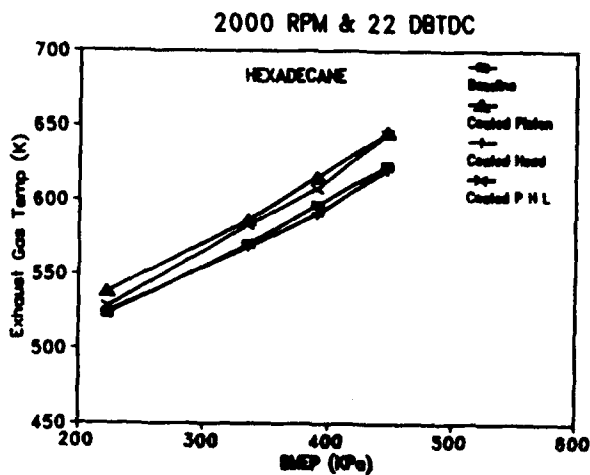
Fig E4(a)

Fig E4(b)

Fig E4(c)
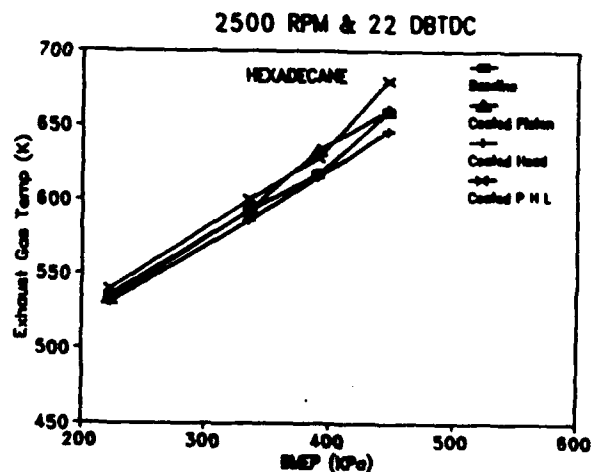
Fig E4(d)

Figure E4

Exhaust Gas Temperature Versus Load for Hexadecane at 22 DBTDC

105
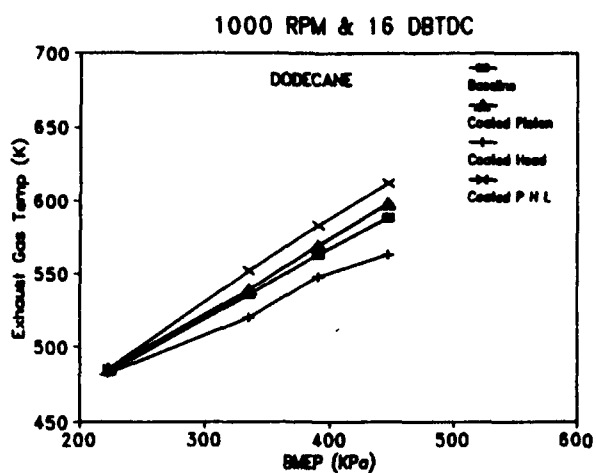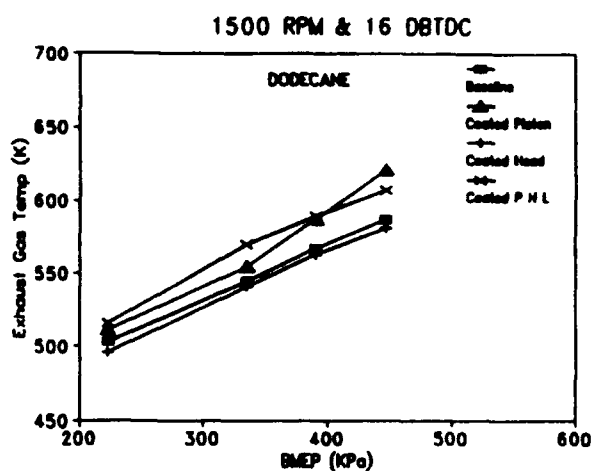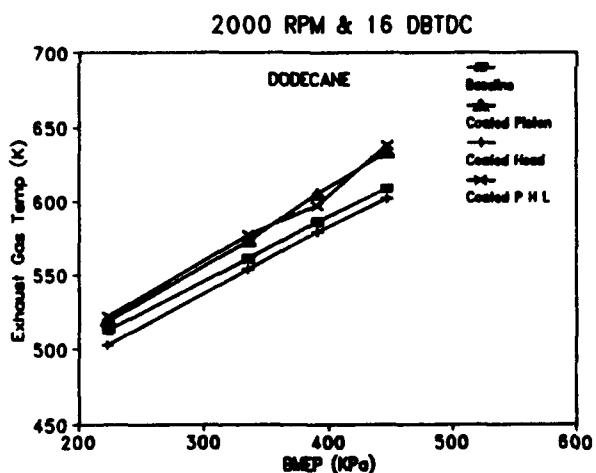
Fig E5(a)

Fig E5(b)

Fig E5(c)
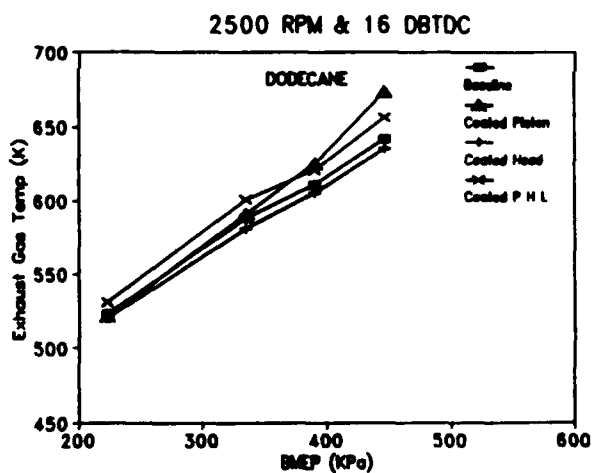
Fig E5(d)

Figure E5

Exhaust Gas Temperature Versus Load for Dodecane at 16 DBTDC

106
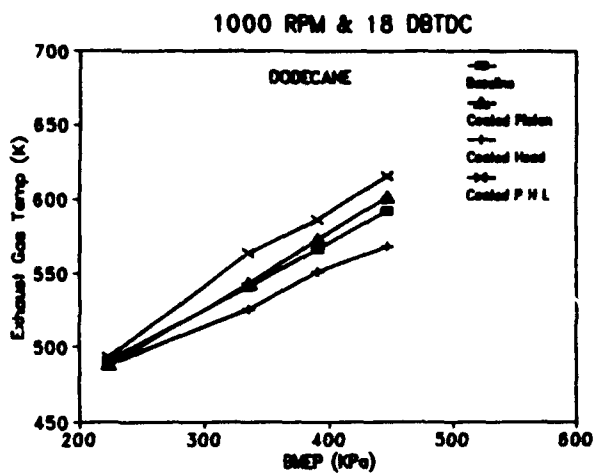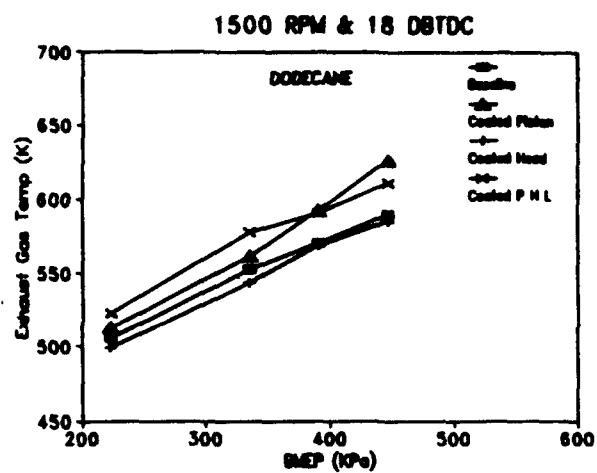
Fig E6(a)

Fig E6(b)

Fig E6(c)
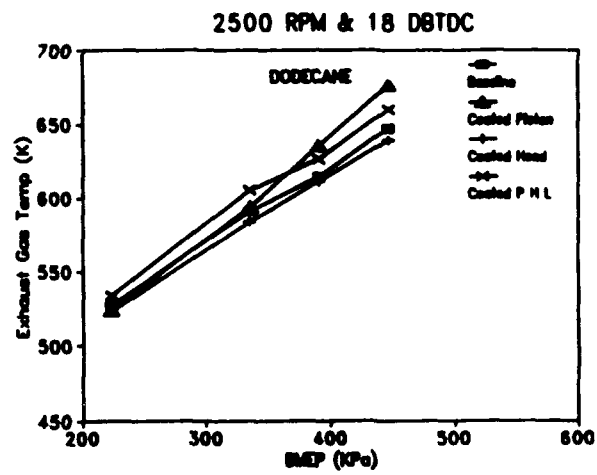
Fig E6(d)

Figure E6

Exhaust Gas Temperature Versus Load for Dodecane at 18 DBTDC

1000 RPM & 20 DBTDC

Fig E7(a)

1500 RPM & 20 DBTDC

Fig E7(b)

2000 RPM & 20 DBTDC
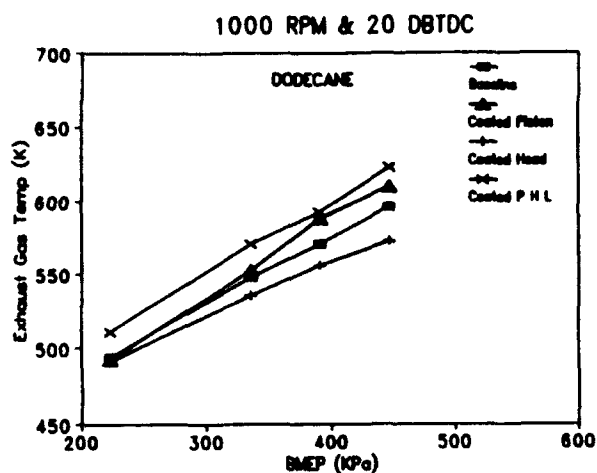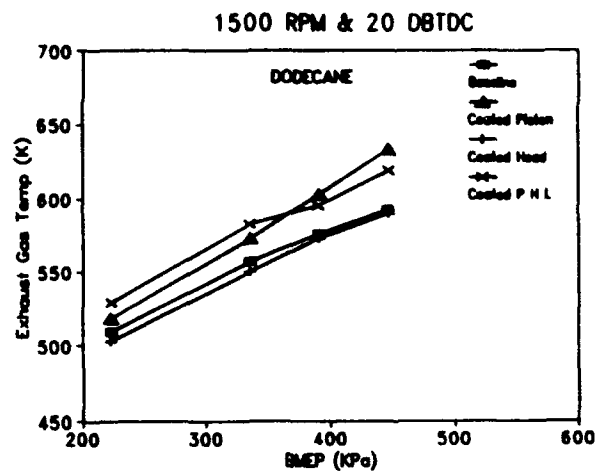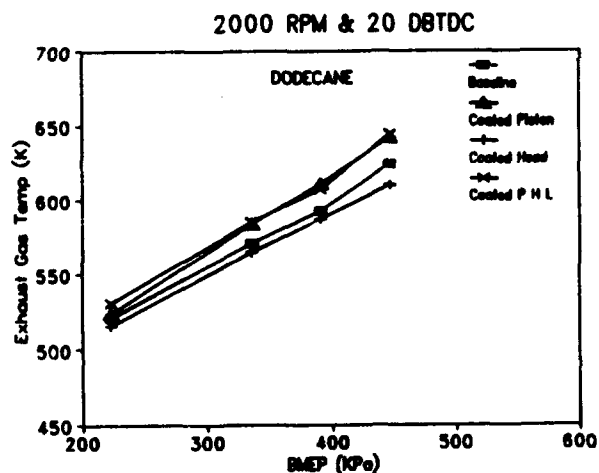
Fig E7(c)

2500 RPM & 20 DBTDC
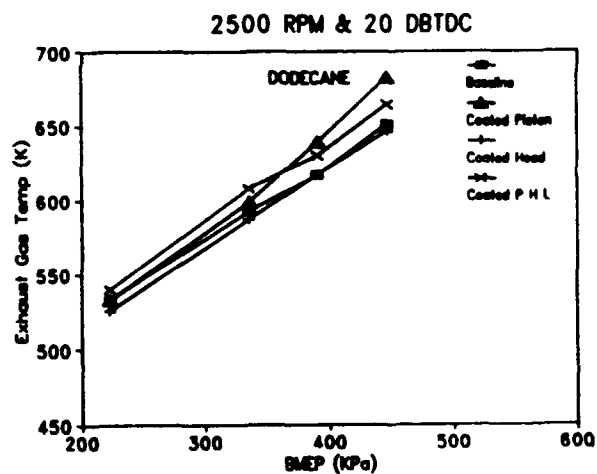
Fig E7(d)

Figure E7

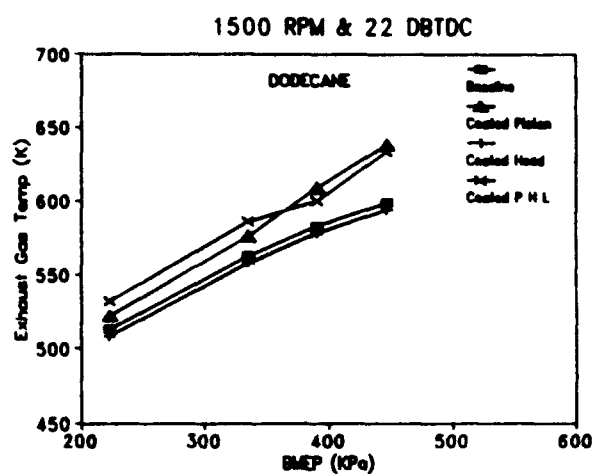**Exhaust Gas Temperature Versus Load for Dodecane at 20 DBTDC**
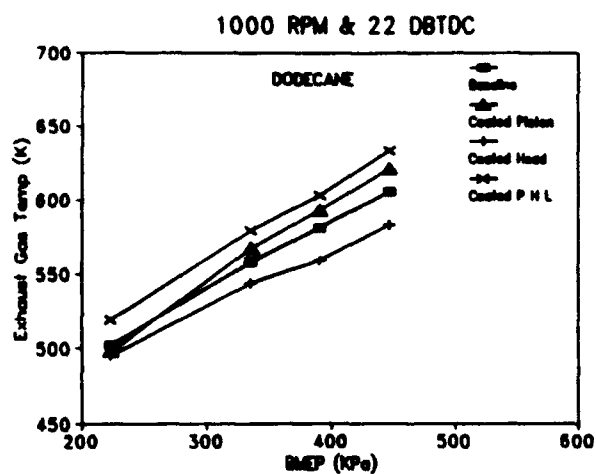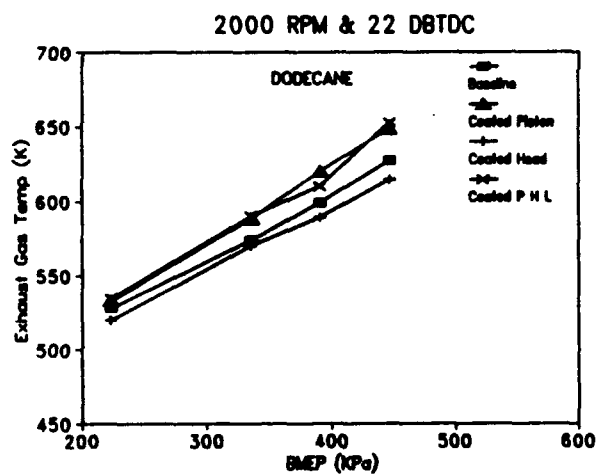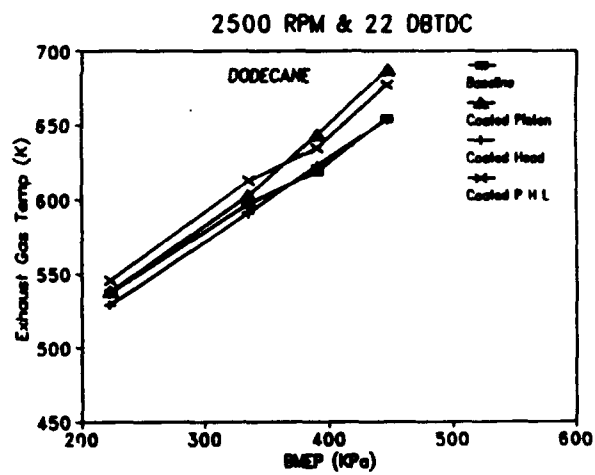
Fig E8(a)

Fig E8(b)

Fig E8(c)

Fig E8(d)

Figure E8

Exhaust Gas Temperature Versus Load for Dodecane at 22 DBTDC